SKI Report 2008:12

Research

Independent Calculations for the SR-Can Assessment

External review contribution in support of SKI's and SSI's review of SR-Can

Philip Maul
Peter Robinson
Alex Bond
Steven Benbow

March 2008

ISSN 1104-1374
ISRN SKI-R-08/12-SE

SKI

SKI Report 2008:12

Research

Independent Calculations for the SR-Can Assessment

External review contribution in support of SKI's and SSI's review of SR-Can

Philip Maul
Peter Robinson
Alex Bond
Steven Benbow

Quintessa Limited, Henley-on-Thames, UK

March 2008

FOREWORD

The work presented in this report is part of the Swedish Nuclear Power Inspectorate's (SKI) and the Swedish Radiation Protection Authority's (SSI) SR-Can review project.

The Swedish Nuclear Fuel and Waste Management Co (SKB) plans to submit a license application for the construction of a repository for spent nuclear fuel in Sweden 2010. In support of this application SKB will present a safety report, SR-Site, on the repository's long-term safety and radiological consequences. As a preparation for SR-Site, SKB published the preliminary safety assessment SR-Can in November 2006. The purposes were to document a first evaluation of long-term safety for the two candidate sites at Forsmark and Laxemar and to provide feedback to SKB's future programme of work.

An important objective of the authorities' review of SR-Can is to provide guidance to SKB on the complete safety reporting for the license application. The authorities have engaged external experts for independent modelling, analysis and review, with the aim to provide a range of expert opinions related to the sufficiency and appropriateness of various aspects of SR-Can. The conclusions and judgments in this report are those of the authors and may not necessarily coincide with those of SKI and SSI. The authorities own review will be published separately (SKI Report 2008:23, SSI Report 2008:04 E).

This report covers issues related to the post-closure evolution of the repository and to the radionuclide transport calculations for the safety assessment.

Bo Strömberg (project leader SKI) Björn Dverstorp (project leader SSI)

FÖRORD

Denna rapport är en underlagsrapport till Statens kärnkraftinspektions (SKI) och Statens strålskyddsinstituts (SSI) gemensamma granskning av Svensk Kärnbränslehantering AB:s (SKB) säkerhetsredovisning SR-Can.

SKB planerar att lämna in en ansökan om uppförande av ett slutförvar för använt kärnbränsle i Sverige under 2010. Som underlag till ansökan kommer SKB presentera en säkerhetsrapport, SR-Site, som redovisar slutförvarets långsiktiga säkerhet och radiologiska konsekvenser. Som en förberedelse inför SR-Site publicerade SKB den preliminära säkerhetsanalysen SR-Can i november 2006. Syftena med SR-Can är bl.a. att redovisa en första bedömning av den långsiktiga säkerheten för ett KBS-3-förvar vid SKB:s två kandidatplatser Laxemar och Forsmark och att ge återkoppling till SKB:s fortsatta arbete.

Myndigheternas granskning av SR-Can syftar till att ge SKB vägledning om förväntningarna på säkerhetsredovisningen inför den planerade tillståndsansökan. Myndigheterna har i sin granskning tagit hjälp av externa experter för oberoende modellering, analys och granskning. Slutsatserna i denna rapport är författarnas egna och överensstämmer inte nödvändigtvis med SKI:s eller SSI:s ställningstaganden. Myndigheternas egen granskning publiceras i en annan rapport (SKI Rapport 2008:19; SSI Rapport 2008:04).

Denna rapport behandlar frågor kopplade till utvecklingen av förvarssystemet efter förslutning och radionuklidtransportberäkningar för säkerhetsanalysen.

Bo Strömberg (projektledare SKI) Björn Dverstorp (projektledare SSI)

Summary

SKB has published the SR-Can assessment of a deep repository for spent fuel at either the Forsmark or Laxemar sites. This is the final assessment prior to a formal regulatory submission.

A number of independent calculations have been undertaken in support of SKI's review of SR-Can. The types of calculations are:

1. direct checks of specified SKB calculations;
2. reproduction of SKB computer calculations with independent codes, to ensure that what SKB has done is properly understood, and to check that the calculations are properly documented; and
3. independent calculations to investigate particular aspects of the safety case.

The data used by SKB in its Performance Assessment calculations have not been subject to detailed review.

The independent calculations provide information on:

1. where independent calculations have been able to provide support for the arguments put forward by SKB;
2. areas where insufficient information has been provided by SKB to enable a third party to reproduce the SR-Can calculations; and
3. areas where calculations lead to questions about the validity of SKB's arguments.

The timescale for the production of the present report has been determined by the timescales for SKI's review of the SR-Can assessment. As a result, some of the independent calculations referred to have not been fully documented, and this will be carried out in 2008.

The following conclusions have been drawn.

1. SKB has worked hard to respond to criticisms of previous performance assessments, and SR-Can is an impressive piece of work.

2. In several areas either insufficient or inconsistent information has been presented so that a full reproduction of SKB's calculations has not been possible. This is an important area where SKB will need to improve the presentation of its assessment for SR-Site.

3. There are several areas where SKB's description of post-closure repository evolution needs to be further reviewed. Overall SKB have given only limited consideration to the coupled processes that will operate before the system reaches a new equilibrium.

4. The calculations of thermal evolution suggest that some canisters may reach temperatures close to the maximum criterion of 100°C. It was not possible to reproduce fully the calculations presented by SKB because of uncertainties over the way that the repository layout was specified.

5. SKB's repository resaturation calculations are not definitive. The resaturation timescales obtained in the QPAC-EBS calculations are generally consistent with the relatively short timescales obtained by SKB, but timescales of much greater than 200 years have been obtained with some combinations of modelling assumptions. Further independent calculations will be undertaken, including consideration of bentonite resaturation.

6. Radionuclide transport calculations using the AMBER code have produced very similar results to those reported by SKB. However, this required a considerable amount of effort because of the need to check a large number of areas with SKB where the information provided in the SR-Can documentation was either incorrect or missing.

7. Insufficient deterministic calculations are given by SKB to enable the reader to understand the key issues presented and to facilitate the reproduction of SKB's calculations by a third party. It is suggested that for each set of probabilistic calculations undertaken in support of comparisons with regulatory criteria, a deterministic case should be documented to illustrate the key points. Further insight into the important features of probabilistic calculations can be obtained by analysing the high consequence runs: this has been undertaken for the Quintessa calculations but was not considered by SKB in SR-Can.

8. The calculated risks may be more sensitive to the choice of parameter probability density functions (PDFs) than implied by SKB. For example, the choice between a triangular and log-triangular PDF for the fuel dissolution rate makes a difference of more than a factor of 2 in the calculated doses.

9. The lost buffer failure mode is critical to the overall risk quantification, and SKB's evaluation of this failure mode appears to be preliminary in nature. The distribution of failure times for canisters is critical, but it has not been possible to verify fully SKB's corrosion calculations. Further consideration of both the calculations presented by SKB and independent evaluations are required in order to provide a more detailed assessment of the validity of the approach taken in SR-Can.

10. The use of the independent Discrete Fracture Network calculations undertaken by Clearwater Hardrock Consulting has enabled alternative hydrogeological parameters to be used in the AMBER radionuclide transport calculations, contributing to an assessment of the robustness of the conclusions drawn by SKB.

Areas where additional independent calculations would be valuable have been identified and these are planned for inclusion in the programme for 2008.

Contents

1 Introduction

In 2004 SKB published their Interim Main Report of the safety assessment SR-Can (SKB, 2004a). The main purpose of that report was to demonstrate the methodology that will be used for safety assessment. In Maul and Robinson (2005a) a number of independent calculations were undertaken in connection with SKI's review of the interim SR-Can report (SKI, 2005). This proved to be a very useful way of investigating key issues in SKB's assessment; in particular, by aiming to reproduce chosen SKB calculations independently, a lot of information was obtained about the strengths and weaknesses of SKB's approach.

SKB have now published the full SR-Can assessment of a deep repository for spent fuel at either the Forsmark or Laxemar sites (SKB, 2006a). This is the final assessment prior to a formal regulatory submission.

A number of independent calculations have been undertaken in support of SKI's review of SR-Can. The types of calculations are:

1. direct checks of specified SKB calculations;
2. reproduction of SKB computer calculations with independent codes, to ensure that what SKB has done is properly understood, and to check that the calculations are properly documented; and
3. independent calculations to investigate particular aspects of the safety case.

These calculations provide information on:

1. where independent calculations have been able to provide support for the arguments put forward by SKB;
2. areas where insufficient information has been provided by SKB to enable a third party to reproduce the SR-Can calculations; and
3. areas where calculations lead to questions about the validity of SKB's arguments.

Independent calculations of radionuclide transport have been undertaken using the AMBER code (Enviros Ltd and Quintessa Ltd, 2007), which was also used in the previously-reported calculations (Maul and Robinson, 2005a). Calculations for the evolution of the Engineered Barrier System (EBS) have been undertaken with version 1.0 of the QPAC-EBS code (Maul et al., 2007).

This report is structured as follows:

- Section 2 gives an overview of the calculations undertaken by SKB in the SR-Can report;
- Section 3 then discusses checks of some calculations that are important for SKB's performance assessment;
- Section 4 describes the QPAC-EBS calculations that have been undertaken to date on the evolution of the EBS;
- Section 5 describes radionuclide transport calculations using the AMBER code, primarily aimed at reproducing selected calculations described by SKB;
- Section 6 describes the use of independent discrete fracture network calculations to provide alternative parameterisations for radionuclide transport in the geosphere;
- Section 7 discusses the programme for future independent calculations; and
- Section 8 summarises the conclusions drawn.

2 Overview of the SR-Can Calculations

2.1 Introduction

The overall impression is that SKB has worked hard to respond to criticisms of previous assessments, and SR-Can is an impressive piece of work. The way that SKB has dealt with the review comments in Maul and Robinson (2005a) and SKI (2005) are summarised in Table 1.

There are some important issues that will not be addressed properly until SR-Site, and this must be a cause of concern.

A summary of the calculations undertaken in SR-Can is given in Section 2.2. This is followed by comments on specific aspects of the assessment. Except where indicated, references are to the main Tier 1 SR-Can report (SKB, 2006a). Additional references for key Tier 2 and Tier 3 documents are given in Table 2 and Table 3.

In this section an overview is given of the SR-Can calculations, giving the background to the Quintessa calculations in Section 3 to Section 6.

Table 1: SKB's Response in SR-Can to Previous Review Comments

Comment	Relevance to SR-Can
The **effects of climate evolution on engineered barriers** have not been analysed in detail in the Interim Report, and this limits the usefulness of the preliminary calculations that have been undertaken.	This is addressed in SR-Can, leading to the buffer erosion scenario.
A key aspect of SKB's approach is the use of the **integrated near-field evolution model**. The information provided on this model demonstrates its capability efficiently to reproduce calculations from individual process models, but insufficient information is given at the present time to justify statements about interactions between processes. In particular it is assumed that relatively short-term thermal and resaturation processes do not affect the properties of the buffer and its longer-term performance.	This appears to be downplayed in SR-Can.
The underlying **methods for considering radionuclide transport** are little changed from SR 97, although useful improvements have been made in some areas. The approach taken means that additional calculations are needed to address issues related to the evolution of the system with time. Whether the overall methodology will enable a comprehensive assessment to be undertaken in practice can only be judged when the full SR-Can assessment is available.	SKB will not have methods to consider time dependence until SR-Site. This must be a cause for concern.
The **documentation** of the models used in PA calculations often relies on references going back over a period of twenty years updated by model validity documents for each model. The production of a single up-to-date supporting document giving full details of the models used would greatly assist the transparency of the safety case presentation.	SKB have tried hard to address this. It is stated in SR-Can Section 2.7.3 that models and data should be documented to enable calculations to be reproduced. This statement is tested in the independent calculations given in this report.

Comment	Relevance to SR-Can
The consideration of **Conceptual Uncertainties** in the supporting Process Report is restricted to the buffer. This restriction greatly limits the usefulness of the Process Report in providing information on the overall methodology. For example, it is not clear whether the approach taken for the buffer will be satisfactory for addressing conceptual model uncertainties in the geosphere.	Advances have been made in SR-Can. Various aspects of conceptual uncertainties will be explored using independent calculations.
SKB have not presented any **deterministic PA calculations**. Without these it is often difficult to understand fully the probabilistic calculations that are presented, although independent AMBER calculations have been able to reproduce the key features of these calculations. It is suggested that deterministic calculations should be part of SR-Can.	SR-Can includes deterministic calculations but these are very limited.
It has been possible to reproduce the key features of the interim SR-Can probabilistic calculations with AMBER, although there remain uncertainties deriving from the way that SKB have modelled the **U-238 decay chain** in different parts of the system.	The way that the actinide decay chains are modelled remains an issue.
A full reproduction of the interim SR-Can calculations was not possible because only summary data from **hydrogeological calculations** are presented. It is suggested that in the SR-Can safety assessment sufficient information should be provided to enable PA calculations to be fully reproduced.	This remains an issue for SR-Can.
SKB's preliminary calculations indicate that safety criteria are likely to be met by a comfortable margin even if a **large fraction of the canisters fail**. The geosphere plays only a minor role in the retardation function. This assertion depends on a number of assumptions, and the independent AMBER calculations show that different assumptions could mean that the safety criteria would be exceeded in this extreme case.	The buffer erosion scenario is considered in detail in the independent calculations.

Table 2: Key Tier 2 Supporting Reports

Topic	Report	Reference	Comments
Data	TR-06-25	SKB (2006b)	Used for all calculations; the most important reference for the current report
Models	TR-06-26	SKB (2006d)	Superficial description of a large number of codes, but useful for tracking references
Initial State	TR-06-21	SKB(2006e)	Includes lots of data relevant to independent calculations
Canister and Fuel Processes	TR-06-22	SKB(2006f)	
Buffer and Backfill Processes	TR-06-18	SKB(2006g)	

Table 3: Key Tier 3 Supporting Reports

Topic	Report	Reference	Comments
Safety Evaluations			
Laxemar	TR-06-06	SKB (2006c)	
Forsmark	TR-05-16	SKB (2005)	
EBS Evolution in General			
Integrated model	R-04-36	Hedin (2004)	Published before SR-Can. It is not clear exactly how far it is used in SR-Can, although the temperature evolution model is used.
Hydrological evolution			
Flow and Transport at Forsmark	R-06-98	Hartley et al. (2006a)	Key report for hydrogeology.
Flow and Transport at Laxemar	R-06-99	Hartley et al. (2006b)	" "

Topic	Report	Reference	Comments
Flows in Glacial Conditions	R-06-100	Jacquet and Siegel (2006)	
Water inflows to deposition holes	R-06-102	Svensson (2006b)	Important background document for some calculations
Effects of spalling	R-06-91	Neretnieks (2006a)	Important for some calculations
Buffer & Backfill Resaturation	TR-06-14	Börgesson et al. (2006)	A key report for repository evolution calculations.
Flows for eroded/cemented buffer	TR-06-33	Neretnieks (2006b)	A key report for the eroded buffer scenario.
Chemical Evolution			
Oxygen consumption	R-06-106	Grandia et al. (2006).	
Physical Evolution			
Buffer piping and erosion	R-06-80	Börgesson & Sandéen (2006)	Looks at experimental information - no modelling. Useful background.
EBS properties			
Bentonite properties	TR-06-30	Karnland et al. (2006)	
Buffer physical & chemical stability	R-06-103	Liu and Neretnieks (2006)	A key report for the buffer erosion scenario.
Models and Data			
COMP23 User's Guide	R-04-64	Cliffe and Kelly (2006)	Refers to the standalone version not the Matlab version actually used in SR-Can
COMP23 validity document	R-06-76	Kelly and Cliffe (2006)	This does not include much new material that was not known at the time of SR-97.
FARF31 validity document	R-04-51	Elert et al. (2004)	" "
Matlab version of NF models	R-06-86	Vahlund and Hermansson (2006b)	

Topic	Report	Reference	Comments
Matlab version of far field models	R-04-50	Vahlund and Hermansson (2006a)	Takes FARF31 and adds colloids. The SR-Can main report states that this covers the Matlab version of COMP23, but this is not the case.
Releases from Fuel	TR-04-19	Werme et al. (2004)	
Solubility Limits	TR-06-32	Duro et al. (2006)	

2.2 Summary of the SR-Can Calculations

The most important sections of the main SR-Can report (SKB, 2006a) in the present context are:

▲ Section 9, which describes the anticipated evolution of the repository; and

▲ Section 10, which describes radionuclide transport calculations.

The Assessment Model Flowcharts (AMFs) described in Section 6.5 and Table 6.7 of that report are also useful in documenting the calculations that SKB has undertaken.

Particular calculations for 'short term' repository evolution include:

1. Groundwater flow in the open repository in SR-Can Section 9.2.3, where the problem of high drawdown at Laxemar should be noted.

2. Groundwater flow in the saturated repository in SR-Can Section 9.3.6, where the way that the transition from 'open' to saturated' conditions is dealt with is not totally clear.

3. Near-field temperature calculations in SR-Can Section 9.3.4.

4. Buffer resaturation in SR-Can Section 9.3.8.

The long-term evolution of the repository depends upon assumptions about climate change. In SR-Can Section 9.4 a reference glacial cycle is described with glacial conditions occurring around 60,000 and 90,000 years after repository closure. Key calculations include:

1. Effects on the buffer of glacial conditions, including colloid release, in SR-Can Section 9.4.8.

2. Canister corrosion rates, particularly with a partially eroded buffer, in SR-Can Section 9.4.9.

SR-Can Sections 11 and 12 use the calculations undertaken to provide risk estimates that can be compared with regulatory criteria.

2.3 General Methodology

SKB's methodology is described in SR-Can Section 2. Some of the issues that this section raises for the present report include:

- The description of the handling of uncertainties in SR-Can Section 2.7 is clear, but independent calculations can be used to investigate whether all uncertainties have been addressed adequately.

- The discussion in SR-Can Section 2.9.2 on handling risk dilution is also clearly presented, in particular the issue of not averaging over different futures with different temperate periods (when the doses are incurred) and the use of 'peak of mean' versus 'mean of peak'.

- In SR-Can Section 2.9.2 it is stated that pessimistic simplifications should be avoided. This is important to avoid bias in comparisons between sites. It is not also straightforward, however, to determine whether a simplification consistently results in pessimistic calculations of impacts.

- Table 10-8 (SR-Can Section 10.5) gives details of how uncertainty and spatial variability have been handled in the pinhole failure calculations. The sensitivity of calculations to the assumed parameter PDFs is one of the issues that can be addressed in independent calculations.

- A discussion of alternative indicators is given in SR-Can Section 2.9.3. This is important for the long-term Ra concentrations in the buffer erosion scenario, but these indicators have not been considered in detail in this report.

2.4 Repository Evolution

2.4.1 General Issues

It is stated that the effects of phased operation are assessed qualitatively in SR-Can Section 9.2.6. This is relevant to short term EBS evolution issues.

2.4.2 The Thermal Phase

The 100°C criterion is now stated in SR-Can Section 7.3.2 to be required in order to limit chemical alterations to the buffer, and reference is made to Section 2.5.9 of the Buffer and Backfill Process Report (SKB, 2006g). Quintessa's understanding is that previously the temperature limit was specified to avoid the deposition of salts on the canister, which appears no longer to be a concern, but now the criterion relates to the need to avoid alteration of the buffer, as limited thermodynamic data are available over 100°C. The calculation of the canister separation distances based on thermal evolution calculations is an important part of the assessment. It appears that some canisters will be very close to the 100°C limit.

It is stated (page 98, SR-Can Section 4.3.2) that the data for thermal property parameters (including uncertainties and variabilities) given in the data report (SKB, 2006b) are well understood because of the direct link to mineralogy. The importance of the heterogeneity in thermal properties needs to be assessed.

SR-Can Section 9.3.6 refers to the importance of thermal effects on groundwater flows once the repository has resaturated, reducing travel times to the biosphere, but little quantitative information is given. It is stated that the thermal phase only lasts for about 1000 y, during which time no radionuclides are released. It is clearly stated that thermal effects on the resaturation phase have not been considered in SR-Can.

2.4.3 Repository Resaturation

Mass balance calculations for oxygen consumption are undertaken in SR-Can Section 9.2.5. These are important for the initial post-closure evolution of the repository.

The resaturation of the repository is discussed in SR-Can Section 9.3.6. It is stated that this should be evaluated using two-phase flow, but a simpler approach has been used to mimic the results in Börgesson et al (2006). The claimed resaturation times are short: in SR-Can Section 9.3.8 it is stated that the resaturation time for the buffer at Laxemar is only 10 years. However, it is stated that if the hydraulic conductivity of the rock is less than 1E-14 m/s, the buffer will not resaturate for a very long time. This begs the question as to whether this is the case for a significant number of deposition holes (particularly at Forsmark).

At the top of p243 it is stated that resaturation modelling methodology is 'still on-going'. Calculation of the resaturation of the repository is an important part of the representation of the EBS evolution, and it is therefore important to undertake independent calculations in this area.

2.5 Canister Failure Modes

SKB consider four failure modes, where a damaged canister can fail and lead to release of radionuclides; these are discussed in Chapter 10 of the main SR-Can report.

The modes are:

- Initial growing pinhole, where a small penetrating defect ultimately grows into a major canister breach;

- Advection/corrosion failure, where an eroded buffer exposes a canister to advection of corrodants and hence to enhanced corrosion rates and ultimately to canister failure;

- Shear movement failure, arising as a consequence of faulting associated with a large earthquake and leading to a loss of canister integrity; and

- Isostatic load failure, where the increased glacial load causes a canister to fail.

In order to analyse the consequences of each of these failure modes, SKB have made various assumptions about the way that the canister damage evolves.

2.5.1 Initial Growing Pinhole

The initial growing pinhole is discussed in Section 10.5 of the main SR-Can report. The analysis does not feed into the reference scenario as it is believed that such initial defects can be ruled out because of the checks made on canisters before emplacement.

Nevertheless, a detailed discussion is presented on the way in which the initial damage will evolve. The SR-Can Data Report, Section 4.4, describes the various processes that eventually cause the damaged region to grow. The key parameter is t_{large}, the time after which a large part of the canister is damaged and no transport resistance is offered. The key processes in determining this time relate to the corrosion of the iron insert. The role of gas, conversion of iron into magnetite, and the consequent filling of the gap between the copper and iron are all complex. SKB note that the sensitivity of the PA calculations to the exact value of t_{large} is small, and conclude that the effort required to further reduce uncertainty is not merited.

In Section 4.4.7 of the SR-Can Data Report it is stated that the large failure may occur at any time between 1,000 and 100,000 years and that 'a uniform distribution of this additional time required for a large failure to develop is therefore assumed'. The 1,000 year start relates to the initial delay in establishing a water conducting path through the copper.

However, in Table 4-2 on the same page, the uniform distribution has become a triangular distribution, T(0, 10^5, 10^5) years. This implies that the most likely time is the longest and that, for example, only a 1% probability of the large failure occurring before 10^4 years, compared to 10% if a uniform distribution had been used. The triangular distribution is quoted in the main report and is presumably what was used in the assessment. In this case it seems that the impact of the discrepancy is small in terms of overall consequences, but it does suggest that improvements are needed in the

procedures for ensuring that the uncertainty distributions used are what the experts recommend.

2.5.2 Advection/Corrosion Failure

The advection/corrosion failure is discussed in Section 10.6 of the main report. This is associated with a loss of buffer material during a glacial melting phase leading to direct exposure of the copper canister to advecting groundwater. This is potentially the most important failure mode. SKB assume that this only happens in deposition holes with high flow rates.

SR-Can Section 9.3.11 discusses bentonite colloid formation and explains why the Ca content of groundwater is important in terms of the critical coagulation coefficient (CCC). Buffer erosion in glacial conditions is then discussed in Section 9.4.8. The 'back of the envelope' calculation for buffer loss is given in Appendix B. The SKB calculations are based on the assumption that corrosion is uniform and occurs across a significant area of the canister (35 cm high over half its circumference), meaning that when penetration occurs a large amount of damage must be assumed in the copper shell.

It is stated (Section 10.6.2) that 'the time required to penetrate the cast iron insert is assumed to be triangularly distributed between 1,000 and 100,000 years, based on the same reasoning for the large failure to occur in the pinhole case…'. The Data Report Section 4.4 is referenced for more elaboration. The basis for this appears weak. The discussion on what leads to the failure for the pinhole case is in a very different context. A small pinhole in an otherwise intact canister in intact bentonite clearly offers substantially more resistance to the ingress of corrodants than a large corroded region of copper with no bentonite subject to advection in the groundwater.

A more plausible description of the evolving canister needs to be developed for this scenario.

In a similar way to the pinhole failure mode, SKB indicate that that actual failure time does not strongly influence the consequences. This is because the doses received are dominated by the ingrowth of daughters in the canister. These persist for a long time due to the immobility of the uranium isotopes. The other contributor to the dose is the instant release fraction of some nuclides, which is also largely unaffected by the time that failure occurs. This suggests that an improved understanding of the evolving canister may not lead to a significant change in the calculated consequences.

2.5.3 Shear Movement Failure

The failure of a canister due to faulting is stated to be unlikely. SKB have therefore taken a simple approach to calculating the consequences. No transport resistance is assumed for the canister after the shear, but the buffer is assumed to be intact with a reduced thickness.

The resistance of the fracture due to transport is neglected as it is assumed that the shearing will increase its transmissivity.

It appears, however, that the buffer-fracture interface resistance on the buffer side is still included. Given that this would be completely reconfigured during shearing, a justification for this assumption should be provided.

2.5.4 Isostatic Load Failure

For the isostatic loading case, it is assumed that the full glacial overburden is transmitted to the canister and that this fails. This failure is assumed to remove the transport resistance from the canister, but the buffer and geosphere are intact.

It appears that the consequences are calculated for the normal flow regime. Only a very brief description is given in the main SR-Can report, presented as a 'what if' calculation since it is thought to have a negligible probability of occurring.

2.6 Hydrogeological Modelling

In SR-Can Section 9.3.6 a summary is given of the detailed hydrogeological calculations that have been undertaken for temperate conditions, with full details being given in Hartley et al. (2006a, 2006b). For Forsmark, both continuous porous medium (CPM) and discrete fracture network (DFN) calculations have been undertaken, the latter for both semi-correlated and fully-correlated fracture length-transmissivity relationships. Only the semi-correlated DFN model has been used at Laxemar. For glacial conditions (SR-Can Section 9.4.6) the key reference appears to be Jaquet and Siegel (2006).

These calculations require detailed assessment, but this is outside the scope of the present report. It is important that independent DFN calculations are undertaken, and the consequences of these compared with SKB's calculations.

2.7 Radionuclide Transport

Reference is made on p384 of the main report to a supporting 'radionuclide transport report'. This would appear to be an error as there does not appear to be such a document.

2.7.1 Near-Field Calculations: COMP23

The basic models appear essentially unchanged since SR-97, but there are some detailed differences, which are discussed in Section 5.1.2. The Matlab implementation of the COMP23 code is described in Vahlund and Hermansson (2006b).

The COMP23 User Guide (Cliffe and Kelly, 2006) discusses fuel/U dissolution, and states that the model with alpha radiolysis has been changed.

2.7.2 Far-Field Calculations: FARF31

The basic models appear essentially unchanged since SR-97. For SR-Can, SKB are sticking to their 1D transport modelling, but reference is made on p402 to the new time-dependent model PORSS which will be used later in parallel with the 1D modelling.

It is stated on p401 that the code has been modified to take t_w and F as input parameters, as these come from DFN calculations.

Colloids are modelled in a modified version of the code in Vahlund and Hermansson (2006a), but this is only considered to be important in glacial conditions (p402), and then geosphere retention is neglected, so the new models are not used.

It is admitted (p402) that the variation of properties in space and time limit the validity of the model calculations and reference is made to the use of the new time-dependent model PORSS for SR-Site.

2.7.3 Probabilistic Calculations

In SR-Can Section 10.4.4 it is stated that analytical methods have been extensively used in PA calculations (to speed up probabilistic runs), but more detailed quality assurance procedures are required. This echoes the concerns that Quintessa staff have previously expressed as to whether the approximations used will be valid across the whole range of parameter values used in probabilistic calculations.

Triangular distributions are widely used for parameter PDFs; this can give big differences between the mode (used in deterministic calculations) and the mean for very skew triangles and so it would be useful to check how important this is in the SKB calculations, although in Section 10.5.10 of the main SR-Can report SKB state that their calculations are not particularly sensitive to the choice of the shape of the parameter PDFs.

3 Checking SKB Calculations

In this section some of the SKB calculations that are considered, on the basis of the discussion in Section 2, to be important for SKB's performance assessment are discussed and checked.

3.1 The Oxygen Consumption Mass Balance

This calculation is given in SR-Can Section 9.2.5, with supporting information in Section 3.5.4 of the Fuel and Canister Process Report (SKB, 2006f). This calculation is important as it affects the early evolution of the Engineered Barrier System.

SKB state that the total available oxygen for early corrosion is 560 moles per canister and that this equates to a potential for the uniform corrosion of 840 μm of copper. This is intended to be a bounding calculation, since in reality most of the oxygen will be consumed in other reactions (with the backfill, buffer and microbially). The figures here are not supported by any details, but it is easy to verify their plausibility and they appear to be correct.

The assumptions behind these calculations need to be better explained and justified.

The assumption of uniform corrosion is important. It is assumed that the oxygen available is shared uniformly between all the canister surfaces in a sealed tunnel section. It is not clear that all the canisters would have equal access to available oxygen and that corrosion would be uniform. The Fuel and Canister Process Report (SKB, 2006f) rules out pitting corrosion but suggests that general corrosion rates may vary by a factor of two across the surface. The question of whether some parts of the surface would be more vulnerable because of their proximity to the tunnel (e.g. the lid) is not addressed.

There are ongoing experiments at Äspö to look at oxygen consumption. Preliminary results are discussed in SKB (2006f) but the claim that these demonstrate rapid oxygen consumption is not clearly explained.

A further complication is that there is a period during which the canisters will have been placed in the deposition holes but the tunnel remains open. During this phase there is an ample supply of oxygen. There appears to be no discussion of the potential for canister corrosion during this phase.

Overall the SKB calculations appear reasonable, but some of the assumptions employed (uniform corrosion and the neglect of corrosion during the operational period) appear questionable.

3.2 Spalling

Spalling is a process that was not considered in the SR-97 calculations and which is potentially significant in determining the release of radionuclides to the geosphere. The effects of spalling on Q_{eq} (the equivalent flow rate at the buffer/fracture interface, which is discussed in Appendix A) is discussed in Neretnieks (2006a) and summarised in SR-Can Section 9.3.6. SR-Can Section 13.8.5 discusses feedback to the RD&D programme.

The treatment of spalling in SR-Can is clearly provisional. There are no data to support the assumptions that need to be made about the properties of the region damaged by spalling. Neretnieks (2006a) sets out a 'worst case' analysis where it is assumed that the damaged region is highly conductive and porous. This leads to significant increases in the Q_{eq} values compared to the undamaged case (Figure 9-36 and 9-37 of the main SR-Can report) – up to values which imply that the buffer resistance becomes more significant. This analysis appears to be sensible in the current context.

The formulae given in Neretnieks (2006a) do not give an explicit relationship between the various velocities and flow rates. The Data Report (SKB, 2006b) does give a relationship, and refers (page 159) to Neretnieks for the capture area – but this term is not discussed in the Neretnieks report. The value given (12.8 m^2) appears to be the product of the capture widths for the vertical and horizontal cases – it is not clear why this product is relevant (the report on hydrogeology, Hartley et al. (2006a), quotes a capture area of 12.8 m^2 in Appendix E.1 but gives a different relationship between the Darcy velocity and the flow rate used in the spalling calculations).

The example given by Neretnieks (Section 4.1 of that report) does not seem to be correctly calculated. There appears to be a factor of 10 wrong somewhere (the values stated for RatioW and RatioL are higher by a factor $\sqrt{10}$ than is given by (11a) and (11b) with the values stated in Table 4-1).

There is a clear need for experimental support for the effects of spalling – particularly if SKB wish to demonstrate that the effect is less significant than currently estimated.

Neretnieks (2006a) gives some reasons for believing that the approach is pessimistic (in particular the conductivity and porosity of the damaged zone), but this relies on a conceptual understanding of this zone and how it interacts with the buffer. Although it is tempting to believe that the swelling buffer prevents the spalling zone from being highly conductive, this relies on the timing of various processes. If the spalling damage occurs before the buffer is saturated then the rock could move into the gap – this would probably not be reversed by the swelling.

Overall the approach taken by SKB appears reasonable, but the documentation of the calculations is not totally transparent, and it is clear that the whole analysis remains preliminary.

3.3 Corrosion and Canister Failure

The corrosion calculations at the start of SR-Can Appendix B are important for the overall case that is being made by SKB. These calculations use the equivalent flow rate concept discussed in Quintessa's report on interface resistances (Maul and Robinson, 2005b) and are summarised here in Appendix A. The reference to 'Liu (2006)' in the SR-Can report is assumed to be to Liu and Neretnieks (2006).

The distribution of failure times for canisters in the eroded buffer failure mode is important for the overall contribution of that failure mode to calculated risks. Information on the calculated distributions is shown in Figure 9-103 and Table 9-22 of the main SR-Can report.

3.3.1 Intact Buffer

The formula given in SR-Can Appendix B for the corrosion rate e (m y^{-1}) for an intact buffer appears to be correct. This can be expressed as:

$$e = [HS^-] Q_{eq} \frac{F f M_{Cu}}{2\pi r_{can} h_{can} \rho_{Cu}} \qquad 3.1$$

where:

$[HS^-]$ is the concentration of sulphide ions in groundwater (mol m^{-3}).

Q_{eq} is the equivalent flow rate (m^3 y^{-1}).

F is the buffer concentration factor representing the ratio between concentrations nearest the fracture and the average over the canister surface. This was assigned a value of 7 by SKB.

f is a stoichiometric factor equal to 2.

r_{can} is the canister radius (0.525 m) and h_{can} is the canister height (5 m).

M_{Cu} is the molar mass of copper (0.06355 kg mole^{-1}) and ρ_{Cu} is the density of copper (8920 kg m^{-3})

No buffer resistance is included. It is stated that this adds little, but this is not true with spalling – then the buffer resistance can be the limiting effect. Thus the calculated corrosion rates will tend to be overstated. This formula has been used to produce Figure 9-62. A sulphide concentration of 1E-5 kmole m^{-3} has been used. All of the other parameters are fixed, so the only variation from hole to hole is due to Q_{eq}. This gives a corrosion rate (in m y^{-1}) of 6.1E-8 times Q_{eq} (in m^3 y^{-1}). Figure 9-62 presents the results as mm y^{-1}, so the relevant factor is 6.1E-5. The distribution of Q_{eq} with spalling is shown in Figure 9-36.

Comparison of Figure 9-36 and 9-62 shows that there is something not fully explained. The CPM result has a factor of approximately 1E-4, whereas the DFN results have a factor of about 2E-5. Thus, neither seems to agree with the Appendix formula and they are not internally consistent. These discrepancies will not change the conclusion that corrosion in the intact case is slow, but demonstrates that the presented results are not quite as described.

An attempt was made to reproduce the distribution for Q_{eq} for Forsmark in the file supplied by Hedin (2007b), but this proved not to be possible with the information given in the SR-Can documentation. This is important for the calculation of doses, and requires further investigation.

3.3.2 Eroded Buffer

The rate of buffer erosion E (kg y^{-1}) is given in Appendix B of the SR-Can report as:

$$E = C_{\max} Q_{eq}, \qquad 3.2$$

where C_{max} is the maximum concentration of bentonite in water, taken to be 50 kg m^{-3}.

The eroded buffer case uses the results from Neretnieks (2006b). In practice, all flows are in the "low flow" category, so that the equivalent flow rate is equal to the total flow rate through the deposition hole.

The formula given in SR-Can Appendix B is based on the corrosion of an area of canister given by

$$A = \pi h_{zone} r_{can}, \quad 3.3$$

where h_{zone} was assigned a value of 0.35 m. The rate of corrosion is then obtained from a modified version of equation 3.1:

$$E = [HS^-] Q_{eq} \frac{f M_{Cu}}{A \rho_{Cu}} \quad 3.4$$

This formula has been used to produce figures 9-102 and 9-103. With a sulphide concentration of 1E-5 kmole m^{-3}, the corrosion rate (in m y^{-1}) is 2.5E-7 times the flow (in m^3 y^{-1}). Figure 9-102 presents the corrosion rate in mm y^{-1}, so the relevant factor is 2.5E-4.

To check figure 9-102 we need the distribution of flows at the deposition hole. This information is not provided in the SR-Can reports. The file provided by Hedin (2007b) gives Darcy velocities. Thus we need an area to get flow rates. We focus on the Forsmark base case. If we take 12.8 m^2 as the area then the 90th percentile of the flow rates is about 2E-3 m^3 y^{-1}, which should give a corrosion rate of 5E-7 mm y^{-1}. Figure 9-102 shows the 90th percentile as about 3E-7 mm y^{-1} so this is reasonably similar. The discrepancy may be due to the actual area used not being 12.8 m^2.

It should be noted that in Figure 9-102 the fully- and semi-correlated DFN lines cross. In Figure 9-36 they do not. This suggests that the Q_{eq} for spalling and the corrosion rate given in SR-Can Appendix B of the SKB report are not both simply functions of Darcy velocity – hence our inability to match them.

Overall, it is very hard to verify these calculations because the way they are documented is not completely clear. Moreover, important parts of the PA inputs (e.g. the distribution of flow rates) are not presented. Calculating the flow rates has proved difficult as the relevant area used is not clear (and probably depends on details of the intersected fracture which are not given). It has therefore not been possible to reproduce the distribution of failure times for canisters in the eroded buffer failure mode which is important for the overall safety case.

3.4 The Gas Pathway

In SR-Can Section 10.9 some simple calculations are undertaken to assess the significance of the radionuclide transport in gas. This pathway is considered to be much less important than the groundwater pathway considered in SR-Can Section 5.

SKB's assessment of the radiological consequences of this pathway appears reasonable. SKB assume that once gas production falls to levels below which the gas can dissolve,

then the buffer will close. This assumption is important since if the buffer does not close, gas production could provide a process for producing an advective pathway through the buffer.

4 QPAC-EBS Repository Evolution Calculations

The calculations described in this Section aim to investigate key issues for repository evolution. Some of the calculations were undertaken with a development version of QPAC-EBS before the finalisation of version 1.0 of the code (Maul et al., 2007). QPAC-EBS is based on Quintessa's multiphysics compartmental modelling code QPAC.

4.1 Thermal Evolution

Although thermal evolution calculations are the most straightforward to undertake, the separation of the canisters is critical for these calculations, and the SR-Can calculations suggest that some canisters may come close to the imposed 100°C maximum temperature criterion.

It is stated that the analytical model described in Hedin (2004) (report R-04-36) is used, and all data employed in the Quintessa calculations have been taken from that source where possible. Results are given in SR-Can Section 9.3.4 and the same calculations are presented in SKB (2005) and SKB (2006c) (reports TR-05-16 and TR-06-06), but it is not clear if the calculations are given in more detail in other unreferenced supporting documents.

4.1.1 Governing Equations

The governing equation for thermal conduction can be written in the following form:

$$\begin{aligned} \frac{\partial Q_H}{\partial t} &= F_{HC} + P, \\ Q_H &= V\rho cT, \\ F_{HC} &= A\nabla\cdot\left(\Gamma\nabla T\right). \end{aligned} \qquad 4.1$$

Here T (K) is the temperature and ρ (kg m^{-3}), c (J kg^{-1} K^{-1}) and Γ (W m^{-1} K^{-1}) are the density, specific heat capacity and thermal conductivity of the medium respectively in the relevant compartment which has volume V (m^3) and may have a source of heat P (W). The heat flux F_{HC} (W) is determined by the cross-sectional area (A, m^2),

temperature gradients across and thermal conductivities in the donor and receptor compartments.

Radiative heat transfer between surfaces is represented by

$$F_{HR} = \varepsilon\sigma(T_1^4 - T_2^4) \qquad 4.2$$

where ε is the total emissivity (-), σ is Stefan's constant (5.6697 10^{-8} W m^{-2} K^{-4}), and T_1 and T_2 (K) are the temperatures of the two surfaces. The emissivity for the interface is determined from the specified emissivities for the two surfaces involved (ε_1 and ε_2,) as given by Hedin (2004):

$$\varepsilon = \left(\frac{1}{\varepsilon_1} + \frac{1}{\varepsilon_2} - 1 \right)^{-1} \qquad 4.3$$

4.1.2 The Source Term

The source term is taken by Hökmark and Fälth (2003) to be represented by a sum of exponential terms:

$$P = P(0) \sum_{i=1}^{7} a_i \exp(-t / t_i). \qquad 4.4$$

Where t is the time since deposition. The values for the coefficients a_i are given in Table 4.

Table 4: Coefficients used by SKB for Canister Power (38 MWd/kgU burnup)

i	t_i (y)	a_i (30 y old fuel)	a_i (40 y old fuel)
1	20	0.07	0.049
2	50	0.713	0.696
3	200	-0.051	-0.059
4	500	0.231	0.271
5	2 000	0.024	0.027
6	5 000	-0.009	-0.010
7	20 000	0.022	0.026

There remain some uncertainties over the interpretation of the methods used by SKB. Table 9-4 in the SR-Can main report indicates that an initial power of 1700 W was used, but it is not totally clear how equation 4.4 was applied. In the QPAC-EBS calculations

described below, it was assumed that the coefficients for 30 y old fuel were used with a time offset of 4.3831 years in order to obtain a power of 1700 W at t=0.

4.1.3 System Description

The basis of the discretisation employed is shown in Figure 1; the canister (assumed to be for BWR fuel) is surrounded by bentonite compartments and there is a backfill compartment at the top of the deposition hole. For simplicity the backfill characteristics have been taken to be the same as those of the buffer. There can be gaps between the canister and the bentonite and between the buffer and the host rock; these are not shown explicitly in Figure 1. The tunnel above the deposition hole is not represented explicitly (its properties are therefore effectively assumed to be similar to the host rock) and there are several rock compartments surrounding the deposition hole. The Upper Buffer/Backfill and Lower Buffer regions shown in Figure 1 were split up into a number of compartments, using a cylindrical grid.

In the QPAC-EBS calculations the outer boundary condition is determined by assuming that, at large enough distances from the source, the temperature drops off as the inverse square of the distance from the source. This is equivalent to specifying that the temperature falls linearly to ambient levels at a specified distance into a final heat sink compartment. If the volume of all of the compartments inside the sink compartment is V_{total}, then an effective radius, r_{eff}, of an equivalent sphere can be calculated, and the distance into the sink compartment at which the temperature falls to ambient levels is taken to be this distance.

In the present calculations the structure used in Hedin (2004), as illustrated in Figure 2, has been used as the basis for a simplified representation. The canister is taken to have a thickness of 50 mm and 12 fuel boxes, each containing 64 fuel pins, are placed in the cast iron insert. Air gaps which exist between the fuel boxes and between the iron insert and the copper canister are not shown explicitly in the figure. The simplified representation used in the QPAC-EBS calculations maintains the radial symmetry, as illustrated in Figure 3. Again, the air gaps between the different materials are not shown explicitly. The radius of the area containing the fuel box has been chosen so that the total cross-sectional area matches that of the 12 fuel boxes. Relevant dimensions are given in Table 5.

The SR-Can documentation does not give details of how the internal structure of the canister is represented in the vertical plane. In the QPAC-EBS calculations the dimensions given in Table 5 were employed with the same air gaps between the different materials as in the radial plane.

4.1.4 Material Properties

Table 6 gives the material properties used in the QPAC-EBS calculations.

Several properties of bentonite depend on the degree of water saturation; such variations were not considered in the SR-Can calculations.

Figure 1: Regions in the Thermal Evolution Calculations

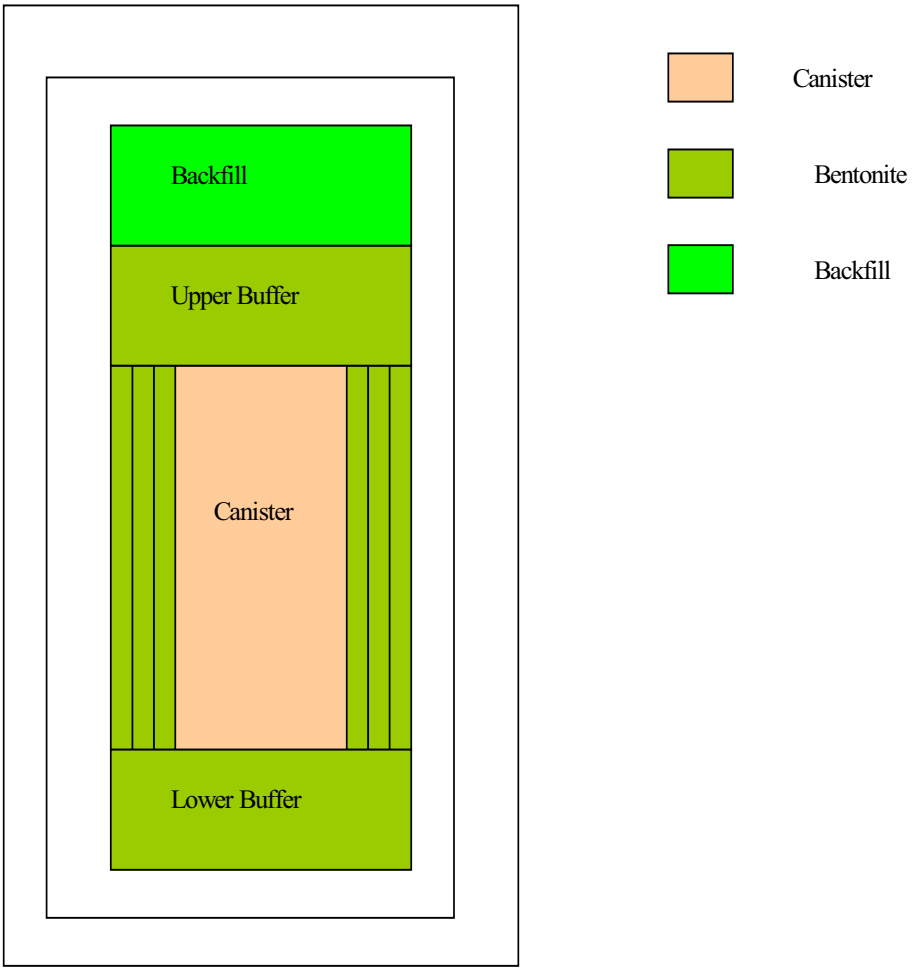

Figure 2: Cross-Section of Internal Structure in a Canister

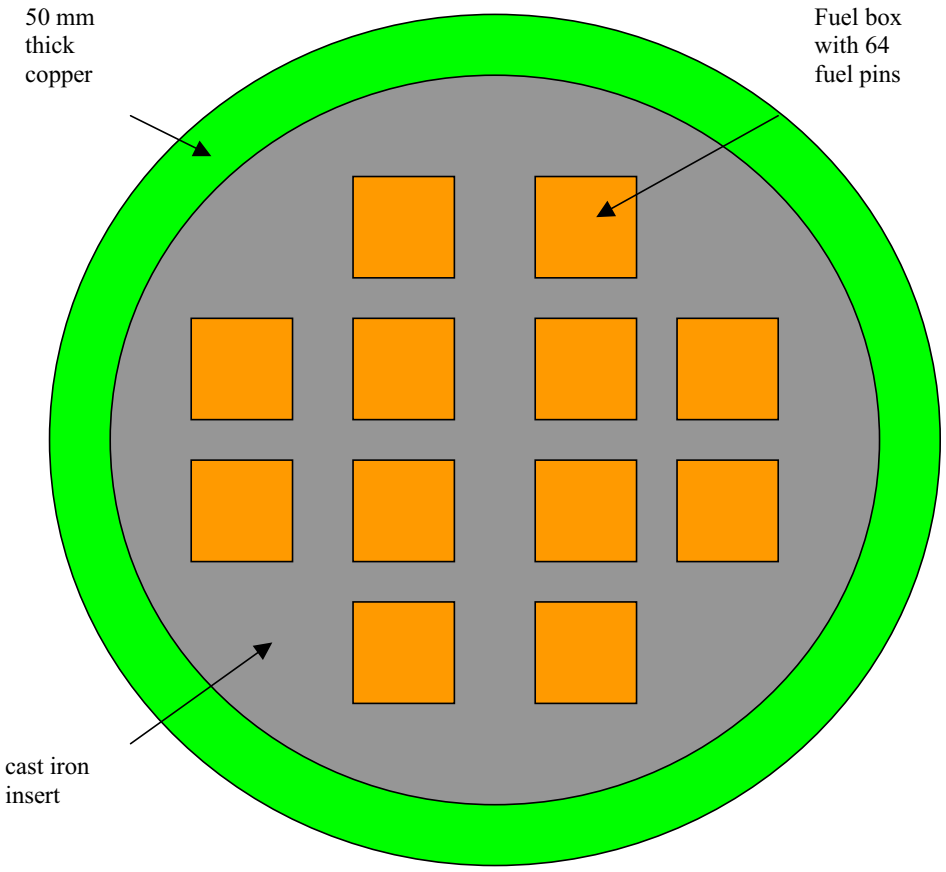

Figure 3: Simplified Radial Geometry for the Canister in QPAC-EBS

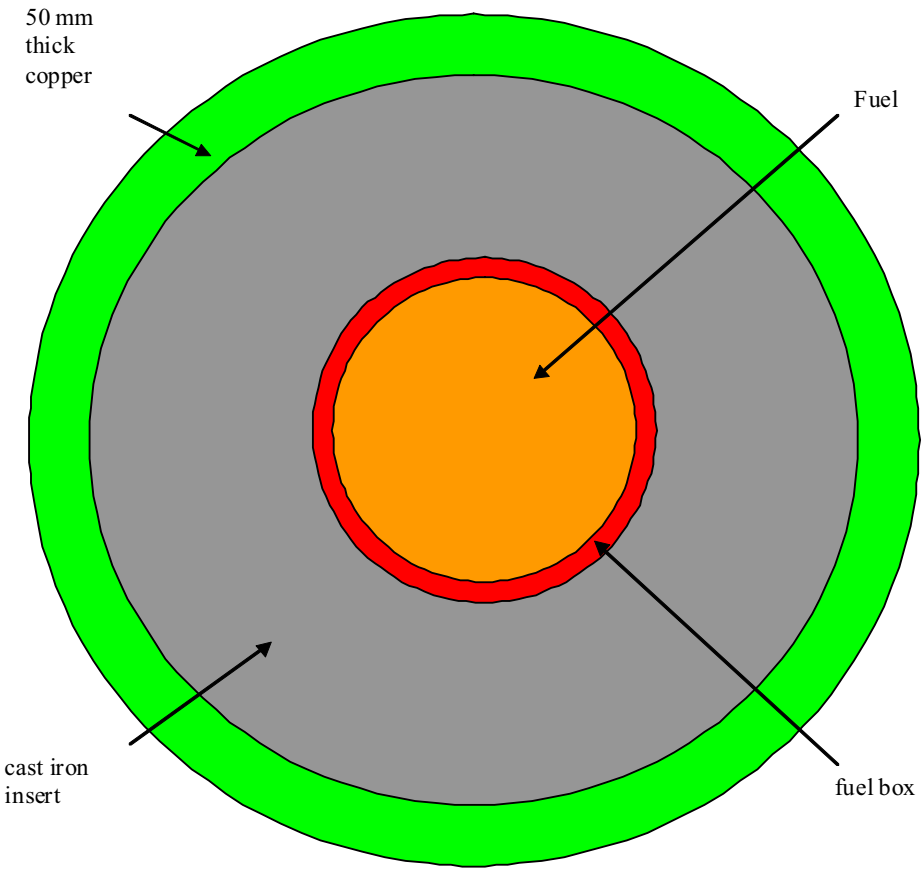

Table 5: System Description Parameters

Parameter	Description	Units	Value used in SKB calculations	Value used in QPAC-EBS calculations	Comment
L_c	Canister length	m	4.83	4.83	
D_c	Canister diameter	m	1.05	1.05	
d_c	Canister thickness	m	0.05	0.05	
L_{box}	Length of fuel box	m	3.68	3.68	
r_{fuel}	Radius of fuel zone	m	-	0.281	Chosen so that cross-sectional area is the same as the 12 square fuel boxes of dimension 0.14 m
r_{box}	Outer radius of fuel box	m	-	$r_{iron\text{-}I} - \delta_{fi}$ 0.289	
δ_{fi}	Width of air gap between fuel box and iron insert	m	0.008	0.008	
$r_{irion\text{-}i}$	Inner radius of cast iron insert	m	-	0.305	Chosen so that cross-sectional area is the same as the 12 square fuel boxes of dimension 0.156 m
$r_{irion\text{-}o}$	Outer radius of cast iron insert	m	-	$r_{can\text{-}I} - \delta_{ic}$ 0.474	
δ_{ic}	Width of air gap between iron insert and canister	m	0.001	0.001	
$r_{can\text{-}i}$	Inner radius of copper canister	m	0.475	0.475	
$r_{can\text{-}o}$	Outer radius of cast iron insert	m	$D_c/2$ 0.525	0.525	Canister thickness is 50 mm

Parameter	Description	Units	Value used in SKB calculations	Value used in QPAC-EBS calculations	Comment
δ_{cb}	Width of air gap between canister and bentonite	m	0.005	0.005	
d_b	Buffer thickness	m	0.35	0.35	
L_{lb}	Buffer thickness below can	m	0.5	0.5	
L_{ub}	Buffer thickness above can	m	1.5	1.5	
L_f	Thickness of backfill at top of deposition hole	m	0.5	0.5	Taken to have the same characteristics as the buffer
δ_{br}	Width of gap between bentonite and rock	m	0.03	0.03	The gap is assumed to be filled with air.
N_c	Number of canisters per tunnel	-	160	159	An odd number of canisters is used in the calculation of background temperatures
M_t	Number of tunnels	-	?	25	This number is not given in Table 9-4 of the main SR-Can report
r_c	Canister separation in a tunnel	m	6	6	Value used for Forsmark. Table 9-4 of the main SR-Can report refers to a value of 7.2 m for Laxemar.
R_t	Distance between tunnels	m	40	40	
T_r	Temperature at repository depth	K	284	284	Value is for Forsmark. Table 9-4 of the main SR-Can report refers to a value of 286.8 K for Laxemar. Hedin (2004) used 12°C.
z_r	Repository depth	m	400	400	Table 9-4 of the main SR-Can report refers to a value of 500 m for Laxemar.

Table 6: Material Property Parameter Values

Parameter	Description	Units	Value used in SKB calculations	Value used in QPAC-EBS calculations	Comment
Γ	Thermal Conductivity - can	W m^{-1} K^{-1}	390?	401	Taken from CRC (Lide and Kehiaian, 1994).
	Thermal Conductivity - fuel box		?	5.0	Calculated as a weighted average of the values for steel, uranium oxide and air.
	Thermal Conductivity - iron		?	80.2	Taken from CRC (Lide and Kehiaian, 1994).
	Thermal Conductivity - air		0.03	0.03	
	Thermal Conductivity - buffer		1.1	1.1	The conductivity of the buffer will actually vary with the degree of saturation.
	Thermal Conductivity - rock		3.34	3.34	The SKB value is for Forsmark. Table 9-4 of the main SR-Can report refers to a value of 2.27 W m^{-1} K^{-1} for Laxemar.
ε	Emissivity- canister inner surface	-	0.03	0.03	
	Emissivity- canister outer surface		0.1	0.1	
	Emissivity- cast iron inner surface		0.3	0.3	
	Emissivity- cast iron outer surface		0.24	0.24	
	Emissivity- fuel box		0.4	0.4	
	Emissivity- bentonite		0.88	0.88	Same value taken for inner and outer surface
	Emissivity- rock		?	0.88	

Parameter	Description	Units	Value used in SKB calculations	Value used in QPAC-EBS calculations	Comment
ρc	Heat Capacity - can	MJ m^{-3} K^{-1}	?	3.44	Taken from CRC (Lide and Kehiaian, 1994) .
	Heat Capacity - fuel box		?	2.32	Calculated as a weighted average of the values for steel, uranium oxide and air.
	Heat Capacity - iron		?	3.23	Taken from CRC (Lide and Kehiaian, 1994).
	Heat Capacity - air		?	7.18E-4	Taken from CRC (Lide and Kehiaian, 1994).
	Heat Capacity - buffer		2.2	2.2	
	Heat Capacity - rock		2.17	2.17	Value used for Forsmark. Table 9-4 of the main SR-Can report refers to a value of 2.24 MJ m^{-3} K^{-1} for Laxemar. Hedin (2004) used 2.08 MJ m^{-3} K^{-1}.

4.1.5 Background Temperatures

To consider the 'background' temperature rise due to neighbouring canisters the non-equilibrium case needs to be considered. An instantaneous point source can be approximated by a uniform temperature in a sphere of radius *R(t)* (m). In order to get back to the equilibrium solution at long times we require that:

$$R^2 = 6\,a\,(t - t'), \tag{4.5}$$

where *a* is the thermal diffusivity ($m^2\ s^{-1}$) given by:

$$a = \frac{\Gamma}{\rho\, c}, \tag{4.6}$$

and t' (s) is the time of the instantaneous point source.

To see this consider:

$$T(r,t) = \frac{3}{4\pi\rho\, c}\int_0^{t_{\max}} \frac{P(t')\,dt'}{R^3} \qquad t > \frac{r^2}{6a}$$
$$t_{\max} = t - \frac{r^2}{6a} \tag{4.7}$$

For a constant source this is readily evaluated to give

$$T(r,t) = \frac{P}{4\pi\,\Gamma r}\left\{1 - \frac{r}{\sqrt{6at}}\right\}, \tag{4.8}$$

which approaches the equilibrium value at long times.

If *P* is varying it is not straightforward to provide a good estimate of the resulting temperature rise. One approach is to use the values of *P* at the ends of the integral to give:

$$T(r,t) \cong \frac{1}{4\pi\,\Gamma r}\left\{P(t - \frac{r^2}{6a}) - \frac{P(0)\,r}{\sqrt{6at}}\right\} \tag{4.9}$$

Another approach is to use a weighted average of *P* to give:

$$T(r,t) \cong \frac{1}{4\pi \Gamma r}\left\{1-\frac{r}{\sqrt{6at}}\right\}\left\{\frac{t^{3/2}P(t-\frac{r^2}{6a})+(t-\frac{r^2}{6a})^{3/2}P(0)}{t^{3/2}+(t-\frac{r^2}{6a})^{3/2}}\right\} \qquad 4.10$$

The background temperature rise at a centrally-placed canister can be calculated from:

$$T_{background}(t) \cong T_r + \sum_{m=-M}^{M}\sum_{n=-N}^{N} T(r_{mn},t) \quad r_{mn} \neq 0$$
$$r_{mn} = \sqrt{(n\ r_c)^2 + (m\ r_t)^2} \qquad 4.11$$

Where T_r (K) is the temperature at repository depth, r_c is the separation between deposition holes in a single tunnel, r_t is the separation between tunnels, N_c, the number of canisters in each tunnel is 2N+1, and the number of tunnels, M_t, is 2M+1.

This approach is adequate for timescales of the order of 10 years but a different approach was used in the present calculations to obtain an approximation that is better over longer periods:

$$T(r,t) \cong T_0(r,t) + \frac{1}{4\pi r}\sum_{n=1}^{N}\{P(t_n)-P(t_{n-1})\}\left\{1-\frac{r}{\sqrt{6a(t-t_n)}}\right\} \quad t-t_n-t_{\min}>0$$
$$t_{\min} = \frac{r^2}{6a} \qquad 4.12$$

Here $T_0(r,t)$ is the temperature function for the initial power as a constant source. The evaluation times in the summation were determined from:

$$t_n = \tau n^{5/4}, \qquad 4.13$$

with the timescale τ set to 1 y. The number of terms N is defined as the largest integer value of n for which $t_n < t$. This numerical integration scheme constrains the number of terms in the summation at early times, prevents excessively large values of N at later times and ensures the relative numerical accuracy at early and late times is similar.

At long times the boundary condition at the surface can become important. Hedin (2004) employed negative mirror sources for each canister above the surface to obtain a zero increase in temperature at the surface, and the same approach was taken in the QPAC-EBS calculations, so that equation 4.11 is modified to:

$$T_{background}(t) \cong T_r + \sum_{m=-M}^{M} \sum_{n=-N}^{N} T(r_{mn}, t) - T(R_{mn}, t) \quad r_{mn} \neq 0$$
$$r_{mn} = \sqrt{\left(n\ r_c\right)^2 + \left(m\ r_t\right)^2} \qquad 4.14$$
$$R_{mn} = \sqrt{\left(n\ r_c\right)^2 + \left(m\ r_t\right)^2 + 2z_r^2}$$

4.1.6 Calculations for Forsmark

The background temperature calculated is uncertain because the way that the repository layout has been represented in SKB's thermal evolution calculations is not clear. An effective number of deposition tunnels of 25 has been used, but the actual repository layout, as described by Brantberger et al. (2006) is more complex; Table 5-2 of that report actually shows 190 deposition tunnels, with 11% of the deposition holes assumed not be used.

Figure 4 shows the calculations for Forsmark without inclusion of the 'background' contribution from other canisters. This can be compared for early times with the SKB calculations in Figure 9-17 of the main SR-Can report, and this is done in Table 7. The SR-Can calculations represent a faster transfer of heat away from the canister. In the QPAC-EBS calculations it can be seen that the thermal gradients take time to establish themselves, but the SR-Can calculations do not show this as constant thermal gradients are maintained from 0.01 years. It is understood that the SR-Can calculations do not include heat storage in the canister. Re-running the QPAC-EBS calculations with no heat capacity in the canister gives essentially identical results to the SR-Can calculations as shown in the last column of Table 7.

Figure 4: Thermal Calculations for Forsmark without Background Contribution

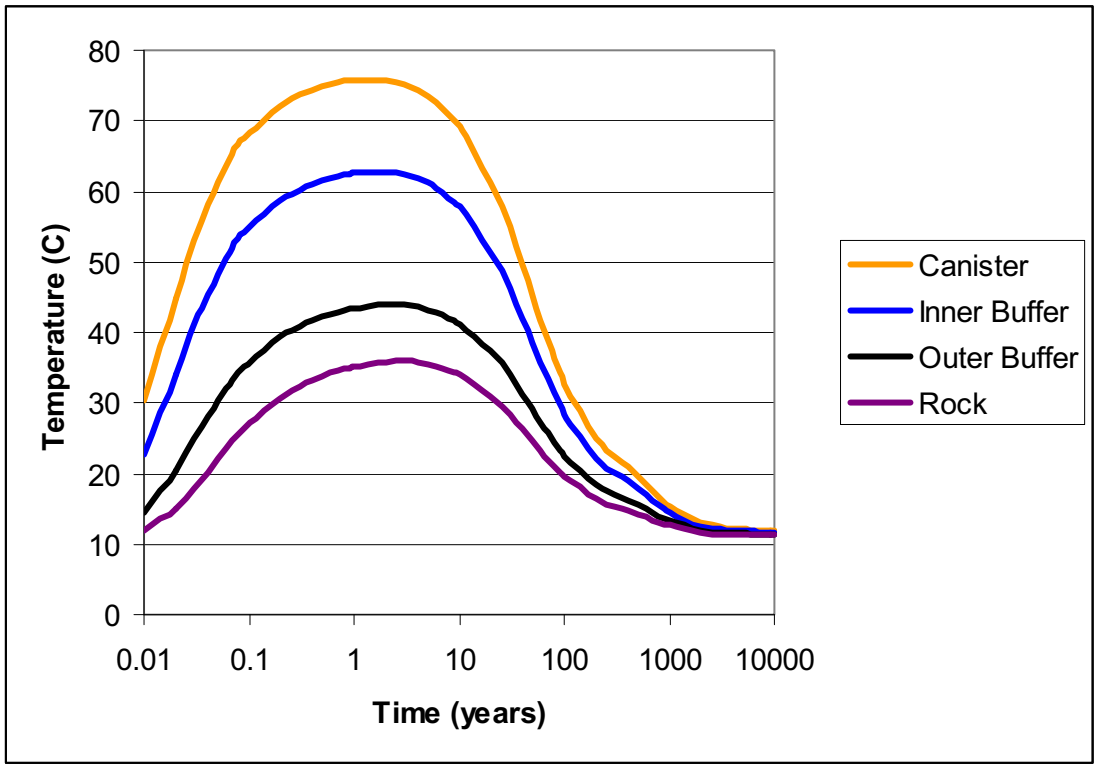

Table 7: Calculations for a Single Canister at 0.1 Years after Deposition

	Temperature (C)		
	SR-Can	QPAC-EBS	QPAC-EBS with no canister heat capacity
Canister	70	74	70
Inner Buffer	57	60	57
Outer Buffer	37	37	37
Rock Wall	29	28	28

Figure 5 gives the results from calculations with the background temperature contribution included and with the heat capacity of the canister omitted and Table 8 gives some comparisons with SKB calculations. The QPAC-EBS calculations give a slightly higher temperature gradient between the canister and the rock, but this is probably due to the relatively coarse discretisation used in the code. The most significant difference derives from the calculation of background temperatures. The

QPAC-EBS calculations give significantly higher background temperatures but, as previously explained, it is not clear what repository layout was actually used by SKB for these calculations.

Figure 5: Thermal Calculations for Forsmark with Background Contribution and No Canister Heat Capacity

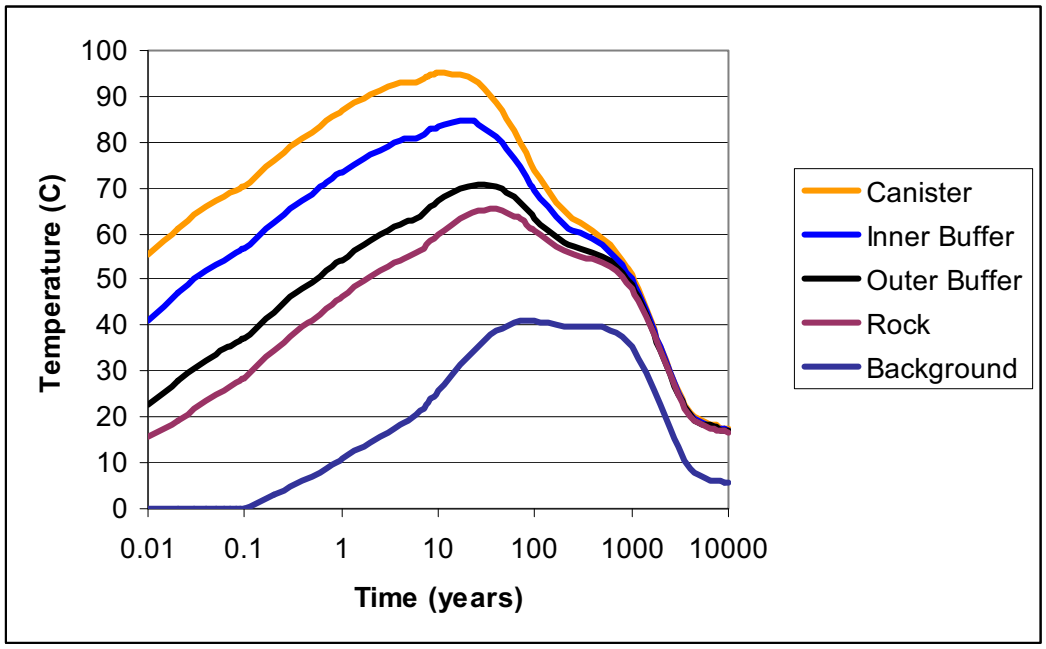

Table 8: Calculations with Background Temperature Contribution

	Temperature (C)					
	t=10 y		t=100 y		t= 1000 y	
	SR-Can	QPAC-EBS	SR-Can	QPAC-EBS	SR-Can	QPAC-EBS
Canister	89	95	66	74	42	51
Inner Buffer	78	84	62	70	41	50
Outer Buffer	62	67	57	64	40	49
Rock Wall	56	60	55	61	39	48

Probabilistic Calculations

Figure 9-18 of the main SR-Can report presents some probabilistic calculations but only one parameter is varied - the rock thermal conductivity. The SKB calculations give a range of about 10°C in the calculated peak temperatures at both the buffer inner surface and the canister outer surface. Additional runs of QPAC-EBS were undertaken

with values of the rock thermal conductivity 3 standard deviations from the mean: 2.68 and 4.00 W m^{-1} K^{-1}. Although the actual magnitudes of the calculated peak temperatures were different because of the uncertainties in the background temperature, the difference between the peak values for these runs was 10°C; totally consistent with the SKB calculations.

4.2 Repository Desaturation and Resaturation

4.2.1 Introduction

Calculations of the desaturation of the open repository can be compared with the results given in SR-Can Tables 9.2 and 9.3. Resaturation calculations for the repository as a whole are given in SR-Can Section 9.3.6 and specifically for the buffer in SR-Can Section 9.3.8. As indicated in SR-Can Section 2.4.3, SKB state that resaturation calculations should be evaluated using two-phase flow, but a simpler approach has been used to mimic the results in Börgesson et al (2006). The claimed resaturation times are short. As indicated by SKI's EBS Review Group (SKI, 2007), further work is required in order to address the consequences of heterogeneous resaturation.

4.2.2 Overview of the Independent Calculations

The primary source of data employed in the calculations is Jaquet and Siegel (2004), R-04-46, where resaturation calculations were undertaken using the ConnectFlow code and simple 2D calculations were presented in an appendix. Some discussion of resaturation times is also presented in Svensson (2006a), along with some simple 2D modelling.

The model geometry is based on the ConnectFlow calculations, consisting of a block of rock 8000 m by 6000 m by 1500 m deep. As shown in Figure 6, the repository is represented as a single 'slab' 20 m thick at 400 m depth (Forsmark conditions) representing the disposal tunnels and bulked associated host-rock. The region was discretised with seven compartments in the X direction, five in the Y direction and five in the Z direction. The repository occupies the central compartment in all three axes.

Figure 6: The Modelled System: Plan (top) and Section (bottom)

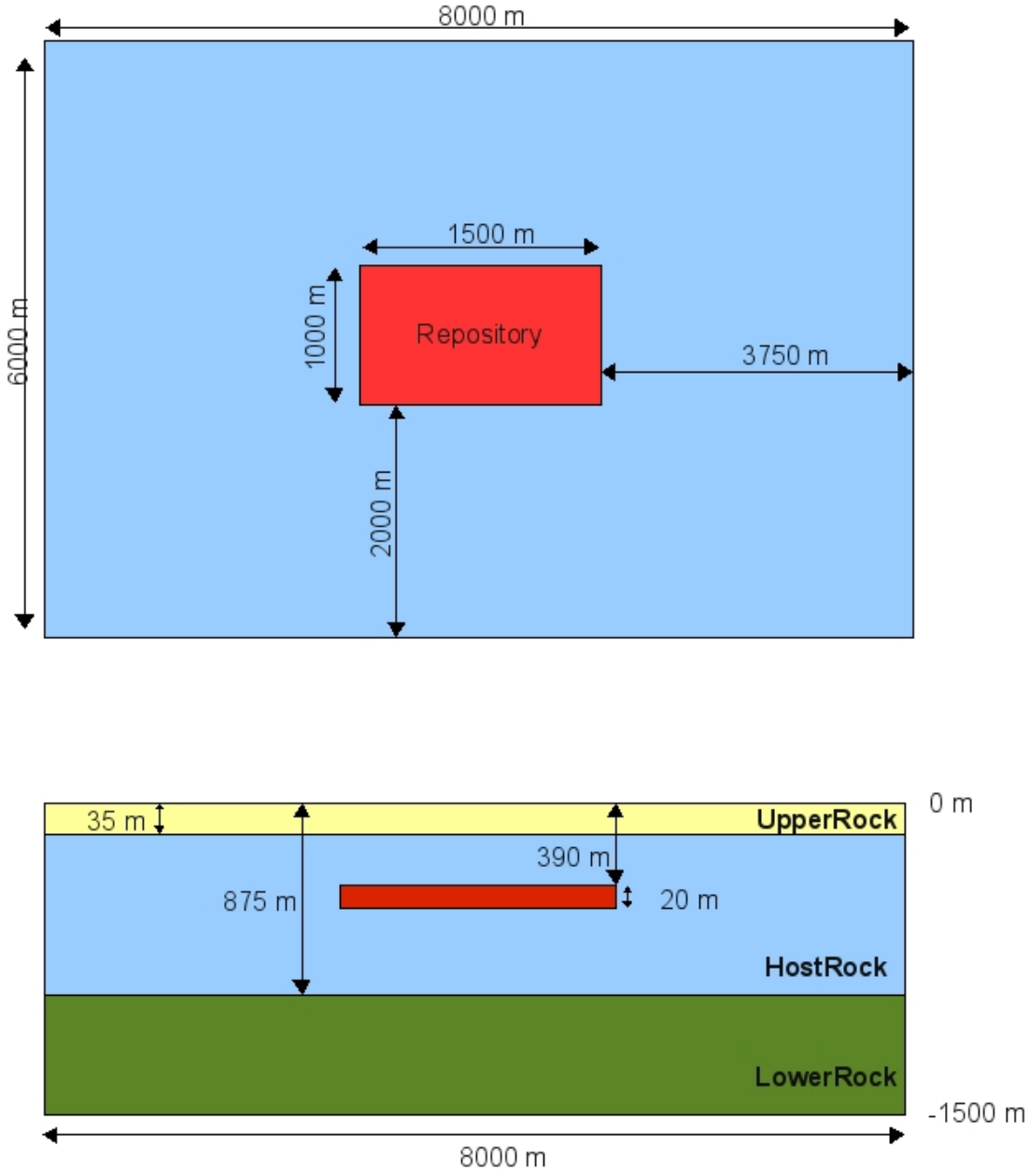

The external boundaries of the model were taken to be hydrostatic columns with atmospheric pressure at 0 m. Different conditions were assumed at the top surface dependent on the calculational case. Following the general approach taken in Jaquet and Siegel (2004), the rock mass was divided into three types: `LowerRock` (-875 m and below), `HostRock` (-875 m to -35 m) and `UpperRock` (-35 m and above). A further material type of `UpperRockUS` was used for the unsaturated zone (0-5 m), although this was not represented in all calculational cases.

It was effectively assumed that the model domain does not take an active part in the near-surface flow zone; hence zero recharge was assumed for all cases at initial conditions (consistent with the general assumptions for 2D modelling employed in Jaquet and Siegel (2004)).

Groundwater was assumed to have a constant density and viscosity. No gas dissolution was represented and air was assumed to behave as a perfect gas.

The relative permeability curves for water were taken from Rutqvist and Tsang (2007), while the relative permeability curves for gas were 'generic' and designed to show only limited retardation of gas permeability with changes in gas permeability. The values used are given in Table 9.

Because of the need to represent the repository in a variety of different states, three 'variant' compartments were used that effectively replace each other in the model according to the time period being represented:

- Variant 0: This is the open working repository where the pressure is fixed at atmospheric pressure and the air saturation is taken to be 0.95 (open tunnels, slightly saturated host rock). This variant is employed for 0-40 years of the simulation.

- Variant 1: This is the post-closure backfilled repository. The initial pressure is atmospheric and the air saturation is taken to be 0.88 (this is less than the saturation for variant 0 because the volume of voids is reduced). This variant is employed for 40-1000 years of the simulation.

- Variant 2: This is the pre-construction state of the rock, fully saturated with the initial pressure being hydrostatic.

Table 9: Relative Permeability Curves

Water		Air	
Saturation	**Permeability**	**Saturation**	**Permeability**
0.0	0.0	0.0	0.0
0.003995	1.321941E-8	0.05	0.00008
0.012166	1.519911E-6	0.10	0.00068
0.034221	4.328761E-5	0.15	0.00233
0.096105	0.000932	0.20	0.00561
0.189809	0.005994	0.25	0.01114
0.295446	0.024201	0.30	0.01961
0.420991	0.073907	0.35	0.03174
0.510656	0.129154	0.40	0.04837
0.624225	0.225701	0.45	0.07042
0.735798	0.359381	0.50	0.09894
0.833423	0.521400	0.55	0.13618
0.917104	0.756463	0.60	0.18065
0.992805	0.830217	0.65	0.23275
1.0	1.0	0.70	0.30752
		0.75	0.39520
		0.80	0.50657
		0.85	0.65562
		0.90	0.95443
		0.95	0.97722
		1.0	1.0

4.2.3 The Main Calculational Cases

The reference calculation had the following features:

- Inflow to the repository was controlled by the backfill, with the permeability of the repository taken to be the same as the backfill.
- The groundwater was assumed to be unconfined, so that a pressure boundary condition at atmospheric pressure was applied with full gas saturation at the top surface (5m).
- Up to 25 mm y^{-1} extra recharge was available, applied as a pressure-dependent source of water in the `UpperRock` region. This represents additional recharge being available as the water is drawn down, and is consistent with the 'best' model in the calculations given in the appendix of Jaquet and Siegel (2004). This was implemented in QPAC-EBS as a transfer (generalised head) condition.

It should be noted that the inclusion of a free surface was apparently not considered in the 3D calculations reported in SR-Can.

A number of additional cases were considered based on the reference case and the details are given in Table 10.

Table 10: Variant Resaturation Calculational Cases

	Case Name	Purpose	Key Changes
1	RefNoUpperInflow	To examine the sensitivity to assumptions about infiltration at the surface	No surface infiltration.
2	RefNoUnsaturatedZone	To examine the impact of the free surface by fixing pressures at the surface	The unsaturated zone was removed and a fixed pressure boundary condition applied.
3	RefAnis	To examine the sensitivity of calculations to vertical anisotropy	Horizontal permeabilities were taken to be a factor of 10 higher than vertical permeabilities for all media.
4	RefAnisNoUpperInflow	To examine the combination of effects from vertical anisotropy and no surface infiltration.	No surface infiltration. Horizontal permeabilities a factor of 10 higher than vertical permeabilities.
5	Ref2D	To examine differences between 3D and 2D flow calculations.	Discretisation in the Y direction removed, with no flow boundary conditions.
6	HighRepK	To examine the sensitivity to the permeability used to control the inflow into the repository.	The permeability of the infilled repository was changed to that of the volume-averaged backfill and host rock.
7	HighRepKNoUpperInflow	1 plus 6	1 plus 6
8	HighKRepNoUnsaturatedZone	2 plus 6	2 plus 6
9	HighRepKAnis	3 plus 6.	3 plus 6.
10	HighRepKAnisNoUpperInflow	4 plus 6.	4 plus 6.
11	LowK	To examine the impact of using the permeability values employed in the 2D calculations in Svensson (2006a).	Different permeability values for the host rock and upper rock units.

4.2.4 Results from the Main Calculations

For the purposes of comparison with the SKB calculations, 'resaturation' has been taken to correspond to the time when the repository compartment was 95% saturated. System equilibration times are also of interest, and these were taken to correspond to the time when pressures returned to 95% of pre-construction conditions.

These calculated timescales are given in Table 11.

Table 11: Resaturation and Pressure Equilibration Timescales

	Case Name	Resaturation Time (y)	Pressure Equilibration Time (y)
0	Reference	23	38
1	RefNoUpperInflow	31	>200
2	RefNoUnsaturatedZone	14	16
3	RefAnis	200	>200
4	RefAnisNoUpperInflow	>200	>200
5	Ref2D	45	84
6	HighRepK	12	32
7	HighRepKNoUpperInflow	18	97
8	HighKRepNoUnsaturatedZone	4	5
9	HighRepKAnis	18	21
10	HighRepKAnisNoUpperInflow	20	41
11	LowK	>200	>200

The variation of resaturation times in Table 11 between the different calculational cases is generally as expected. The following points should be noted:

1. The removal of the upper boundary inflow lengthens equilibration and resaturation times.

2. The introduction of anisotropy tends to increase resaturation times, but causes strong compartmentalisation of the system, such that the pressure re-equilibration times at depth are closer to that of the repository resaturation

times. The near-surface pressure re-equilibration takes a great deal longer than in the reference case.

3. The absence of an unsaturated zone by holding the pressure constant at the surface greatly shortens resaturation times by providing a ready source of water and preventing the permeability restrictions associated with water desaturation.

4. The presentation of the system as a two-dimensional problems leads to much longer resaturation and pressure re-equilibration times.

5. The low permeability case gives rise to extremely long resaturation times.

All of these results give confidence that the models are behaving in line with the conceptual model.

Typical resaturation/re-equilibration times of around 15 – 25 years are quoted from the ConnectFlow work in Jaquet and Siegel (2004), with a variety of assumptions and ranges of parameterisation. The results in Table 11 are generally consistent with these timescales when the same fully saturated representation of the upper surface boundary condition is employed, although the QPAC-EBS times never drop below 10 years for the reference case and are skewed towards the longer time periods.

Figure 7 and Figure 8 show the evolution with time of the saturation and pressure in the repository for the reference case and the other 3D cases with the reference permeabilities (Cases 0-4). The following two figures show the evolution of saturation and pressure in the compartments above the repository for the reference case.

The general form of these curves is as one would expect from this type of modelling and the general conceptual model. Upon excavation and desaturation of the repository, water pressures drop, as do water saturations. The drop in water saturation is a reflection of the fact that the 25 mm y^{-1} inflow at the top boundary is insufficient to maintain full water saturation under these vertical water head gradients. The view as to whether such desaturation is likely is dependent on the degree to which the near-surface hydrogeology has the capacity to supply groundwater to depth and also to permit air ingress into the deeper system. It is not clear whether this is the case for the sites being considered and does not appear to be discussed in any great detail in the SKB documentation. This is a key uncertainty and, as seen in Table 11, this has a large impact on the expected resaturation times.

Figure 7: Repository Resaturation for 3D Calculations with Reference Permeabilities

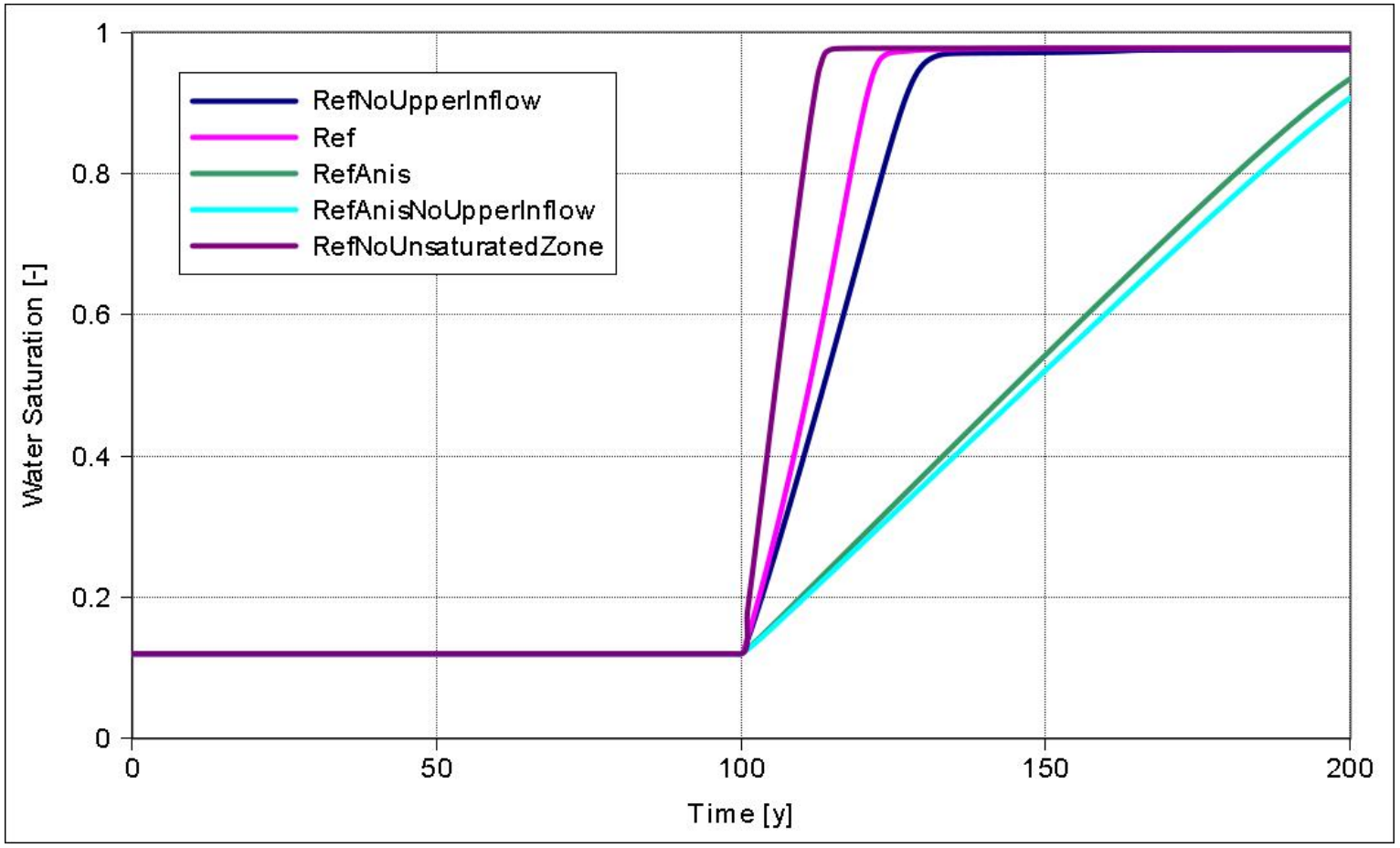

Figure 8: Repository Pressure Evolution for 3D Calculations with Reference Permeabilities

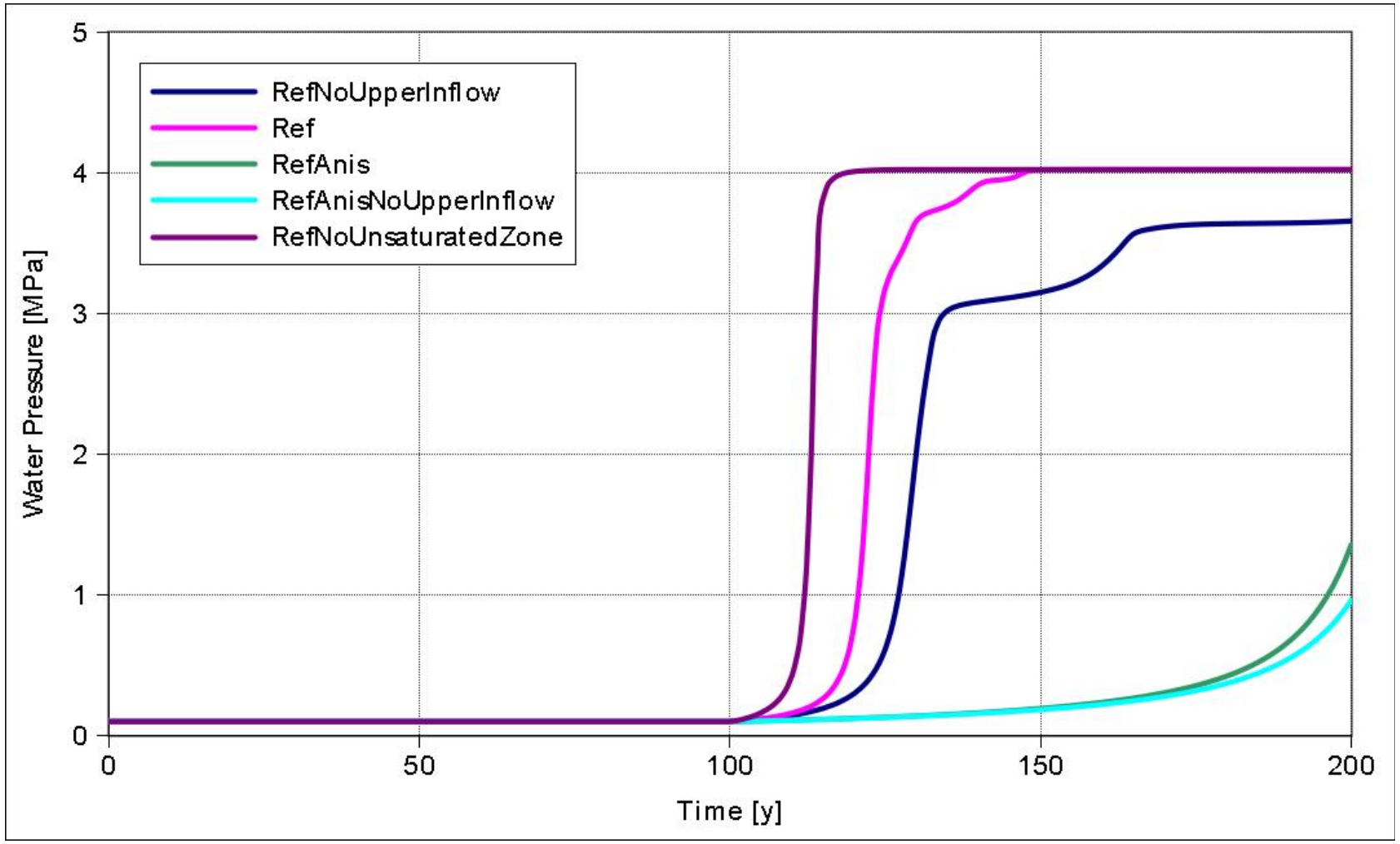

Figure 9: Evolution of Saturation in Compartments above the Repository for the Reference Case (ascending compartment numbers indicate ascending height above the repository)

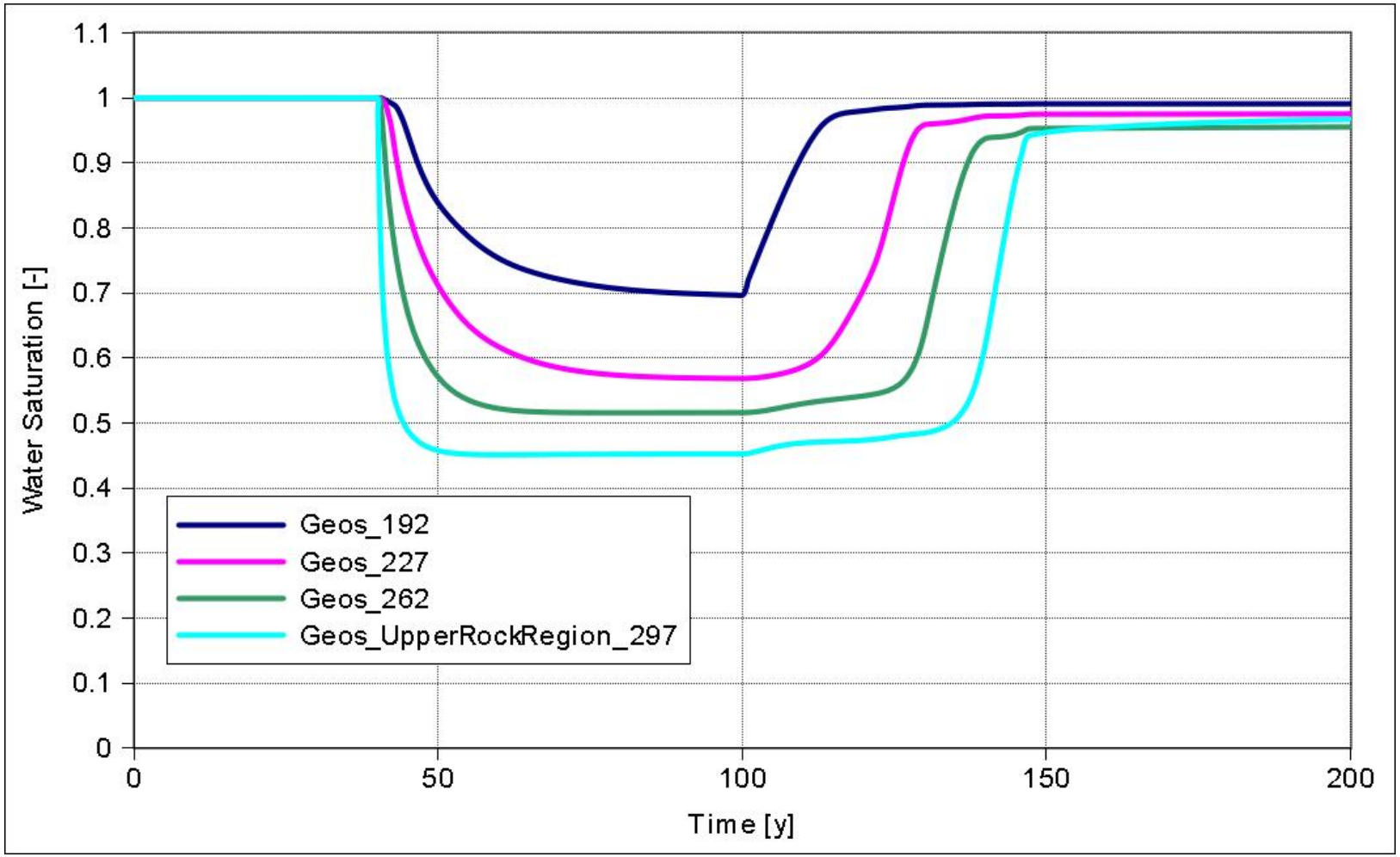

Figure 10: Evolution of Pressure in Compartments above the Repository for the Reference Case (ascending compartment numbers indicate ascending height above the repository)

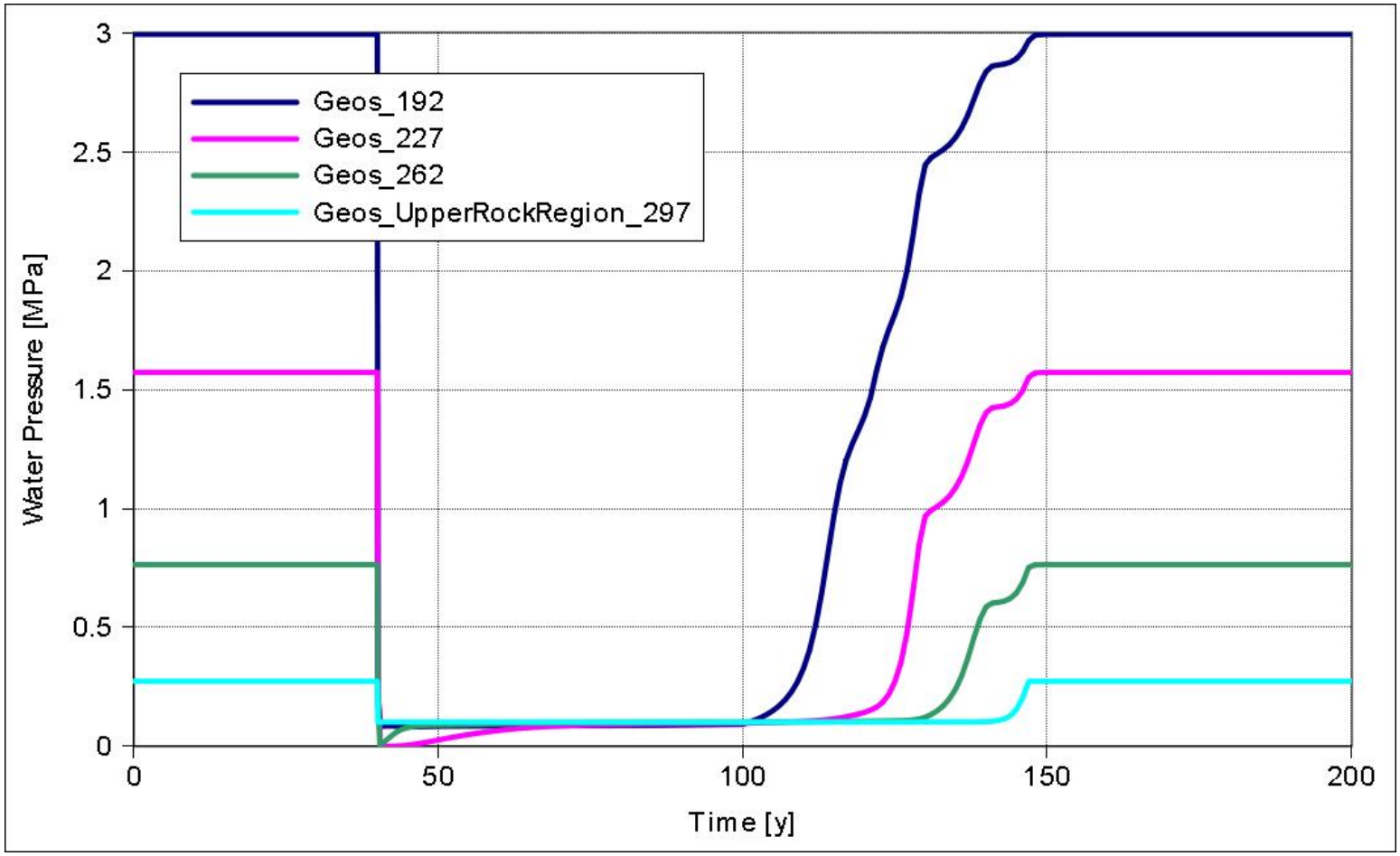

Upon closure of the repository, the QPAC-EBS calculations show the resaturation of the repository and the compartments above it occurs in a staggered fashion with progressive resaturation of each compartment. In contrast, the pressures tend to respond together with full system equilibration occurring at approximately the same time. Both of these behaviours are consistent with the conceptual model employed. As a result, the quoted repository saturation and pressure re-equilibration times tend to bracket the time period over which the system returns to a steady state.

The pressure profiles tend to show a 'stepping' of pressures. These are artefacts of the model parameterisation and geometry. The use of relative permeability curves with large compartments results in individual compartments controlling system resaturation. This in turn means that the rate of pressure rise is locally controlled by the saturation state of a particular compartment. This tends to introduce unphysical steps into the pressure profile as compartments change water saturations. However, the general pressure response averaged over the steps is reasonable. Such behaviour illustrates some of the problems associated with using field data at performance assessment scales and at coarse resolutions.

4.2.5 Additional Calculational Cases

In order to further investigate this issue further, three additional cases were run based on the reference case but using a step change in relative permeability for water from 1 to 0.001 at 0.95 water saturation with the gas relative permeability function left unchanged. This effectively gives a constant relative permeability for unsaturated compartments, representing the bulk loss of permeability in unsaturated compartments. The three additional cases were defined as follows:

- RefStepKrel is the reference case but with the step relative permeability function
- RefStepKrelAnis has a 10:1 vertical anisotropy
- RefStepKrelAnis2 has a 5:1 vertical anisotropy

The results for repository water saturation and pressure are shown in Figure 11 and Figure 12. The simplified relative permeability curve has had the expected effect and the pressure curves have been smoothed. Table 12 gives the resaturation and pressure equilibration timescales for these calculations.

Figure 11: Repository Resaturation for 3D Calculations with a Step Change Relative Permeability for Water

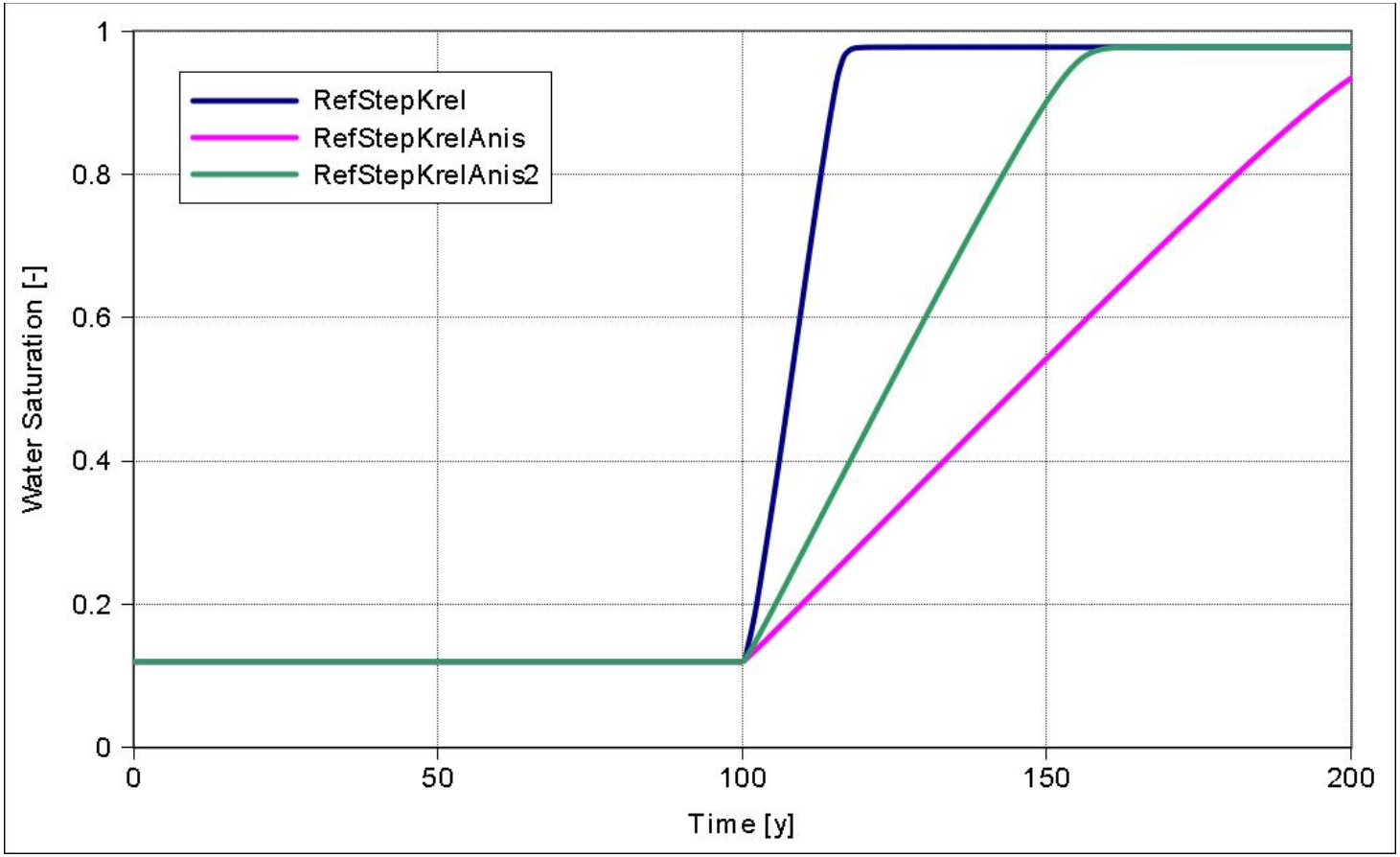

Figure 12: Repository Pressure Evolution for 3D Calculations with a Step Change Relative Permeability for Water

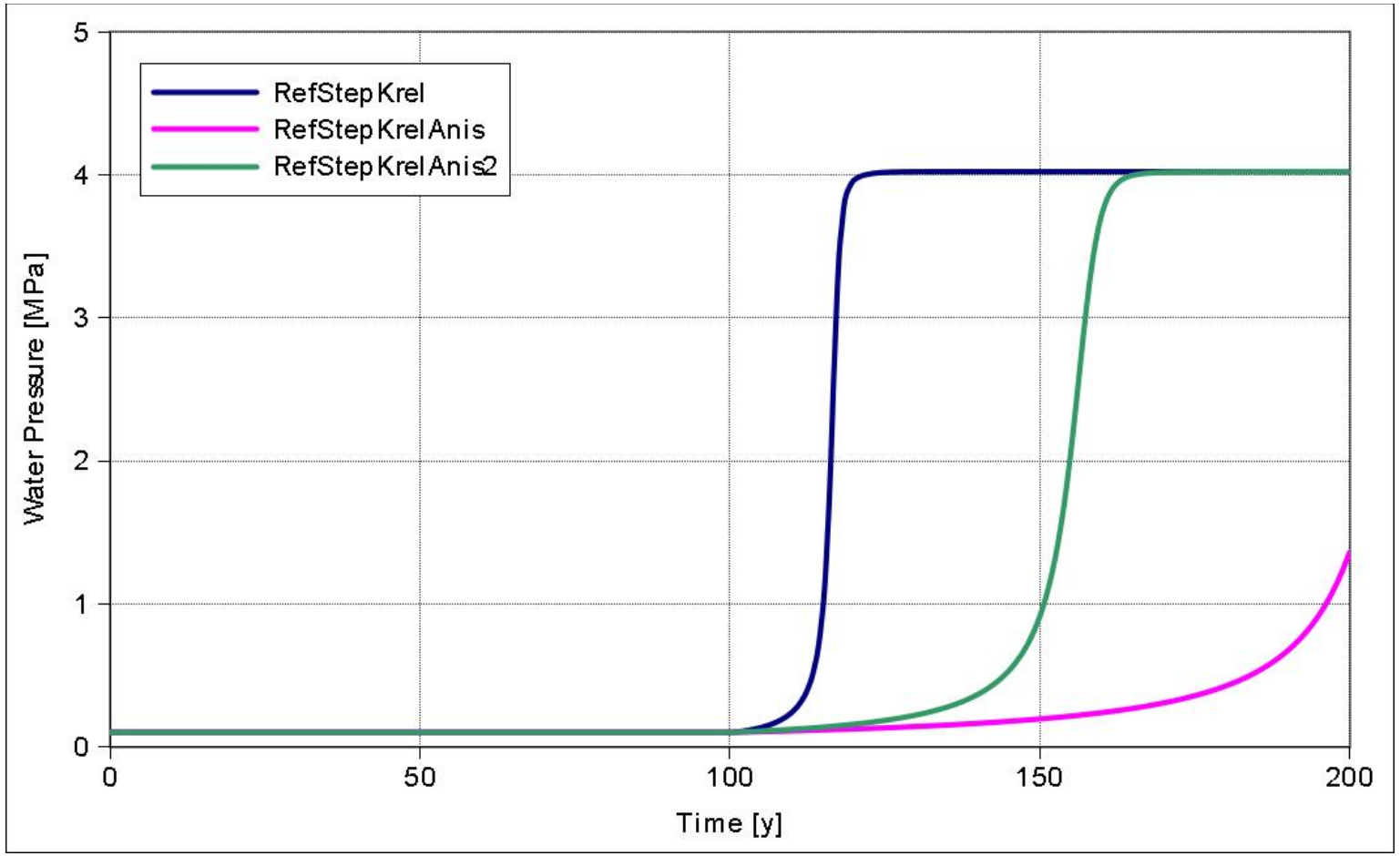

Table 12: Resaturation and Pressure Equilibration Timescales for Cases with a Step Change in Relative Permeability for Water

	Case Name	Resaturation Time (y)	Pressure Equilibration Time (y)
12	RefStepKrel	17	19
13	RefStepKrelAnis	>200	>200
14	RefStepKrelAnis2	55	61

The assumption of a 0.001 relative permeability for unsaturated compartments does give different results from the reference cases, but this is to be expected and could be rectified by appropriate adjustments to the step change relative permeability. The challenge is to choose parameters in performance assessment models such as QPAC-EBS so that the simplified relative permeability forms give the same bulk behaviour as that expected by the more detailed (but unsuitable) smaller scale parameterisation. This is currently being investigated with additional QPAC-EBS calculations which will be reported in 2008.

4.2.6 Summary

The resaturation timescales obtained in the QPAC-EBS calculations are generally consistent with the relatively short timescales obtained using the ConnectFlow code in Jaquet and Siegel (2004). However, timescales of much greater than 200 years have been obtained with some combinations of modelling assumptions. As would be expected, the hydraulic conductivity of the host rock and backfill are dominant.

The representation of the unsaturated zone properly is important and the assumption of groundwater pressures being fixed at surface through desaturation significantly reduces the estimated resaturation time. This expected behaviour of the near-surface hydrogeology under repository desaturation conditions needs to be examined in more detail, or any existing work providing this information more clearly brought into the arguments regarding resaturation times.

The choice of relative permeability curves with the coarse discretisation employed in QPAC-EBS is an important issue for the application of the code, and this is currently being investigated.

4.3 Canister Corrosion

QPAC-EBS calculations are being undertaken that are capable of representing canister corrosion for both an intact and eroded buffer. A simple representation of the system to be modelled is shown in Figure 13.

The main aims of these calculations are:

1. to calculate corrodant transport rates to the canister and canister corrosion rates with an intact buffer which can be compared with the SR-Can values;

2. to represent the evolution of the system (e.g., pH of water in the buffer) as the buffer is eroded by glacial meltwater; and

3. to calculate corrodant transport rates to the canister and canister corrosion rates with an eroded buffer which can be compared with the SR-Can values.

By representing the evolution of the system, rather than just the start and end points, it is possible to investigate some aspects of the problem that cannot be addressed with SKB's approach.

When buffer erosion takes place it is necessary to model the mechanical processes involved or to represent these in a simplified way (as SKB do). Currently the development of a QPAC-EBS model to deal with mechanical processes is being undertaken in the THERESA project (Bond et al., 2007).

The modelling is planned to be undertaken in the following stages:

1. A suitable discretisation of the system will be defined and a corrodant transport model will be implemented with no buffer erosion. This will enable simple comparisons to be made with canister corrosion rates referred to in SR-Can.

2. A simple representation of buffer erosion will be used that does not depend on chemistry processes in order to obtain an initial representation of how canister corrosion rates might evolve.

3. A chemical model will be introduced in order to be able to represent the evolution of groundwater chemistry, including pH.

4. The Hydro (H), Mechanical (M) and Chemical (C) processes will be coupled in order to be able to simulate canister corrosion with an eroding buffer.

Figure 13: System Geometry (from Arcos et al., 2006)

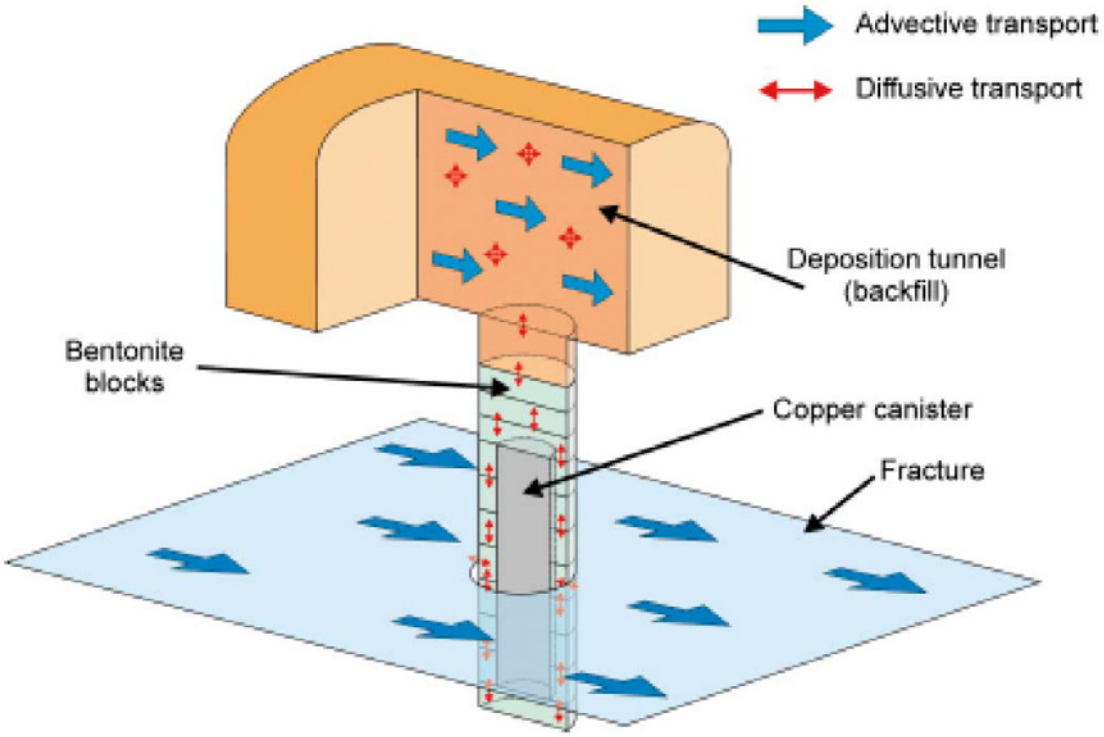

The results of these calculations will be presented in detail 2008, but progress made to date is discussed in Appendix C.

5 Reproducing the SR-Can Radionuclide Transport Calculations

In this section selected calculations presented by SKB are reproduced using the AMBER code in order to gain a full understanding of what SKB has done, and to provide the basis for additional independent calculations. The calculations are restricted to the groundwater transport pathway; the gas pathway is considered briefly in Section 3.4.

The AMBER case file has been reproduced in QPAC-EBS. This will enable coupled calculations to be undertaken in future involving both the evolution of the EBS and radionuclide transport. The representation of radionuclide transport in QPAC-EBS uses the same model as that developed for corrodant transport (see Section 4.3). Radionuclide transport using QPAC-EBS will be reported in 2008, but references are made in this Section to areas where this implementation has already proved to be useful.

5.1 The Pinhole Failure Mode

This failure mode is not considered likely to occur by SKB, but it has been studied in detail in previous assessments (including SR-97) and, as discussed in Section 2.5, it provides information that is relevant to calculations for other potential failure modes.

5.1.1 The SR-97 AMBER Case File

The AMBER model used for reproducing the SR-97 radionuclide transport calculations has been used as the basis for reproducing the SR-Can calculations. For convenience details of this case file are first reproduced here.

Figure 14 and Table 13 give details of the modelling blocks used in the near field, some of which are broken down into a number of compartments. Table 14 lists the release pathways from the near field to the geosphere that have been addressed historically. The pathway Q4 was not considered by SKB in the SR-Can assessment, as it was assumed to be less important than the other pathways.

Figure 14: Discretisation of the Near Field

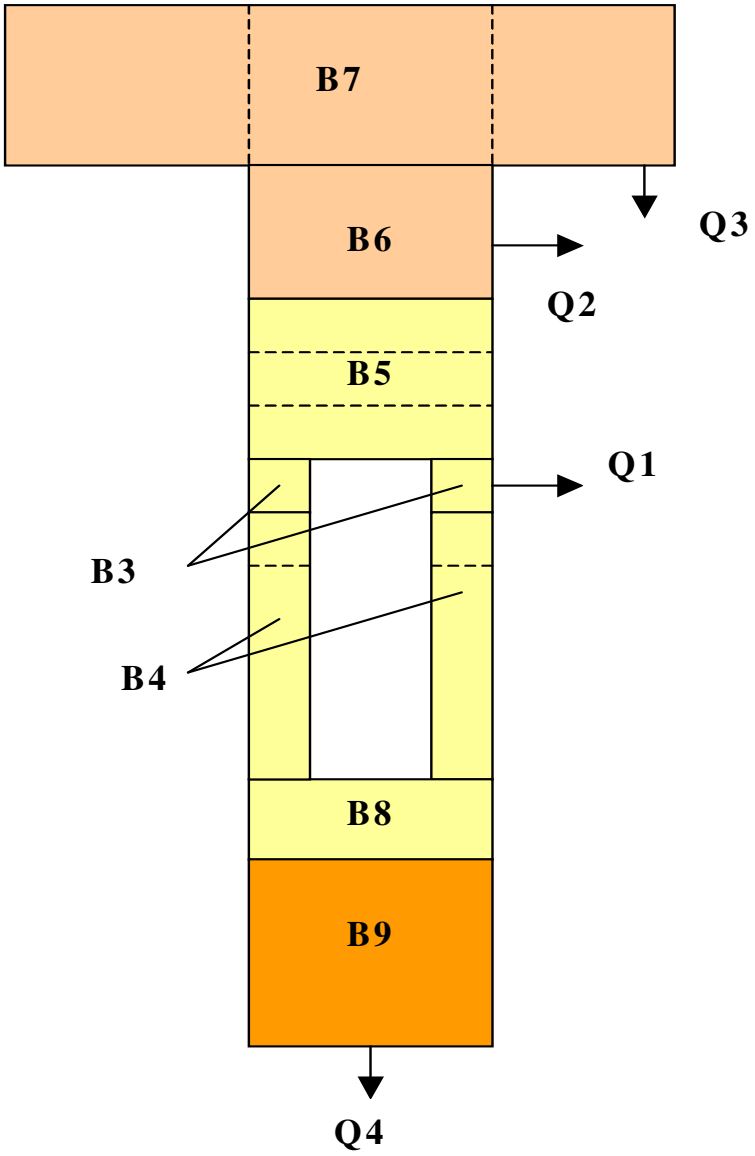

Table 13: Near-Field Blocks

Block	Description	Number of compartments	Comment
B1	Inside the canister (water)	1	Not shown explicitly in Figure 14
B2	The hole in the canister (water)	1	Not shown explicitly in Figure 14
B3	The buffer next to the hole	6 annular compartments of equal thickness (0.058 m)	The height of these compartments is 0.5 m

B4	The rest of the buffer around the canister	2 annular compartments, each of the full thickness, one above the other	The upper compartment is 1.0 m high and the lower 3.33 m high
B5	The buffer above the canister	3 equal layers	The height of these compartments is 0.5 m
B6	The backfill at the top of the deposition hole	1	The height of this compartment is 1.0 m
B7	The tunnel backfill	3	The geometry is hard to understand. It has been assumed that each compartment has the full tunnel cross-section of 12.24 m^2, with the centre one the width of the deposition hole (1.75 m) and the others 2.125 m wide (6 m in total)
B8	The buffer below the canister	1	The height of this compartment is 0.5 m
B9	Rock below the deposition hole	1	The height of this compartment is 3.0 m

Table 14: Near-Field Release Routes

Route	Location
Q1	From the outer B3 compartment
Q2	From the B6 block
Q3	From one of the outer B7 compartments
Q4	From the rock below the deposition hole

Diffusional transfers can take place in horizontal or vertical directions, and these were specified by SKB in terms of resistances between compartments. For diffusion in a given direction, the resistance between compartments *i* and *j* is given by:

$$\Omega^{ij} = \frac{1}{2}\left(\frac{d^i}{D^i A^i}+\frac{d^j}{D^j A^j}\right), \qquad 5.1$$

where A (m^2) is the area perpendicular to the direction of transport, D ($m^2\ s^{-1}$) is the effective diffusion coefficient, and d (m) is the length of the compartment in the direction of radionuclide transport.

Alternatives representations of the diffusional resistance are possible, in particular by employing a common interface area between the two compartments. The use of this

approach in the QPAC-EBS implementation has demonstrated that this does make a small but significant difference to calculated radionuclide transport rates.

The associated transfer rate between compartment *i* and compartment *j* is λ^{ij} (s^{-1}) given by:

$$\lambda^{ij} = \frac{1}{\kappa^i \Omega^{ij}}, \quad 5.2$$

where κ^i (m^3) is the capacity of compartment *i* defined by:

$$\kappa^i = \theta^i R^i V^i, \quad 5.3$$

where θ^i (-) is the compartment porosity, R^i (-) is the retardation coefficient for the radionuclide in question and V^i (m^3) is the compartment volume.

Analytical expressions are used for the transfer resistances from the source term into the buffer. For the canister-hole resistance we have:

$$\Omega = \frac{d_{Hole}}{D A_{Hole}}, \quad 5.4$$

where d_{Hole} (m) is the length of the hole.

The resistance for the buffer-hole interface is taken as:

$$\Omega = \frac{1}{D\sqrt{2\pi A_{Hole}}}. \quad 5.5$$

The four release locations have different properties. The fracture zones (Q1 and Q3) have extra resistance because of the small size, while Q2 and Q4 just have a flow resistance.

The flow resistances are represented by:

$$\Omega = \frac{1}{A_q \sqrt{q}}, \quad 5.6$$

where A_q is a lumped parameter with values 0.03, 0.1, 1 and 1 $m^{2.5}$ $y^{-0.5}$ for Q1-Q4 respectively. Here q (m s^{-1}) is the near-field Darcy flux (taken to have a value of 0.002 m y^{-1}). This resistance was considered in Neretnieks (1979) is discussed in more detail in Appendix A.

For Q1 and Q3 additional resistances are added according to

$$\Omega = \frac{B}{D}, \qquad 5.7$$

where B is another lumped parameter with dimensions m^{-1}. For Q1 this had a value of 0.9 m^{-1} and for Q3 0.333 m^{-1}. The theory behind this representation is given by Neretnieks (1986).

As explained in Appendix A, B can be written in terms of Neretniek's parameter F

$$B = \frac{F}{A_f} = \frac{F}{2\pi rb}, \qquad 5.8$$

where r is the radius of the deposition hole (0.875 m), A_f is either the area of the fracture or half of it (which is not totally clear) and b is the fracture half-width. According to Vahlund and Hermansson (2006b), SKB use F and A_f as inputs: these parameters are described as the plug length and plug area. It is not clear whether SKB are taking A_f *to* be the whole area of the fracture or not. In Appendix F of Vahlund and Hermansson (2006b) the data shown in Table 15 are given, and the resulting implied value of the parameters B and b are calculated; the units have been assumed as these are not given explicitly.

Table 15: Parameters for Diffusive Resistances

	Plug Length F (m)	Plug Area A_f (m²)	B (m^{-1})	b (m)
Q1	5E-4 (0 with spalling)	5.5E-4	0.9	1E-4
Q2	0	1	-	
Q3	0.002	0.006	0.33	1E-3

The values of B are the same as for SR-97, and so no changes are needed to the AMBER case files, although this resistance has now been excluded when spalling is present.

In the geosphere, the flowing fracture was discretised into 5 compartments, consistent with a Peclet number in the region of 10. Six rock matrix compartments were associated with each fracture compartment, with the sizes of the matrix compartments increasing by a factor of 3 from the fracture to the diffusion limit.

It was assumed that the walls of the fracture compartments (to a depth δ) are in equilibrium with flowing water. This introduces an effective fracture retardation coefficient R_f given by

$$R_f = 1 + \frac{2\,\delta(\theta + \rho K_d)}{b}, \qquad 5.9$$

where θ is the rock porosity (dimensionless), ρ is its density (kg m^{-3}), b is the fracture half-aperture (m) and K_d is the relevant equilibrium sorption coefficient (m^3 kg^{-1}). This is effectively the same as introducing a very thin first rock matrix compartment, and can be important for strongly sorbed radionuclides. A value for δ of $2\,10^{-3}$ m was employed.

The calculations reported here use the same approach as employed in the SR-97 calculations, but alternative approaches to discretisation are possible and may be used in future calculations using either AMBER or QPAC-EBS.

The doses incurred in the biosphere for a specified radionuclide are calculated simply by multiplying the flux into the geosphere Φ by a biosphere factor Γ (Sv Bq^{-1}):

$$H = \Gamma\Phi, \qquad 5.10$$

Source Term

The amount of each radionuclide available for transport from the canister through the pinhole depends upon the initial inventory I (Bq), the instantaneously available fraction, α, and the fuel dissolution rate λ_F (y^{-1}). This amount also depends upon the

relevant solubility limit S (mol m^{-3}). No transport is assumed to take place until a time t_{min}.

The area of the pinhole is assumed to increase suddenly from a small initial value (when the transport resistance is large) to a very large value (when the transport resistance is negligible) at time t_{large}.

5.1.2 Developments for the SR-Can Case File

The main differences between the SR-97 AMBER Case File and the SR-Can Case File are given here.

System Geometry

According to Xu (2007) the geometry of the system in SR-Can has not been changed from that used in SR-97, although this is not made clear in the SR-Can documentation. Minor changes to the surface areas of the tunnel compartments have been made for compatibility with information given in Vahlund and Hermansson (2006b).

Transport Pathways

As stated previously, SKB do not consider the Q4 pathway in SR-Can.

Equivalent Flow Rates

The flow resistances in equation 5.6 are defined as the reciprocal of the equivalent flow rates.

Equation 6.6.2 of the Data Report gives a contribution to the equivalent flow rate for pathway Q1 when spalling is considered:

$$Q_{eq}^{spall} = 1.13\sqrt{\frac{D_p q_d A W_{zone} L_{zone} \varepsilon_{zone} f}{d_{zone}}}\,, \qquad 5.11$$

In the deterministic calculations described by SKB a value of 2.2E-4 m^3y^{-1} was obtained with a Darcy velocity q_d of 6E-6 m y^{-1}. This appears to be consistent with the following parameter values taken from Neretnieks (2006a):

$$D_p = \frac{D_w}{10} = 1E-9\, m^2 s^{-1}$$
$$A = 12.8\, m^2$$
$$W_{zone} = 0.2\, m$$
$$L_{zone} = 8\, m$$
$$\varepsilon_{zone} = 0.01$$
$$d_{zone} = 0.1\, m$$
$$f = 0.1$$

Based on this calculation, the following expression has been used in the AMBER calculations:

$$Q_{eq}^{spall} = Q_{ref} \sqrt{\frac{q_d L_{zone}}{q_d^{ref} L_{zone}^{ref}}}. \qquad 5.12$$

Where q_d^{ref} has a value of 6E-6 m y^{-1}, L_{zone}^{ref} has a value of 8 m and Q_{ref} has a value of 2.2E-4 m^{3}y^{-1}.

It is not clear whether this is totally compatible with the calculations given in SR-Can.

The correct value to take for the Q3 pathway is also not totally clear. Equation 6.6.4 of the Data Report gives the value for this pathway as:

$$Q_{eq3} = 4 w_z \sqrt{\frac{q_d D_w L_z \varepsilon_r}{\pi}} \qquad 5.13$$

w_z had a value of 2.5 m assigned to it, L_z was set to 7 m and ε_r had a value of 5E-6, so that

$$Q_{eq3} = a\sqrt{q_d}$$

The constant a is 5.93E-3 m$^{2.5}$ y$^{-0.5}$. This expression was used in the AMBER calculations.

An additional term is added when there is advective flow in the tunnel.

$$Q_{eq3,adv} = \frac{L \varepsilon A}{\tau} \qquad 5.14$$

Here the porosity of the tunnel ε is taken to be 0.36, and cross-sectional area of the tunnel A is taken to have a value of 12.566 m^2 (Vahlund and Hermansson, 2006b). The

distance travelled in the tunnel L and the travel time to the fracture τ are given in the files produced by the DFN code. The travel times in the tunnels appear very long.

Transport Resistances

Based on information given by Hedin (2007c), the diffusive transport resistance at the buffer/rock interface is neglected when spalling takes place, although it is not clear why this is considered to be appropriate.

Advective Flows

Advective flows are included in the tunnel (only diffusive flows were included in the Quintessa SR-97 Case File). The details of the parameter values used by SKB to represent this process are not totally clear from the SR-Can documentation. The COMP23 input file supplied by SKI includes the following parameters:

- TW_TUN_3. Travel time in the tunnel (used when determining advective flow rates), here denoted by τ_T. The deterministic calculation input file had a value of 1E6 y.
- L_TUN_3. Length travelled in the tunnel (used when determining advective flow rates), here denoted by L_T. The deterministic calculation input file had a value of 30 m.
- UR_3. Velocity in the fracture adjacent to the deposition tunnel (used when determining the equivalent flow rate for the Q3 interface). The deterministic calculation input file had a value of 5E-6 m y^{-1} (the units are not actually stated).
- LR_TUN_3. Distance from the deposition hole to the advective fracture. The deterministic calculation input file had a value of 4 m.

It is assumed that the advective transfer rates between compartments i and j in the tunnel are given by:

$$\lambda^{ij} = \frac{L_T \vartheta^i A^{ij}}{\tau_T \kappa^i}, \qquad 5.15$$

where A^{ij} is the interface area between compartments. It is not clear that this approach mirrors that employed by SKB.

The length of the third tunnel compartment has been increased by 1m from the SR-97 value to tie in with the value of LR_TUN_3 used in the COMP23 input file.

Anion Exclusion

Anion exclusion is considered in the buffer and backfill, so the porosity values used are now element-dependent. Anion exclusion is assumed to apply to C, Cl, I and Se.

Solubility Limits

PDFs for solubility data are given in the figures in Section 3.4 of the SR-Can Data Report based on the calculations described in Duro et al. (2006). The sample files proved by Hedin (2007b) have been used directly for probabilistic calculations. According to Hedin (2007a), the median values of these PDFs were used by SKB in deterministic calculations, and the same approach has been used in the AMBER calculations.

Sorption Coefficients

SKI use correlated sorption coefficients. Values of K_d for elements (in a given redox state) in the same correlation group are correlated. The way that these correlations have been implemented has not been stated explicitly in the SR-Can documentation, but has been clarified in Hedin (2007c).

A value x is obtained from a uniform distribution [0, 1] and an input value y is then calculated as $y = F^{-1}(x)$, where $F(y)$ is the cumulative distribution function for the input variable in question. In a particular realisation, the same x is used for all elements belonging to the same correlation group.

SKB make frequent use of triangular and log-triangular distributions. Consideration of cumulative density functions for these PDFs is given in Appendix B.

For the K_d distributions that are piece-wise uniform in log-space (Section 6.7.8 and Table A-43 of the Data Report) the Data Report gives: the lower bound, LB; the 25th percentile, P25; the best estimate, BE; the 75th percentile, P75; and the upper bound, UB. In this case:

$$\text{If } 0 < x < 0.25 \text{ then } \log(K_d) = \log(LB) + x/0.25 * [\log(P25) - \log(LB)]$$
$$\text{If } 0.25 < x < 0.75 \text{ then } \log(K_d) = \log(P25) + (x - 0.25)/0.5 * [\log(P75) - \log(P25)]$$
$$\text{If } 0.75 < x < 1 \text{ then } \log(K_d) = \log(P75) + (x - 0.75)/0.25 * [\log(UB) - \log(P75)]$$

Hedin (2007c) stated that in reality these correlations had little effect on the SR-Can calculations.

Geosphere Transport Parameters

SKB use data 'triples' for the correlated parameters F, t_w and Q_{eq} based on the work described in Hartley et al (2006a, b). The sample files proved by Hedin (2007b) have been used directly for probabilistic calculations. According to Hedin (2007a), the data in these sample files do not include a factor of 10 division referred to on page 407 of the main SR-Can report to account for channelling effects.

The SR-Can documentation makes it clear that not all of the particles that are tracked reach the surface, although it is not clear exactly how this issue is dealt with.

Hedin (2007c) has indicated that a flag OKFLAG in the supplied input files has the following interpretation:

OKFLAG = 0 means particles do reach the surface

OKFLAG = 1 means particles never started at all because of no fractures

OKFLAG = 2 means particles still going in a tortuous path to get out

OKFLAG = 3 means the DFN calculation was stopped due to mass-balance problems

OKFLAG = 4 means that the particle got stuck close to the repository in a closed stagnant loop of fractures/tunnel

Only particles for which OKFLAG = 0 are used in the radionuclide transport calculations.

5.1.3 Data used in the SR-Can AMBER Calculations

Table 16 gives details of the parameter values used. For all calculations it has been assumed that Friedland Clay has been used for the backfill and that highly saline conditions are present.

In Section 10.5.3 of the SR-Can report SKB state that because the radionuclide is strongly sorbed in both the near field and geosphere, Pb-210 is not included in calculations in those parts of the system. In order to test the assumption that releases of Pb-210 from the geosphere are not significant, this radionuclide has been included in the AMBER calculations. In order to do this assumptions have had to be made about the values of some model parameters where they are not given in the Data Report tables.

Although not made clear in the SR-Can documentation, the deterministic calculations are all for the Forsmark Site (Hedin, 2007a).

The SR-Can documentation does not make it clear what chemical form is assumed for C in each part of the system. According to Hedin (2007a), the conservative assumption of methane in the near field and carbonate in the far field was used, and so this conservative approach was employed in the AMBER calculations.

It should be noted that both triangular and log-triangular PDFs have been considered for the fuel dissolution rate. The Data Report appears to indicate that the original expert recommendation was for a triangular distribution, but a log-triangular distribution was actually employed in the calculations. This is one of the key parameters for determining over risks.

For a parameter that has a triangular distribution between the limits $x=a$ and $x=c$ with peak at $x=b$, the mean value of the parameter is $\frac{(a+b+c)}{3}$. For the values chosen by SKB for fuel dissolution, this would give a mean value of 3.7E-7 y^{-1}.

For a parameter that has a corresponding log-triangular distribution the mean value of the parameter is given by:

$$\frac{2}{(\log c - \log a)}\left[\frac{a}{(\log b - \log a)} + \frac{c}{(\log c - \log b)} - \frac{b(\log c - \log a)}{(\log b - \log a)(\log c - \log b)}\right].$$

In this expression the logarithms are natural logarithms. For the values chosen by SKB for fuel dissolution, this would give a value of 1.5E-7 y^{-1}, which is over a factor of 2 lower than for the triangular distribution.

5.1.4 Approximations in the SR-Can AMBER Case File

The following simplifications have been made.

1. The same geosphere transport parameters have been taken for each of the transport pathways Q1, Q2 and Q3 when all the pathways are considered together. Alternatively, each pathway can be considered separately. To provide different geosphere parameters for the different pathways would require significant changes to the structure of the AMBER model. This is much easier to undertake in QPAC-EBS, and consideration will be given to this in future calculations.

2. Reducing conditions are assumed throughout, and this determines the chemical form assumed for some elements that can be in more than one redox state. Future calculations may require consideration of different redox states for the same element.

Table 16: Data Values for Pinhole Scenario Calculations

Parameter/Units	Definition	Deterministic value	PDF	Comments
A_h (m^2)	Area of pinhole	Initial value corresponding to a radius of 2 mm	-	
b (m)	Fracture half aperture. This is not an SKB input parameter, but is defined from F/t_w	-	-	
B (m^{-1})	Geometrical factor in definition of interface diffusive resistances for Q1 and Q3.	Values taken from Hedin (2001): 0.9 for Q1 and 0.333 for Q3	-	It is not clear if these values have been used in the SKB calculations.
D (m^2 y^{-1})	Effective diffusivity	From PDF	Bentonite data from Table A-11 of Data Report. Triangular distributions for each element. Backfill data from Table A-17 of Data Report. Triangular distributions for each element. Rock values from Data Report Tables A-40 and A-41. Anion exclusion for C, Cl, I and Se with reduction factor of 10. Expressed as the product of a site-specific formation factor (log-normal) and element-dependent diffusivity	

Parameter/Units	Definition	Deterministic value	PDF	Comments
F (y m^{-1})	Geosphere transport resistance	Main Report Table 10-5: 4E6 y m^{-1} for Q1; 6E6 for Q2; and 6E6 for Q3	Sample file provided by Hedin (2007b)	
I (Bq)	Radionuclide inventory per canister	Table A-2 of Data Report.	-	
K_d (m^3 kg^{-1})	Equilibrium sorption coefficients	From PDF	Bentonite values from Table A-13 of Data Report. Backfill values from Table A-19 of Data Report. Rock values from Table A-43/A-44 of Data report for non-saline conditions. Range of values for Pb assumed to follow those for Ra. Log-triangular distributions in each case	
L (m)	Geosphere transport distance. (This is not an SKB input parameter).	A representative value of 500 m has been taken.	-	
q (m y^{-1})	Darcy velocity at deposition hole wall	Table 10-5 of Main report: 6E-6 m y^{-1} for Q1	-	Used in specification of Q_{eq} when spalling is included
Q_{eq} (m^3 y^{-1})	Equivalent flow rates at the deposition hole	Table 10-5 of Main SR-Can report. Spalling is assumed for Q1. 2.25E-4 m^3 y^{-1} for Q1 1E-5 m^3 y^{-1} for Q2 5E-3 m^3 y^{-1} for Q3	Sample file provided by Hedin (2007b)	

Parameter/Units	Definition	Deterministic value	PDF	Comments
S (mol m^{-3})	Solubility limit	Median values of PDF	Sample file provided by Hedin (2007b). Pb solubility assumed to follow that for Ni.	
t_{large} (y)	Time when pinhole size increases in area	Table 10-3 of main report: 10 000 y.	-	
t_{min} (y)	Time when radionuclide transport is initiated.	Table 10-3 of main report: 1000 y.	-	
t_w (y)	Geosphere travel time	Table 10-5 of main report: 40 y for Q1 60 y for Q2 and Q3.	Sample file provided by Hedin (2007b)	
v (m s^{-1})	Transport velocity in the geosphere. This is not an SKB input parameter, but is defined from F/t_w	-	-	
α (-)	Instantaneous release fractions	From PDF	Table A-4 in Data Report. Realistic values used.	
Γ (Sv Bq^{-1})	Biosphere factor	Values taken for Forsmark. Table 10-1 of Main Report. SR-97 value used for C.	-	Separate values given for Pb-210 but not Po-210- see discussion in the text.
Δ (m)	Maximum penetration depth into rock matrix	0.03 (Hedin, 2007a)	Data report P194.	The basis of the choice for the deterministic calculations is not clear. See Hedin (2007c)

Parameter/Units	Definition	Deterministic value	PDF	Comments
θ (-)	Porosity	Buffer: Constant values for cations From PDF for anions	Buffer: Table A-11 of Data Report. Triangular PDfs for anions. Backfill: Table A-11 of Data Report. Triangular PDfs for anions. Rock: Table A-42 of data report (Forsmark value: log-normal with mean: -3.03 and standard deviation of 0.20.	
λ_F (y^{-1})	Fuel dissolution rate	From PDF	Data Report Section 3.3: triangular or log-triangular with minimum 1E-8, peak 1E-7 and maximum 1E-6	Both triangular and log-triangular distributions have been considered- see note in the text.
ρ (kg m^{-3})	Bulk density	Bentonite value from P80 of data report: 1700 kg m^{-3} Generic rock density - see Table A-36 of data report: 2600 kg m^{-3}	-	

5.1.5 Deterministic Calculations

The deterministic calculations presented by SKB are for Forsmark. Other than the biosphere dose factors, the only parameters that would differ between the two sites would be the matrix porosity in the geosphere and the formation factors used in the calculation of effective diffusivities in the rock matrix. These differences are small, and so separate calculations have not been undertaken for Laxemar.

Figure 15 gives the results for the first set of AMBER calculations for the flux from the near field for pathway Q1; some radionuclides with very low releases have been omitted from the figure for clarity. This figure can be compared directly with Figure 10-14 in the main SR-Can report. When compared with the SKB numerical calculations, the results are very close. Table 17 compares the values and times of the calculated peak fluxes for Q1. The SKB values are approximate, as they have been read from the relevant figure in the SR-Can report.

Figure 16 gives the corresponding results for fluxes from the geosphere, and Table 18 gives the peak fluxes. These can be compared directly with Figure 10-15 in the main SR-Can report. Again, a comparison between the two sets of calculations shows that the results are very close.

Figure 15: AMBER Deterministic Calculations for the Near-Field Flux for the Pinhole Failure Mode at Forsmark: Pathway Q1

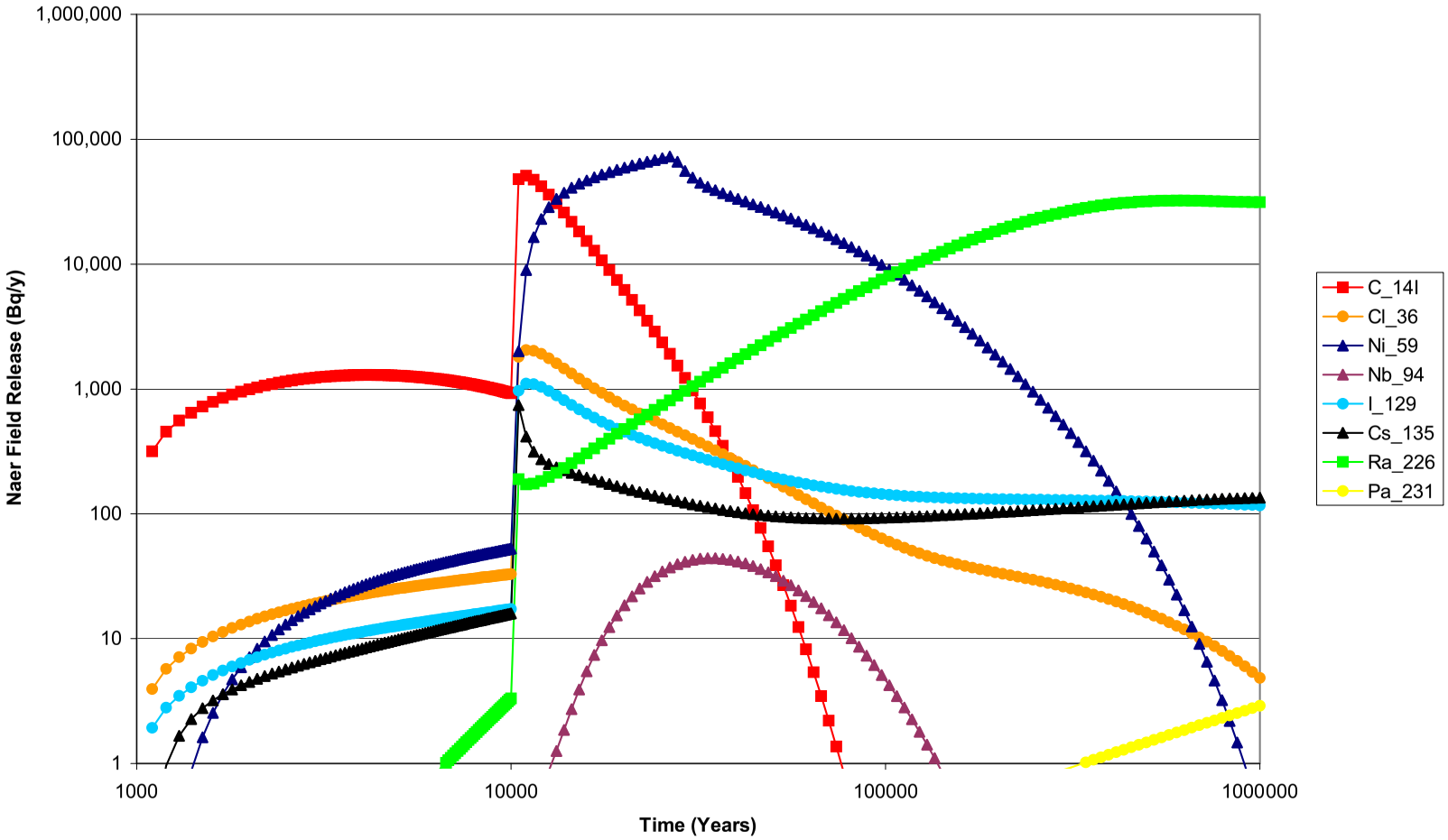

Table 17: Peak Flux Deterministic Calculations for the Near Field for Pathway Q1

Radionuclide	Peak Flux (Bq y^{-1})		Time of Peak Flux (y)	
	AMBER	SKB	AMBER	SKB
C-14	8E4	1E5 (1E5)	1E4	1E4
Ni-59	8E4	5E4 (2E4)	3E4	2E4
Ra-226	3E4	3E4 (3E4)	1E6	1E6
Cl-36	3E3	6E3 (6E3)	1E4	1E4
I-129	2E3	3E3 (3E3)	1E4	1E4
Cs-135	7E2	4E2 (3E2)	1E4	1E4
Nb-94	5E1	5E1 (2E1)	3E4	3E4

Note: The SKB values in parentheses are for analytical calculations

Table 18: Peak Flux Deterministic Calculations for the Far Field for Pathway Q1

Radionuclide	Peak Flux (Bq y^{-1})		Time of Peak Flux (y)	
	AMBER	SKB	AMBER	SKB
C-14	6E3	6E3 (4E3)	2E4	2E4
Cl-36	3E3	5E3 (4E3)	1E4	1E4
I-129	2E3	3E3 (2E3)	1E4	1E4
Ni-59	2E3	2E3 (4E2)	2E5	2E5
Cs-135	3E1	4E1 (8E1)	1E6	1E6

Note: The SKB values in parentheses are for analytical calculations

Figure 16: AMBER Deterministic Calculations for the Far-Field Flux for the Pinhole Failure Mode at Forsmark: Pathway Q1

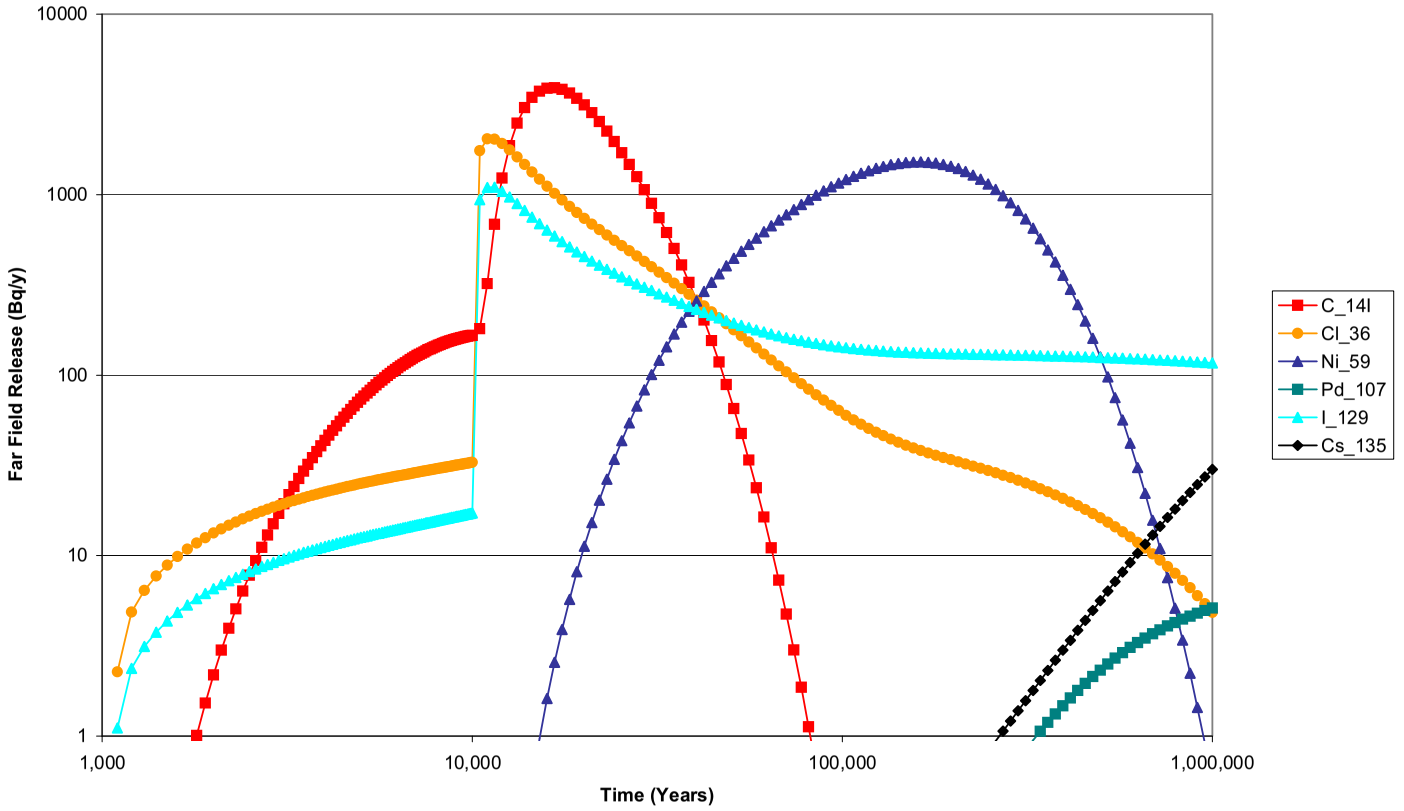

Figure 17 gives the near field releases for the pathway Q2, where the fluxes are significantly smaller than for the Q1 pathway. These calculations can be compared with those given by SKB in Figure B-4, in the Appendix to the main report. Table 19 gives the calculated peak fluxes. Overall the results are similar.

Table 19: Peak Flux Deterministic Calculations for the Near Field for Pathway Q2

Radionuclide	Peak Flux (Bq y^{-1})		Time of Peak Flux (y)	
	AMBER	SKB	AMBER	SKB
Ra-226	3E2	4E2	1E6	1E6
C-14	1E3	4E2	1E4	1E4
Cl-36	5E1	6E1	1E4	1E4
I-129	3E1	3E1	1E4	1E4
Ni-59	3E1	3E1	1E5	1E5
Cs-135	4E0	6E0	1E6	1E6

Figure 5 gives the near field releases for the pathway Q3 and Table 20 gives the calculated peak fluxes. These calculations can be compared with those given by SKB in Figure B-4, in the Appendix to the main report. Here the AMBER fluxes are much higher for some radionuclides, suggesting that the way SKB has represented advective flow in the tunnel has not been correctly represented in the AMBER calculations.

Table 20: Peak Flux Deterministic Calculations for the Near Field for Pathway Q3

Radionuclide	Peak Flux (Bq y^{-1})		Time of Peak Flux (y)	
	AMBER	SKB	AMBER	SKB
Ra-226	3E3	1E2	1E6	1E6
C-14	4E3	2E3	2E4	2E4
Cl-36	4E2	2E2	3E4	3E4
I-129	2E2	9E1	3E4	3E4
Cs-135	1E3	9E1	1E6	1E6

Figure 17: AMBER Deterministic Calculations for the Near-Field Flux for the Pinhole Failure Mode at Forsmark: Pathway Q2

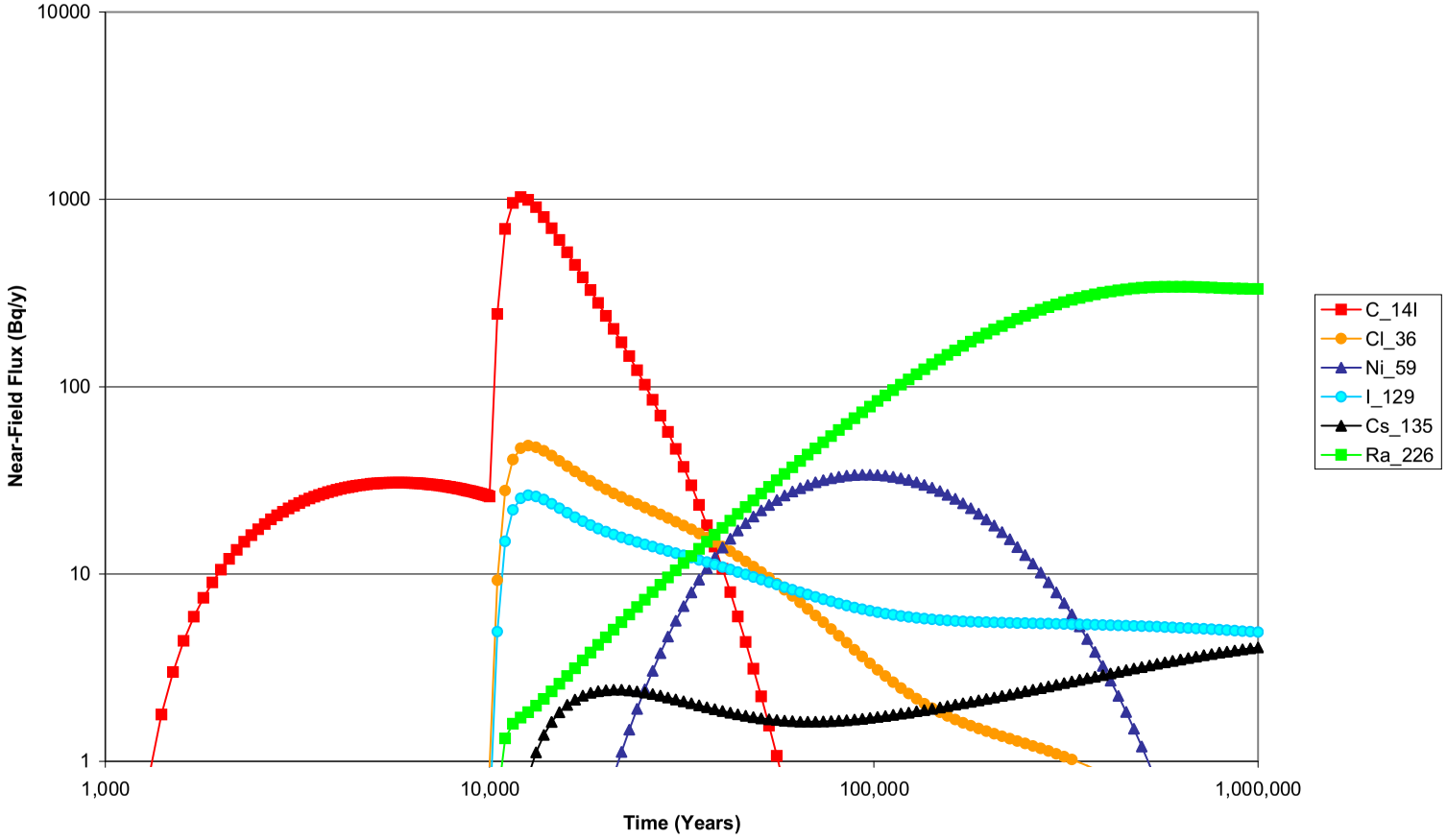

Figure 18: AMBER Deterministic Calculations for the Near-Field Flux for the Pinhole Failure Mode at Forsmark: Pathway Q3

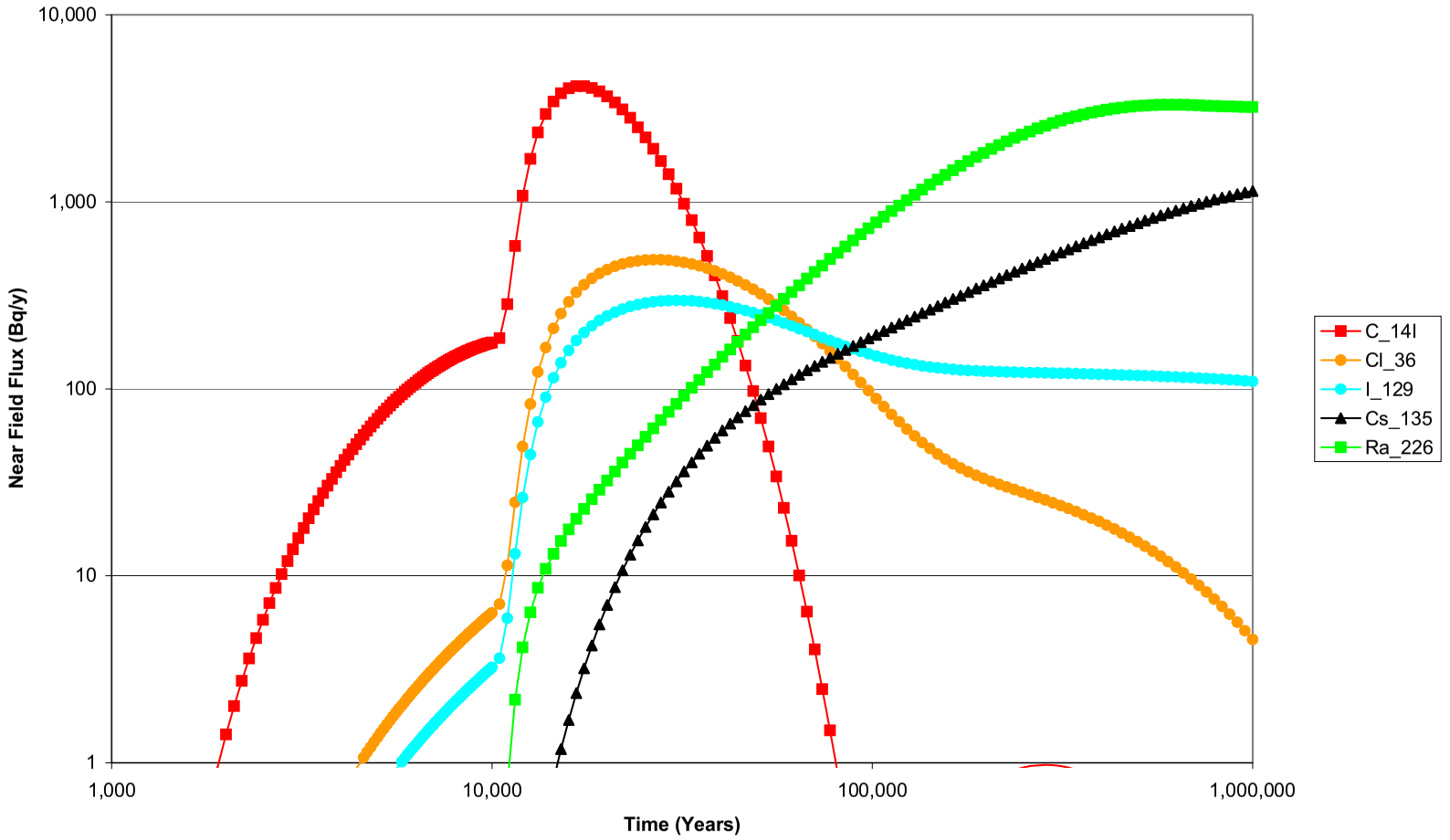

5.1.6 Probabilistic Calculations

Forsmark

Figure 19 shows AMBER probabilistic calculations for the Forsmark site obtained with 4000 samples with just pathway Q1 modelled and with a triangular PDF used for the fuel dissolution rate. The run time for such calculations is about two days. This figure can be compared with Figure 10-20 in the SR-Can main report. The overall features are very similar for times up to about 10^4 y, but at long timescales the AMBER values for the mean and 99th percentile are around an order of magnitude higher than the SR-Can values.

Figure 20 shows the corresponding figure with the use of a log-triangular PDF for the fuel dissolution rates. The calculated doses are typically a factor of 2-3 higher, as would be expected from the discussion in Section 5.1.3. Henceforth all the AMBER calculations shown use a triangle PDF for the fuel dissolution rate except when otherwise indicated.

Figure 21 shows the contribution to the mean dose from the key radionuclides. This figure compares well with Figure 10-18 in the SR-Can main report, although the doses from Ra-226 and Pb-210 are somewhat higher at long times. The Pb-210 dose calculated by AMBER is not obtained in the SR-Can calculations because, as previously noted, SKB do not model this radionuclide in the near field and geosphere; it is not clear that this will necessarily be an appropriate approximation for all possible parameter values in probabilistic calculations.

In Figure 10-19 of the SR-Can main report SKB gives dose calculations based on fluxes from the near field. Corresponding AMBER calculations are given in Figure 22, and it can be seen that the results compare very closely.

Figure 19: AMBER Probabilistic Calculations for Biosphere Doses for Forsmark (triangular PDF for fuel dissolution rate)

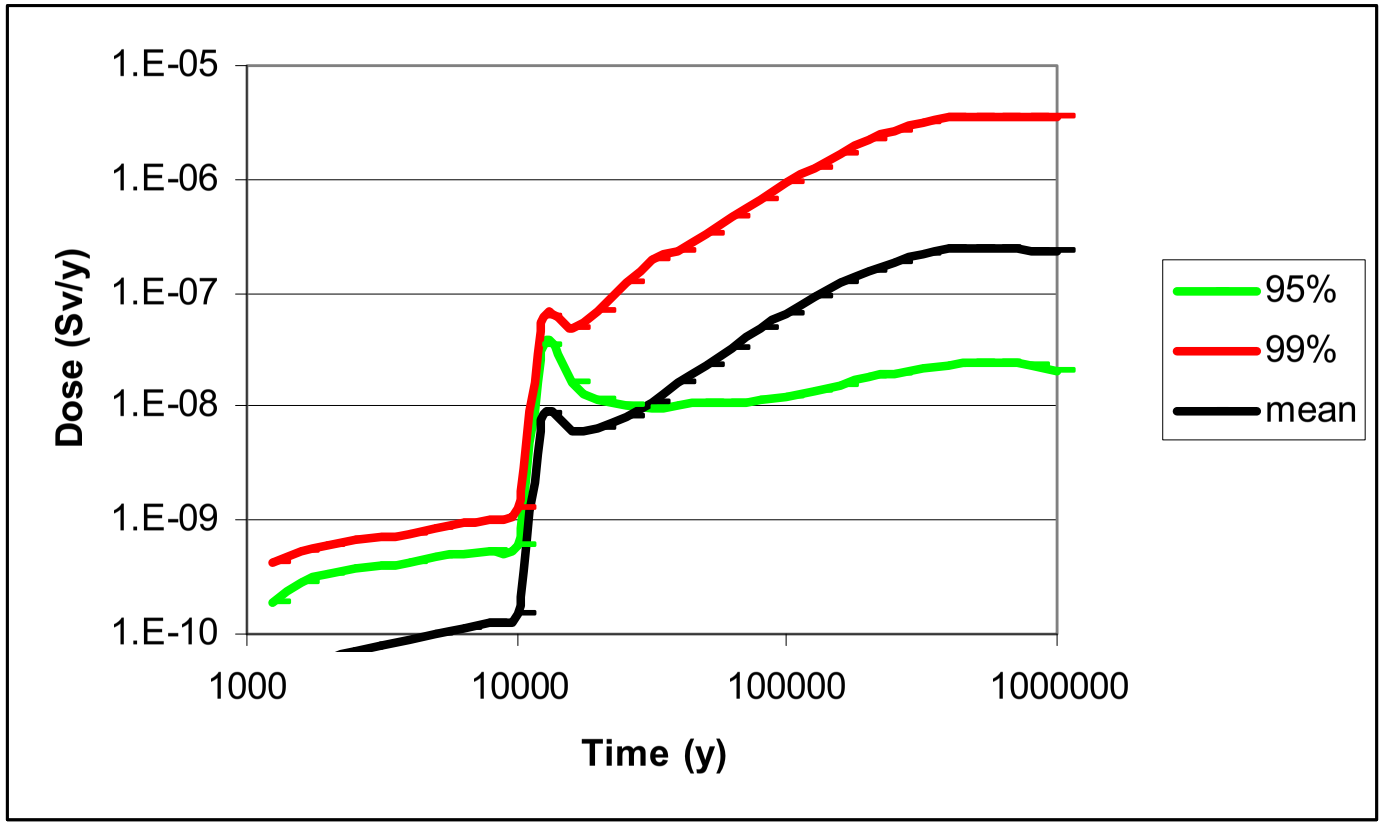

Figure 20: AMBER Probabilistic Calculations for Biosphere Doses for Forsmark (log-triangular PDF for fuel dissolution rate)

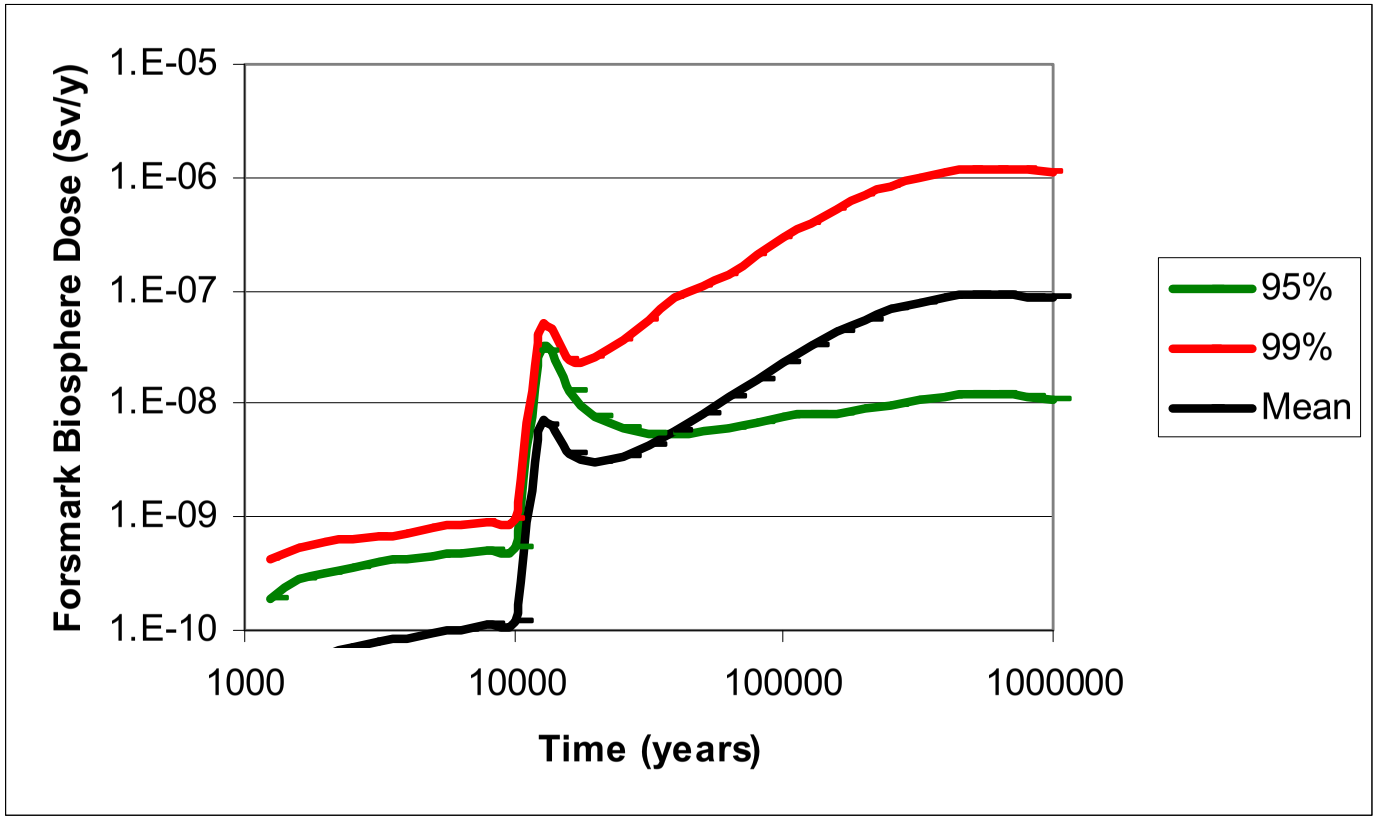

Figure 21: AMBER Probabilistic Calculations for Biosphere Doses for Forsmark for Pathway Q1 - Key Radionuclides (log-triangular PDF for fuel dissolution rate)

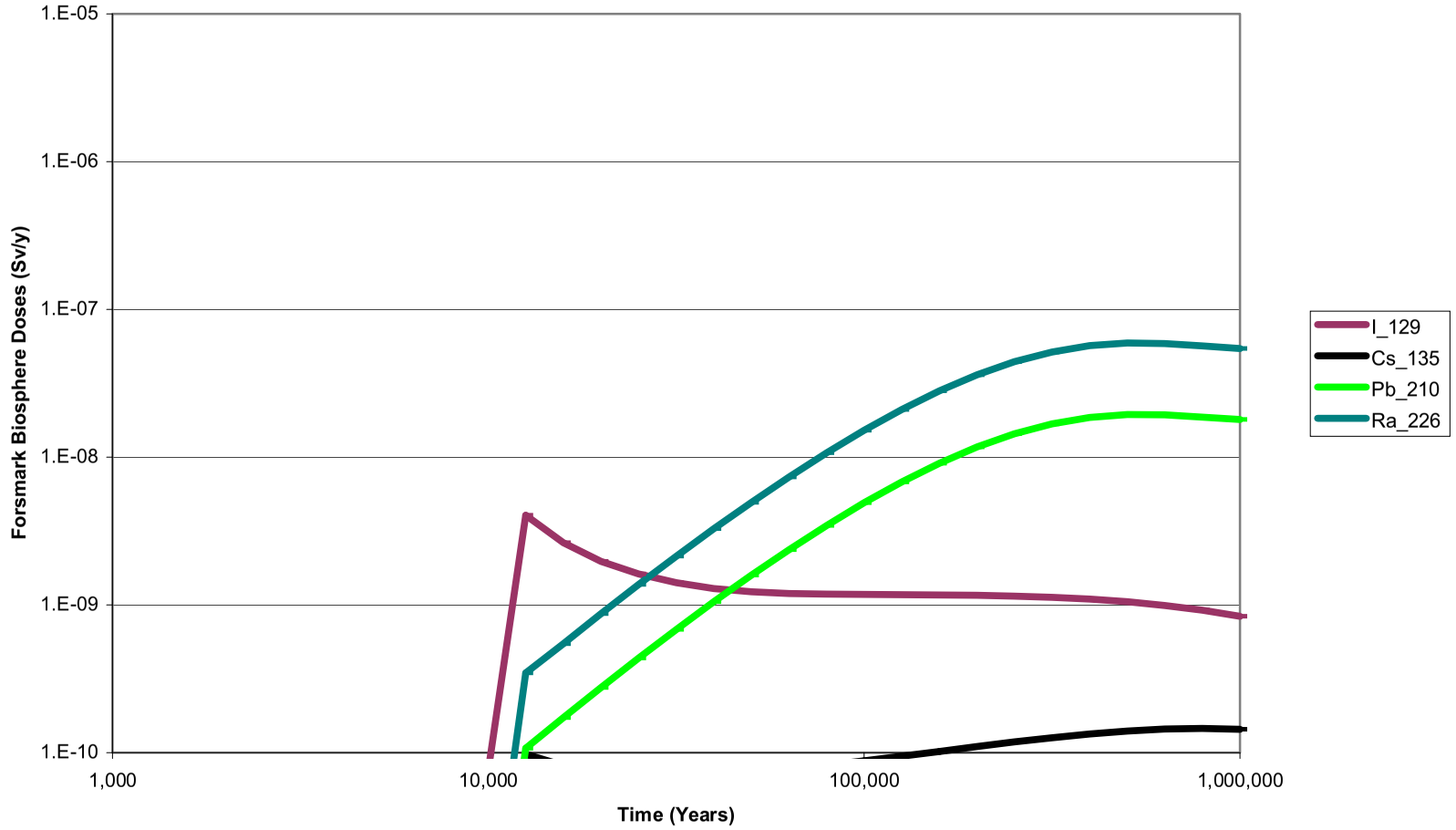

Figure 22: AMBER Probabilistic Calculations for Near Field Biosphere Doses for Forsmark for Pathway Q1 (log-triangular PDF for fuel dissolution rate)

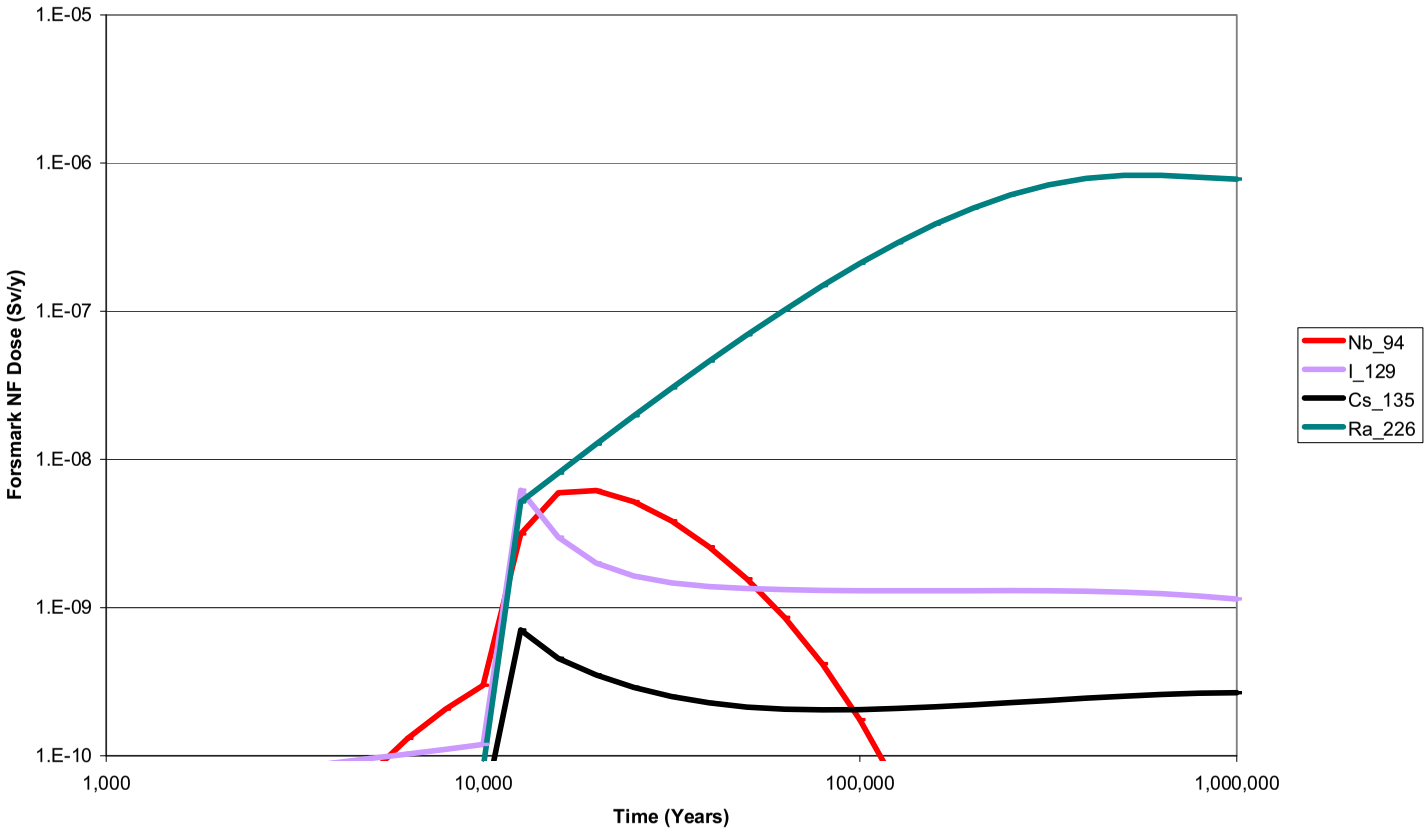

The runs giving the 5 highest geosphere doses at a million years are summarised in Table 21.

Table 21: Characteristics of the Five Runs with Highest Doses for Calculations using the SKB Geosphere Data

Quantity	Units	Run Number				
		643	**1369**	**1515**	**2207**	**3216**
Dose at 1E6 y	Sv y^{-1}	2E-4	6E-5	5E-5	5E-5	5E-5
Dose at 1E6 y without Pb/Po	Sv y^{-1}	3E-5	7E-6	6E-6	4E-5	2E-5
Q_{eq} (SKB input file)	m^3 y^{-1}	2E-2	9E-3	2E-3	7E-4	6E-3
Q_{eq} with spalling (calculated)	m^3 y^{-1}	5E-1	0.58	0.12	4E-2	0.18
F	y m^{-1}	378	236	5280	4250	2400
t_w	y	1.3	1.1	7.1	1.2	6.8
Fracture half aperture, b	m	4E-3	5E-3	1.4E-3	2.7E-3	2.8E-3
Fracture velocity, v	m y^{-1}	376	439	70	44	74
K_d for Ra in rock	kg m^{-3}	0.2	2.4	0.2	6E-3	5E-2

As would be expected, the high dose runs have relatively high equivalent flow rates at the buffer/fracture interface, low geosphere travel times and low transport resistances compared with the overall population of runs; this can be seen by comparing the parameter values in Table 21 with the distributions shown later in this section.

For these high dose runs, the calculated contribution from Pb-210 and Po-210 is dominant. As previously discussed, SKB do not model the transport of Pb-210 in the near field and geosphere.

Figure 23 to Figure 25 show some scatter plots to indicate the range of the three correlated 'data triple' parameters and how these influence the calculated doses. Regression lines are shown on these figures simply to give a general indication of the trends. The direction of these trends is what would be expected, but the regression coefficients are low. It is only when there is a combination of high equivalent flow rate at the buffer/fracture interface, low geosphere travel times and low transport resistance that relatively high doses are calculated.

Figure 23: Scatter Plot of Dose at 1E6 y against Geosphere Travel Time for Calculations using the SKB Geosphere Data

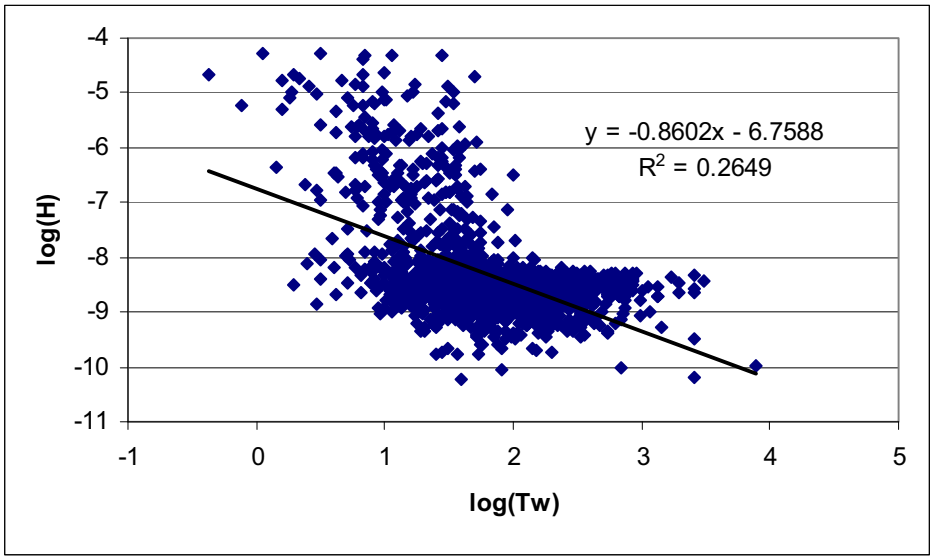

Figure 24: Scatter Plot of Dose at 1E6 y against Geosphere Transport Resistance for Calculations using the SKB Geosphere Data

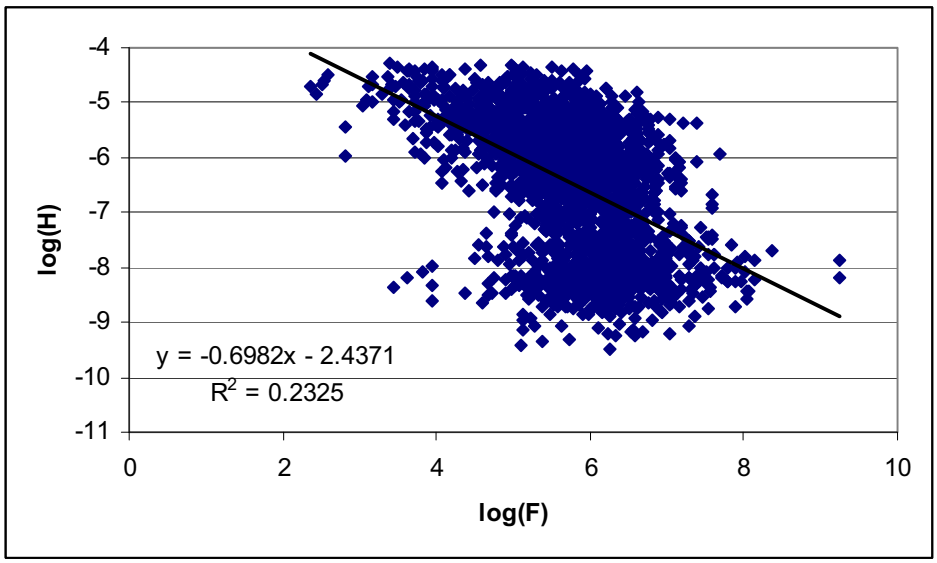

Figure 25: Scatter Plot of Dose at 1E6 y against Calculated Equivalent Flow Rate for Calculations using the SKB Geosphere Data

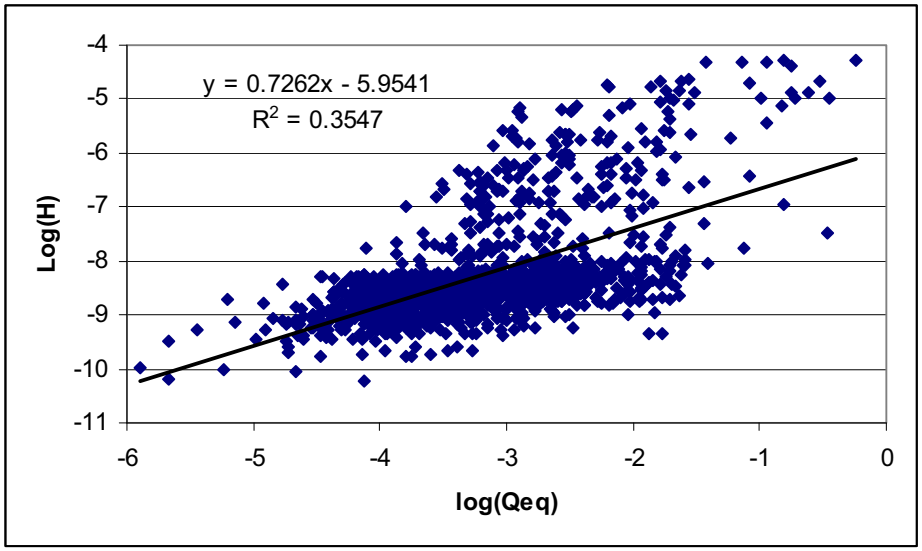

Figure 26 shows how the dose calculated using the flux from the near field varies with the equivalent flow rate for the deposition hole (pathway Q1). Runs with negligible flows for pathway Q1 have been omitted. There are effectively two populations: those where the doses derive from pathway Q1, and those that derive from pathway Q2 and/or Q3.

Figure 26: Scatter Plot of Near Field Dose at 1E6 y against Calculated Q1 Equivalent Flow Rate for Calculations using the SKB Geosphere Data

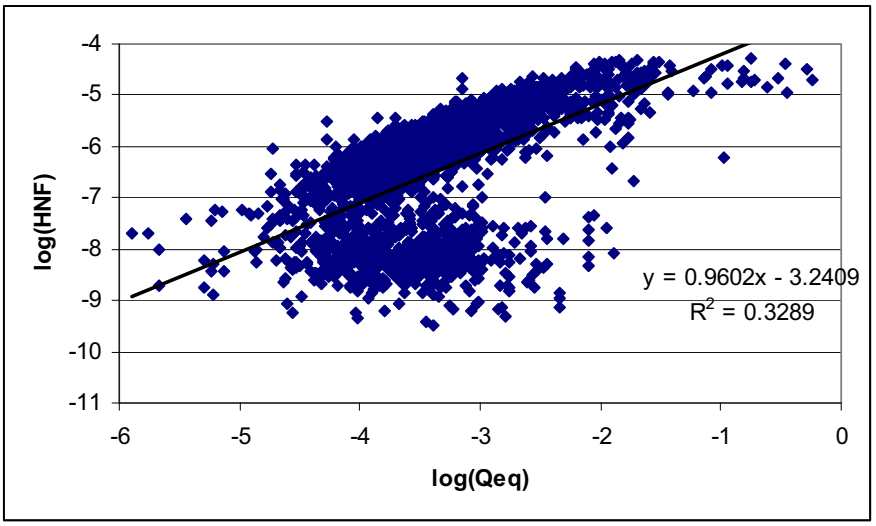

Figure 27 gives the corresponding calculation with only the doses deriving from the Q1 pathway being considered. Here the residual scatter is mainly due to the two orders of magnitude of uncertainty in the fuel dissolution rate.

Figure 27: Scatter Plot of Near Field Dose due to Pathway Q1 at 1E6 y against Calculated Q1 Equivalent Flow Rate for Calculations using the SKB Geosphere Data

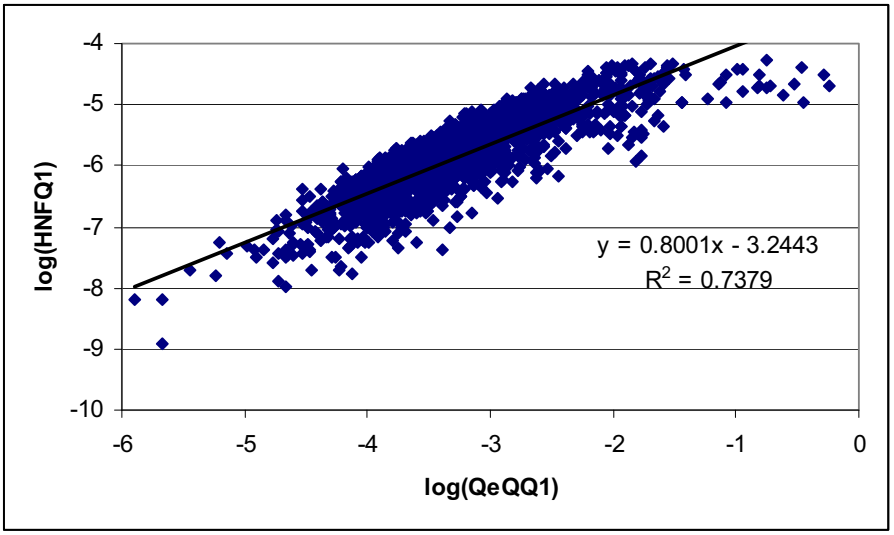

Laxemar

Figure 28 shows AMBER probabilistic calculations for the Laxemar site obtained with 4000 samples with just pathway Q1 modelled; the run time for such calculations is about two days. This can be compared with Figure 10-22 in the SR-Can main report. There are detailed differences between the AMBER and SKB calculations but the overall features are very similar. AMBER calculates somewhat higher doses at long times. Figure 29 shows the contribution to the mean dose from the key radionuclides.

In Figure 10-21 of the SR-Can main report SKB gives dose calculations based on fluxes from the near field. Corresponding AMBER calculations are given in Figure 30, and it can be seen that the results compare very closely.

Figure 28: AMBER Probabilistic Calculations for Biosphere Doses for Laxemar (log-triangular PDF for fuel dissolution rate)

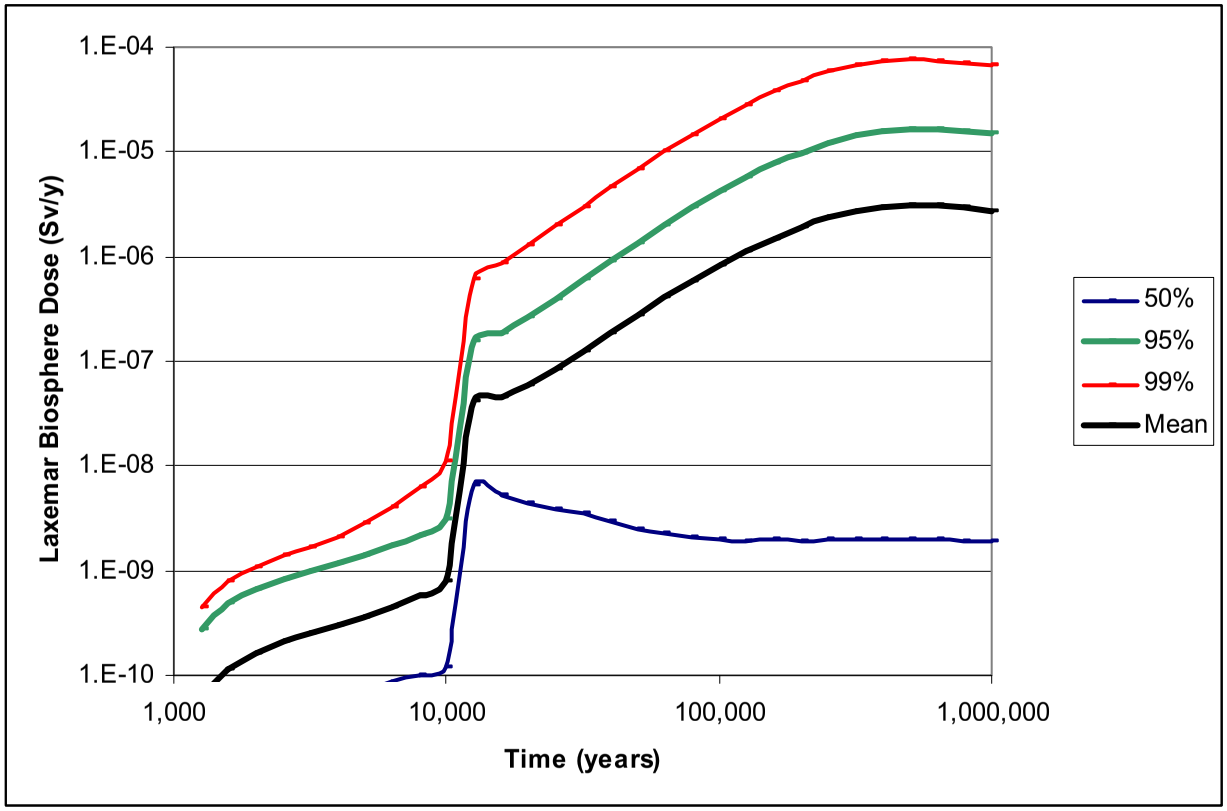

Figure 29: AMBER Probabilistic Calculations for Laxemar for Pathway Q1- Key Radionuclides (log-triangular PDF for fuel dissolution rate)

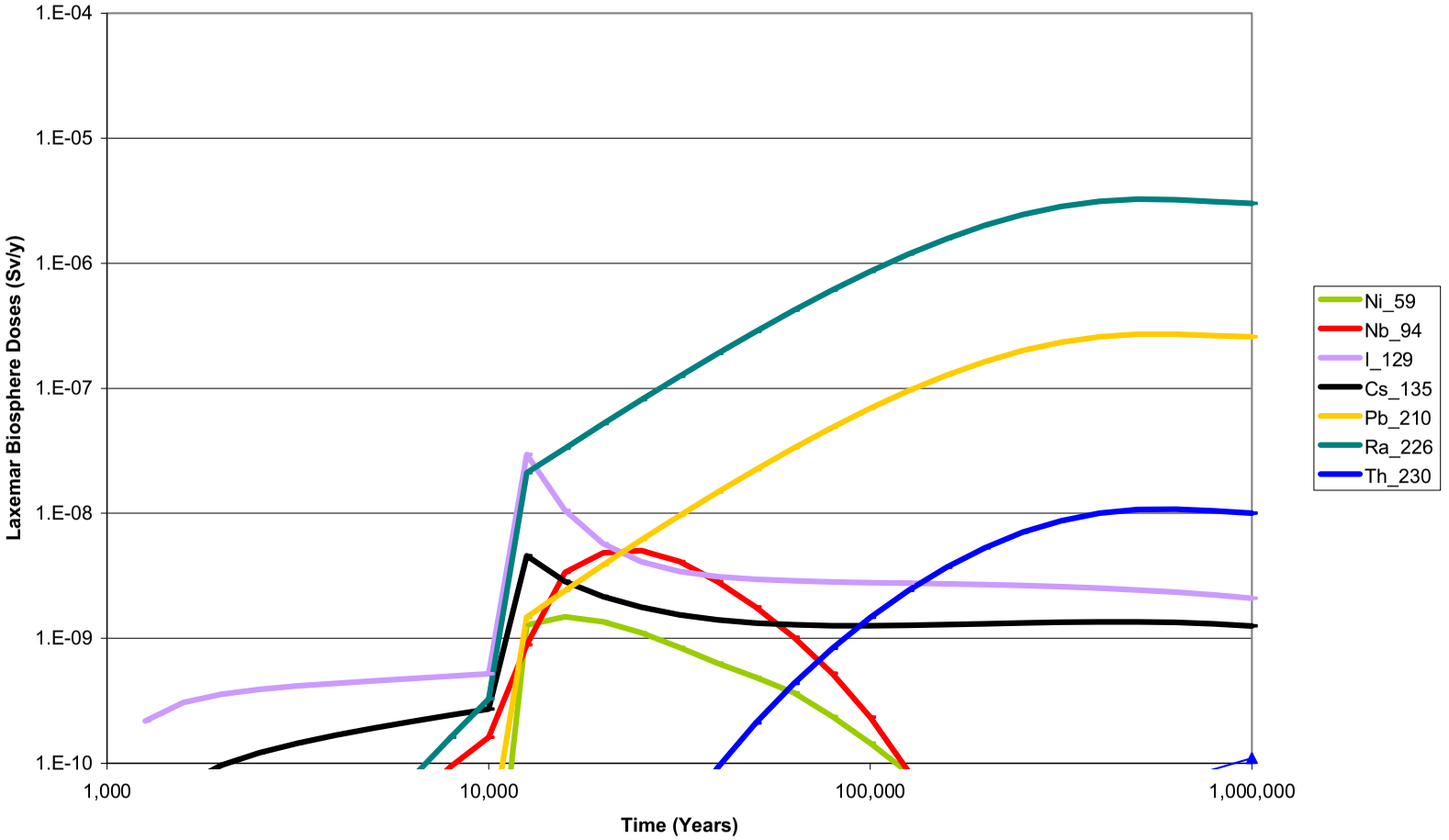

Figure 30: AMBER Probabilistic Calculations for Near Field Biosphere Doses for Laxemar for Pathway Q1 (log-triangular PDF for fuel dissolution rate)

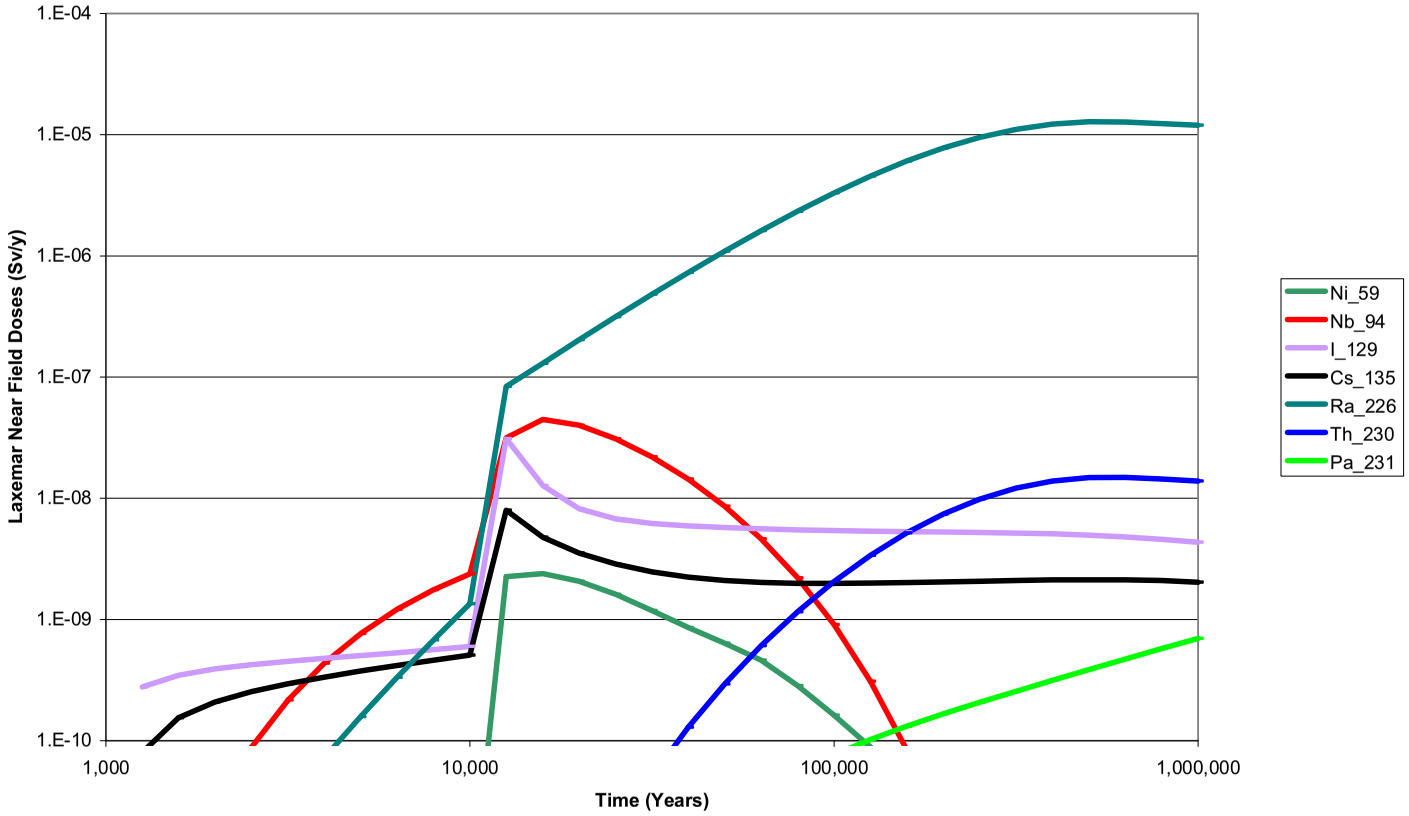

5.2 The Lost Buffer Failure Mode

In this failure mode the canister is assumed to fail at a calculated time (see the discussion in Section 3.3) and there is then an additional delay before the resistance to radionuclide transport from the canister is assumed to fall to zero. The calculations for this failure mode are actually much simpler and quicker to reproduce in AMBER than for the pinhole failure mode because there is no radionuclide transport in the buffer.

5.2.1 Deterministic Calculations

Table 22 gives values of the parameters that were employed that differ from the values used for the pinhole scenario in Table 16. It should be noted that SKB spread the period over which the instantaneous release fractions for Ni-59 and Nb-94 left the canister once failure occurred. This change has not been reproduced in the AMBER calculations.

The calculations reported in the main SR-Can report are for a high equivalent flow rate, Q_{eq}, although this is not made clear in the documentation, and no value is given. SKB's deterministic calculations consider fluxes from the near field only; it would have been helpful to report in addition quantities depending on the far field flux.

Figure 31 compares well with Figure 10-40 in the SR-Can report, but there are detailed differences. The SR-Can calculations have no contributions from long-lived fission products such as Cs-135, I-129 and Sn-126; the AMBER calculations have small contributions from these radionuclides. This may be an error because Figure 10-41 does have a contribution from Cs-135.

Figure 10-41 of the SR-Can report gives modified (analytical) calculations with Th retained in the canister, and these are compared with the full numerical calculation in Figure B-1. SKB indicate in Section 10.6.5 of the SR-Can report that radionuclide in-growth is not included for this failure mode (although it is not clear why). As a result, if co-precipitation of Th occurs in the canister, more Ra-226 will be released. This is an example of where it is not straightforward to identify conservative assumptions in systems as complex as the one being modelled here. Effectively reducing the solubility of Th results in higher doses, which may not necessarily have been expected. This illustrates the importance of undertaking systematic sensitivity studies without preconceptions about whether particular parameter combinations are conservative or optimistic choices.

AMBER calculations were undertaken where the solubility of all Th isotopes has been reduced to effectively zero and the resulting calculations in Figure 32 are similar, but

not identical to the SKB calculations in Figure 10-41 of the SR-Can report; in general the AMBER calculations are closer to the SKB numerical calculations than to the analytical calculations. The AMBER calculations show an increase in the dose from Ra-226, presumably because when the radionuclide is released from the canister rather than as a result of in-growth in the geosphere, there is less decay in the rock matrix. The Pb-210 dose also increases in the AMBER calculations, but there appears to be no change in the analytical SR-Can calculations for this radionuclide, and it is absent in the numerical calculations.

Table 22: Data Values for the Lost Buffer Scenario Calculations

Parameter/Units	Definition	Deterministic value	PDF	Comments
F (y m^{-1})	Geosphere transport resistance	Assumed to be the same as for the pinhole case.	Values given in Table 10-10 of SR-Can main report for Forsmark	
$Q_{eq\ (}$m^3 y^{-1})	Equivalent flow rates at the deposition hole	1.0 m^3 y^{-1} for Q1 (not specified in SR-Can documentation)	Values given in Table 10-10 of SR-Can main report for Forsmark	
S (mol m^{-3})	Solubility limit	Median values of PDF	Sample file provided by Hedin (2007b)	SKB assumed U remains precipitated but all other elements are not solubility limited.
t_{large} (y)	Time of loss of transport resistance from canister	1E5 y	Triangular (1000, 1E5, 1E5) years after t_{min}	
t_{min} (y)	Time when radionuclide transport is initiated.	1E5 y	Values given in Table 10-10 of SR-Can main report for Forsmark	
t_w (y)	Geosphere travel time	Assumed to be the same as for the pinhole case.	Values given in Table 10-10 of SR-Can main report for Forsmark	

Figure 31: Deterministic Calculations for Forsmark for the Advective Failure Mode (log-triangular PDF for fuel dissolution rate)

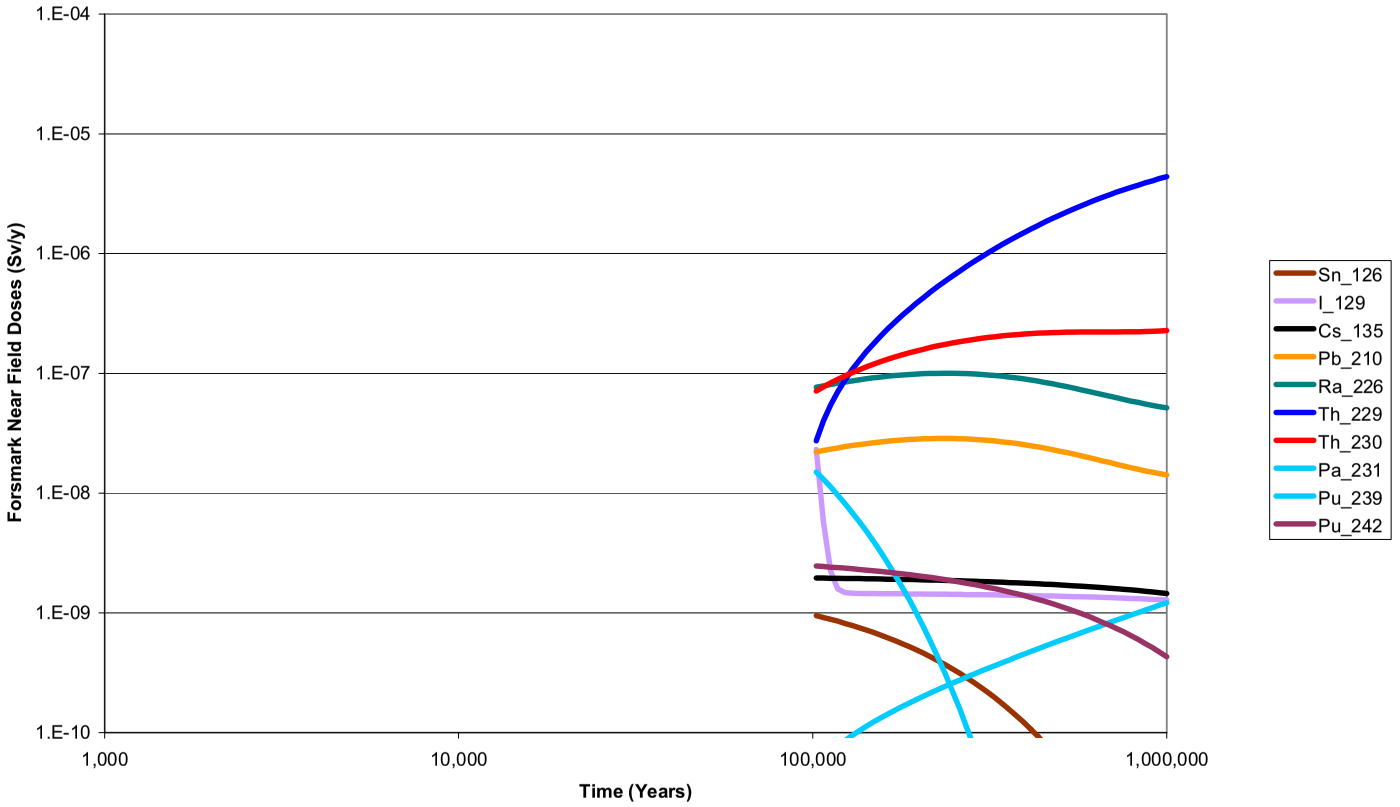

Figure 32: Deterministic Calculations for Forsmark for the Advective Failure Mode with Th retained in the Canister

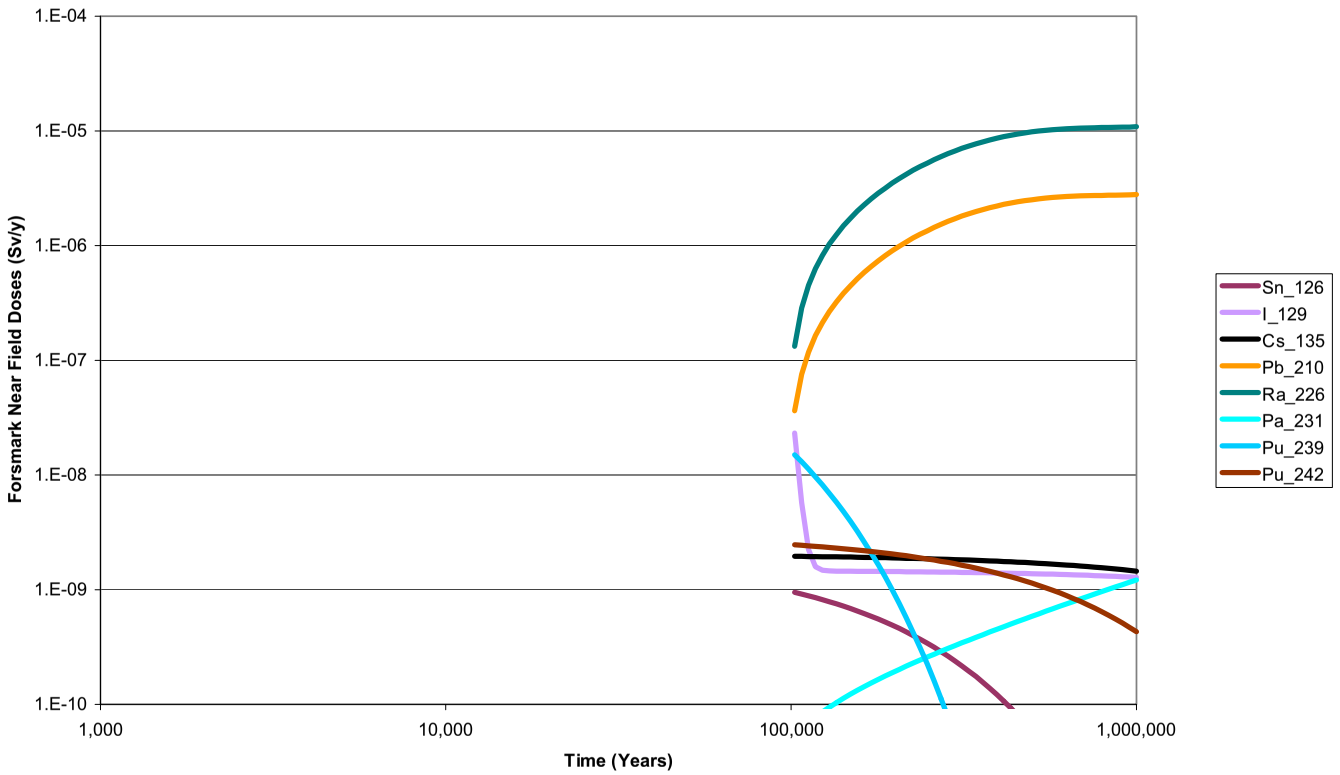

5.2.2 Probabilistic Calculations

Based on the discussion given in Appendix B, it appears that SKB's probabilistic calculations for the lost buffer failure mode use the alternative model where Th-230 is retained in the canister, but this is not totally clear.

Just 10 'triples' for the correlated hydrogeological parameters F, t_w, and Q_{eq} are given for this failure mode in Table 10-11 of the main SR-Can report. The AMBER calculations take 10 failed canisters in each run for one set of transport calculations.

The AMBER calculations shown in Figure 33 were undertaken with 4000 samples. They compare well with Figure B-2 and Figure 10-42 in the SR-Can report, but there are the following detailed differences:

- The AMBER calculations give slightly higher doses for Cs-135.
- The SKB calculations do not consider Pb-210.

Both the SKB and AMBER calculations show fluctuations in the calculated doses that may be due to the calculations of the mean values not having fully converged.

Figure 33: Probabilistic Calculations for Forsmark for the Advective Failure Mode with Th retained in the Canister (log-triangular PDF for fuel dissolution rate)

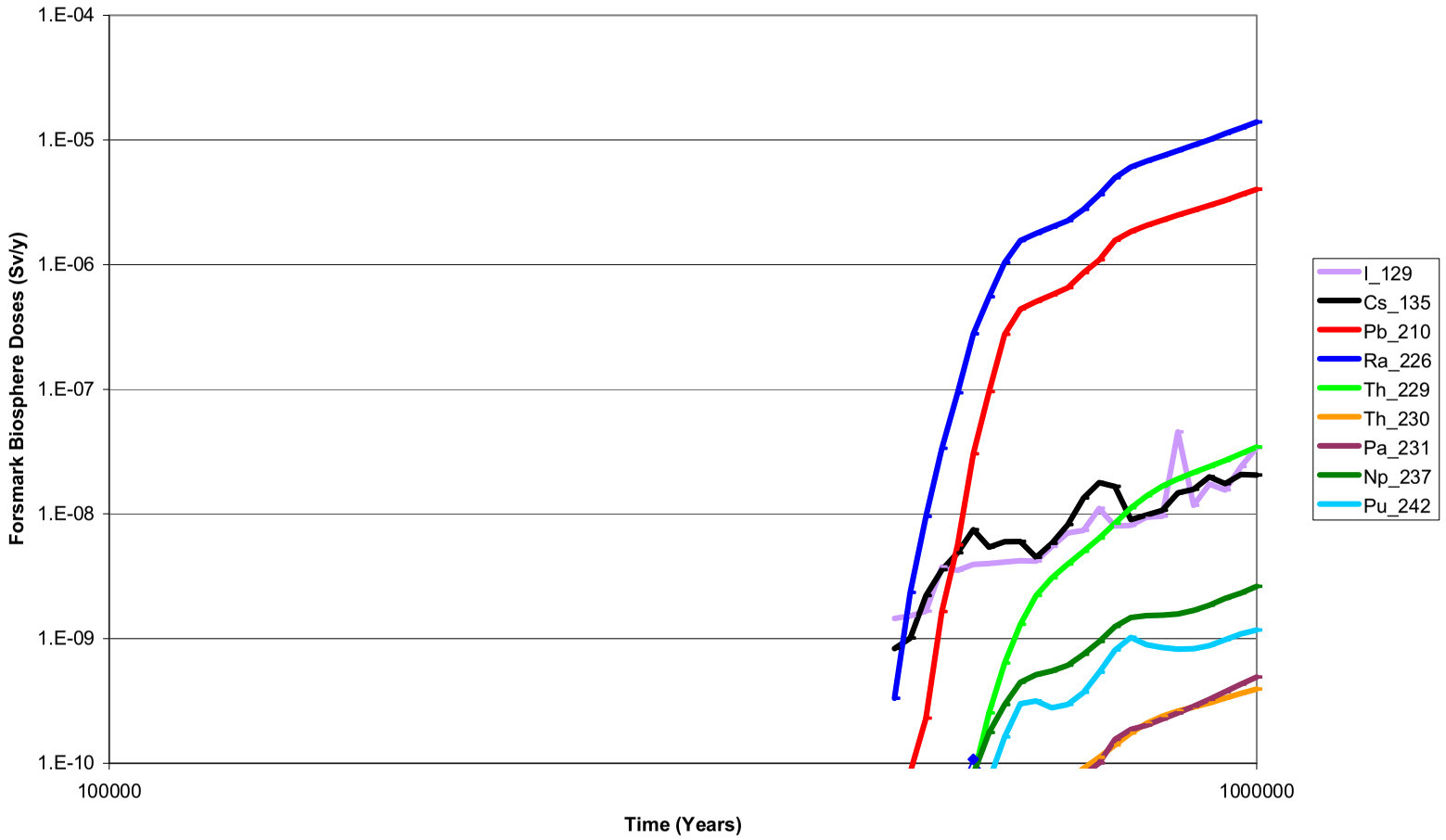

5.2.3 Discussion

The risks calculated from this failure mode depend critically on two key inputs: the calculated canister failure times and the assumed fuel dissolution rate. The calculation of the failure times is discussed in Section 3.3. The first failure time calculated by SKB is not until nearly 500, 000 years at Forsmark. By this time most of the original inventory has decayed, and this is the main reason why the calculated risks are compatible with the relevant regulatory criterion; this is a key part of SKB's overall case.

The dependence of calculated mean doses on the value of the fuel dissolution rate is shown in Figure 10-44. Dissolution rates greater than around 1E-5 y^{-1} do not significantly increase doses as this corresponds to the timescale for which radionuclide transport can take place.

5.3 Mechanical Failure Modes

5.3.1 Shear Movement Failure

Figures 10-50 and 10-51 in the main SR-Can report give calculations for this failure mode. The key assumptions in the modelling are:

- The failure is assumed to be effectively instantaneous, so that the parameters in the AMBER model t_{min} (y) and t_{large} (y) have the same value.
- The lateral thickness of the buffer is reduced from 35 cm to 20 cm.
- A high equivalent flow rate is assumed of 1 $m^3\ y^{-1}$.
- A uniform distribution for the probability of a canister failing is assumed between 0 and a million years, with different cumulative probabilities for the two sites.

AMBER calculations have not been undertaken to reproduce the SR-Can calculations, because it is considered that little additional insight would be gained beyond that obtained for the pinhole and adjective failure modes; the risk calculations depend primarily on the probabilities assumed for the event happening. However, independent calculations, possibly with different underlying assumptions could be useful (see Section 7).

5.3.2 Isostatic Load Failure Mode

As discussed in SR-Can Section 10.8, the consequences of this failure mode can be assessed for the calculations produced for the pinhole failure mode. No additional AMBER calculations have therefore been undertaken.

5.4 Summary

Radionuclide transport calculations using the AMBER code have produced very similar results to those reported by SKB at Forsmark. However, this required a considerable amount of effort because of the need to check with SKB a large number of areas where the information provided in the SR-Can documentation was either incorrect or missing. These include:

- SKB did not make it clear that the reported deterministic calculations for the pinhole scenario were for the Forsmark site.
- The SR-Can documentation does not make it clear what chemical form was assumed for C-14 in the radionuclide transport calculations.
- The description of the probability density function for rock sorption coefficients in Table 10-3 of the main SR-Can report is erroneous: as confirmed by SKB, piecewise uniform distributions were actually used.
- The matrix diffusion depth used in deterministic calculations is not that which is implied in the SR-Can report: SKB has indicated that the value used was 0.02 m, rather than the peak of the probability density function (10 m).
- The details of the inclusion of advective flow in the tunnel in the near field calculations using COMP23 appear not to be given in the SR-Can documentation. Overall, the documentation for the way that the COMP23 code has been used to undertake the near field calculations appears to be incomplete.
- The values of radionuclide solubilities used in deterministic calculations were not provided in the SR-Can documentation. In addition, it was only after the solubilities data file used in probabilistic calculations was provided by SKB that satisfactory comparisons could be achieved with the probabilistic calculations for the pinhole failure mode; it would not be possible for a third party to reproduce these calculations without the additional information given in the solubilities data file.

- Data 'triples' are used for the correlated hydrogeological parameters F, t_w and Q_{eq}. It was only after the file used by SKB for these parameters in probabilistic calculations that satisfactory comparisons between the two sets of calculations could be achieved; again, it would not be possible for a third party to reproduce these calculations without the additional information given in the solubilities data file.

- The precise approach employed by SKB to represent the selection of data values for correlated sorption coefficients is not clear from the SR-Can documentation.

- The deterministic calculations reported for the lost buffer failure mode employ a high equivalent flow rate, Q_{eq}, although no value is given.

- Based on the discussion given in Appendix B, it appears that SKB's probabilistic calculations for the lost buffer failure mode use the alternative model where Th-230 is retained in the canister, but this is not totally clear.

Insufficient deterministic calculations are given by SKB to enable the reader to understand the key issues presented and to facilitate the reproduction of SKB's calculations by a third party. It is suggested that for each set of probabilistic calculations undertaken in support of comparisons with regulatory criteria, a deterministic case should be documented to illustrate the key points.

The independent radionuclide transport calculations have illustrated how the consideration of individual high consequence runs can provide insight into results obtained using probabilistic calculations. It is suggested that SKB should consider doing this in future assessments.

6 Radionuclide Transport Calculations Using Independent Geosphere Data

6.1 Background

SKB's radionuclide calculations considered in Section 5 depend critically on the discrete fracture network (DFN) flow and transport calculations undertaken for the two sites. SKI is funding independent DFN calculations to be undertaken by Clearwater Hardrock Consulting. Dedross et al. (2006) have shown how output from

such calculations can be visualised, using bespoke software developed for that purpose, and used to provide input to AMBER radionuclide transport calculations.

Geier (2007) describes a set of independent DFN calculations that have been undertaken for the two sites. Output files for the Forsmark sites, with and without spalling, have been produced. These calculations consider only the Q1 pathway through the deposition hole.

6.2 Data Triples

In the SR-Can calculations described in Section 5 use is made of 'data triples' that define the important characteristics of path: the equivalent flow rate at the deposition hole, Q_{eq} ($m^3\ s^{-1}$), the integrated F ($s\ m^{-1}$) value and the total travel time t_w (s). Corresponding information is provided by the independent DFN calculations; the integrated F value and travel time are given directly at the end of the particle path data files, and the equivalent flow rate can be calculated from information on Q, the total flow around the deposition hole (in SKB (2006b) the flow rate q corresponds to Q in the present notation).

The equivalent flow rate for a deposition hole is given by SKB to be:

$$Q_{eq} = 4W\sqrt{\frac{D_w L q \varepsilon_f}{\pi}}\ . \qquad 6.1$$

W (m) is the distance of interest perpendicular to the fracture plane;

D_w ($m^2\ s^{-1}$) is the diffusivity of water;

L (m) is the relevant contact length with the buffer in the direction of groundwater flow;

q ($m\ s^{-1}$) is the Darcy velocity; and

ε_f (-) is the flowing porosity of the fractured rock.

Equation 6.1 is only valid if W contains at least one fracture on average.

For Forsmark SKB take W to be the canister height (5 m), L is half the circumference of the deposition hole (2.8 m), D_w has a value of 0.0316 $m^2\ y^{-1}$, and ε_f has a value of 5E-6.

With the low fractured rock porosity taken by SKB, if the separation between fractures is W (so that there is just one fracture in the flow region of interest), this would give a fracture aperture of 2.5E-5 m.

The Darcy velocity can be estimated from

$$q = Q / A, \qquad 6.2$$

where A is the relevant 'capture' area perpendicular to the flow, taken to be 12.8 m^2, as in Section 5.1.2, although it is not clear that this is necessarily the appropriate value to employ.

When spalling is considered in the calculations SKB include an additional contribution to the equivalent flow rate as given in equation 5.11. The following expression has been used corresponding to equation 5.12:

$$Q_{eq}^{spall} = 0.091\sqrt{q}\,. \qquad 6.3$$

Here the constant term 0.091 has units of m$^{5/2}$ y$^{-1/2}$.

Based on the above discussion, the following specification has been used for Q_{eq} when using alternative 'data triples' for 1D radionuclide transport calculations in the geosphere:

- In the absence of spalling equations 6.1 and 6.2 are used together with the parameter values employed by SKB, subject to the constraint that $Q_{eq} \le Q$. The flow rate Q is obtained directly from the DFN output files.
- In the presence of spalling an additional contribution to Q_{eq} is obtained from equations 6.2 and 6.3.

6.3 Calculations without Spalling

The calculations in this section are for zone A-C of the Forsmark repository without inclusion of spalling effects on the equivalent flow rate.

Figure 34 can be compared with Figure 19 and Figure 20 where the SKB geosphere 'data triples' were employed.

Figure 34: Doses Calculated using Independent DFN Data (No Spalling)

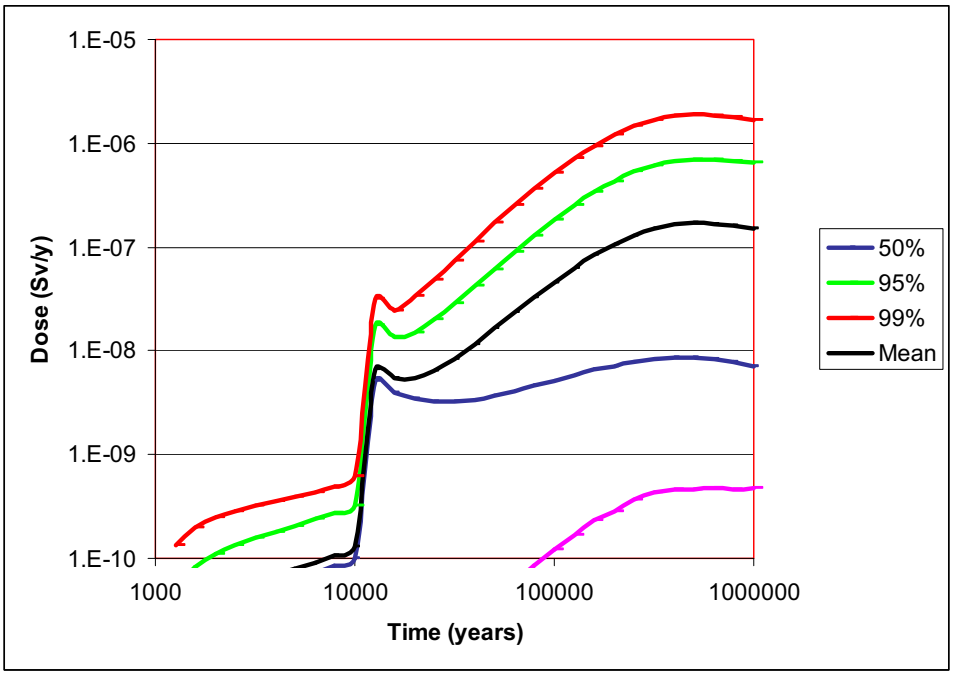

The 99th percentile dose is very similar but the mean and 95th percentile are higher. More of the deposition holes had significant flows through them than in the SKB case, so here calculations can be seen for the 5th and 50th percentiles; these do not appear in the calculations using the SKB data triples.

Figure 35 gives the corresponding calculations with contributions from Pb-210 and Po-210 omitted. As expected, the 99th and 95th percentiles are reduced due to the contributions from these radionuclides with very short geosphere transport times, but the mean value is little changed.

Figure 35: Doses Calculated using Independent DFN Data (No Spalling) omitting Pb-210/Po-210

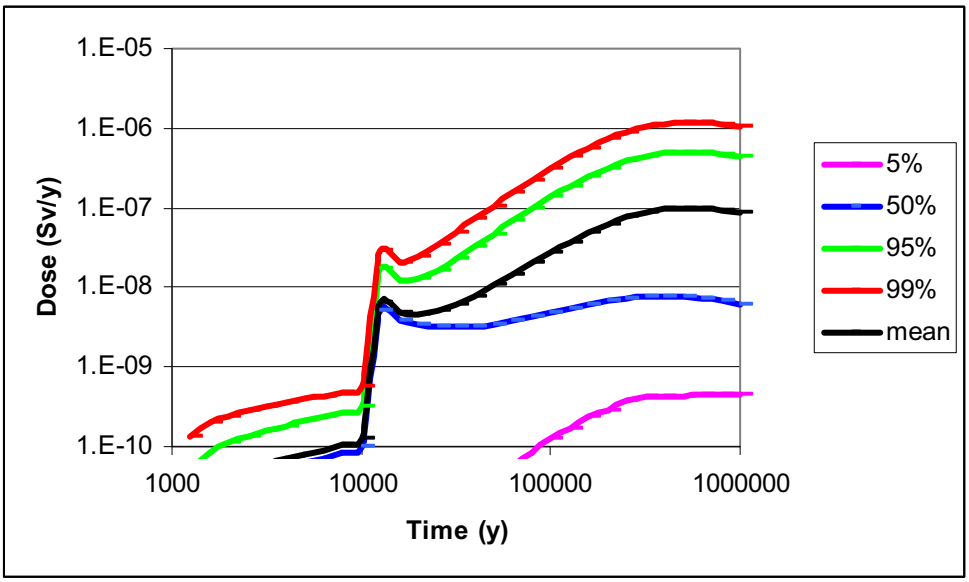

A scatter plot of the calculated doses at 1E6 y against the equivalent flow rate in the deposition hole showed no real pattern. Figure 36 and Figure 37 give the scatter plots for geosphere travel time and transport resistance. The range of transport resistances is similar to that found in the SKB calculations of Section 5.1.6 but the calculations shown here have a much larger fraction of very short (less than 10 years) geosphere travel times.

Figure 36: Scatter Plot of Dose at 1E6 y against Geosphere Travel Time for Calculations using the Independent DFN Data (no spalling)

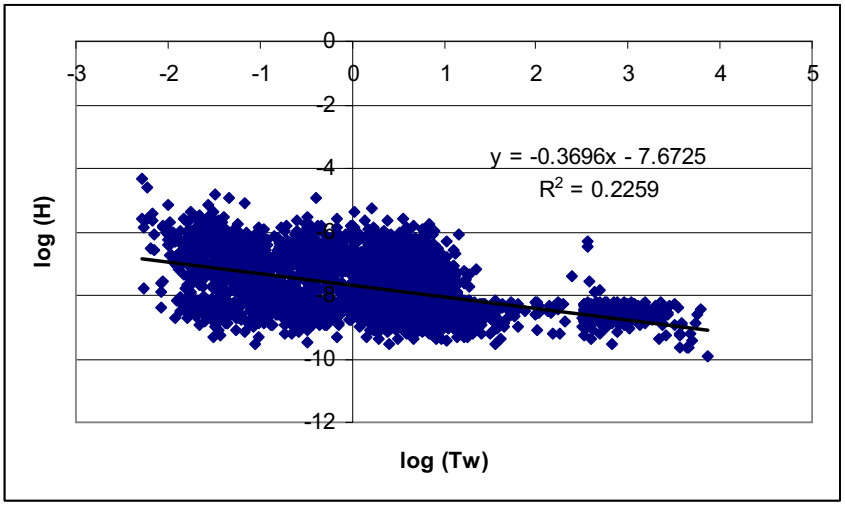

Figure 37: Scatter Plot of Dose at 1E6 y against Geosphere Transport Resistance for Calculations using the Independent DFN Data (no spalling)

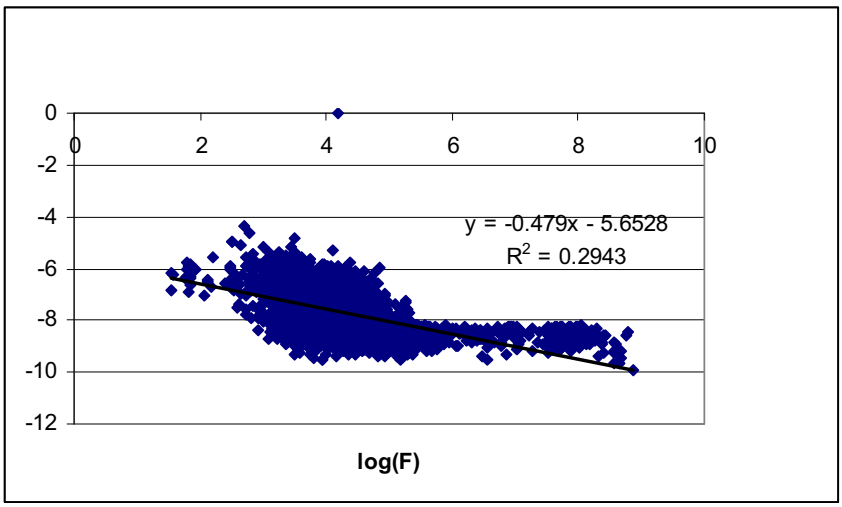

The runs giving the 5 highest geosphere doses at a million years are summarised in Table 23. Compared with the calculations using SKB data, much smaller fracture apertures are calculated, corresponding to the much smaller geosphere transport times.

Table 23: Characteristics of the Five Runs with Highest Doses for Calculations using Independent DFN Data (no spalling)

Quantity	Units	Run Number				
		1372	913	3682	395	2639
Dose at 1E6 y	Sv y^{-1}	5e-5	3e-5	2e-5	1e-5	1e-5
Q_{eq} (SKB input file)	m^3 y^{-1}	6E-4	6e-4	3e-4	1e-4	8e-5
F	y m^{-1}	516	601	3240	317	311
t_w	y	5E-3	6e-3	3e-2	4.7e-2	4e-1
Fracture half aperture, b	m	1E-5	1e-5	1e-5	1.5e-4	1.3e-3
Fracture velocity, v	m y^{-1}	9.7E4	8.32e4	1.54e4	1.07e4	1.25e3
K_d for Ra in rock	kg m^{-3}	3.4	0.17	0.10	2.65	3.1

There is a stronger correlation between the dose calculated with the flux from the near field and the equivalent flow rate than was observed in Section 5.1.6, as can be seen in Figure 38.

Figure 38: Scatter Plot of Near Field Dose at 1E6 y against Equivalent Flow Rate for Calculations using the Independent DFN Data (no spalling)

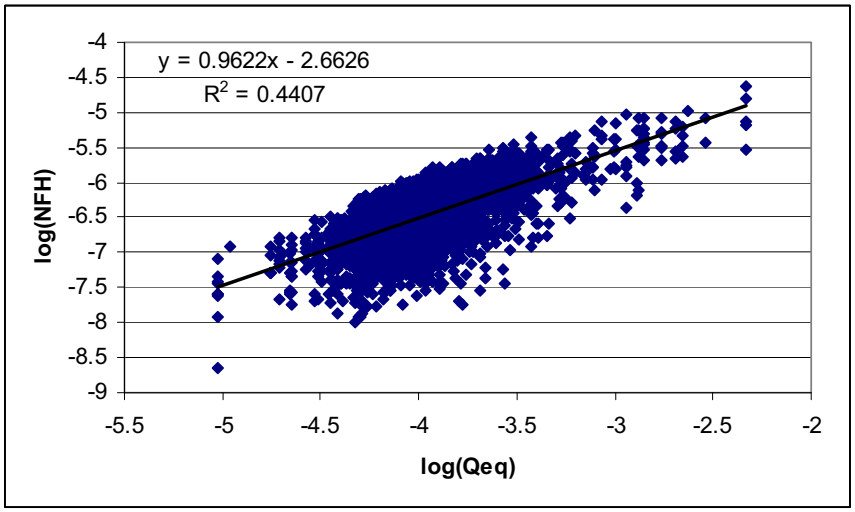

Again, the residual spread is largely explained by the two orders of magnitude variation in fuel dissolution rate.

6.4 Calculations with Spalling

Figure 39 and Figure 40 show the calculated doses using the independent DFN data with spalling included. Mean doses are typically an order of magnitude higher than those shown in Section 5.1.6 and Section 6.3. This observation is consistent with that made by SKB in Section 10.5.7 of the SR-Can report.

Figure 39: Calculated using Independent DFN Data (With Spalling)

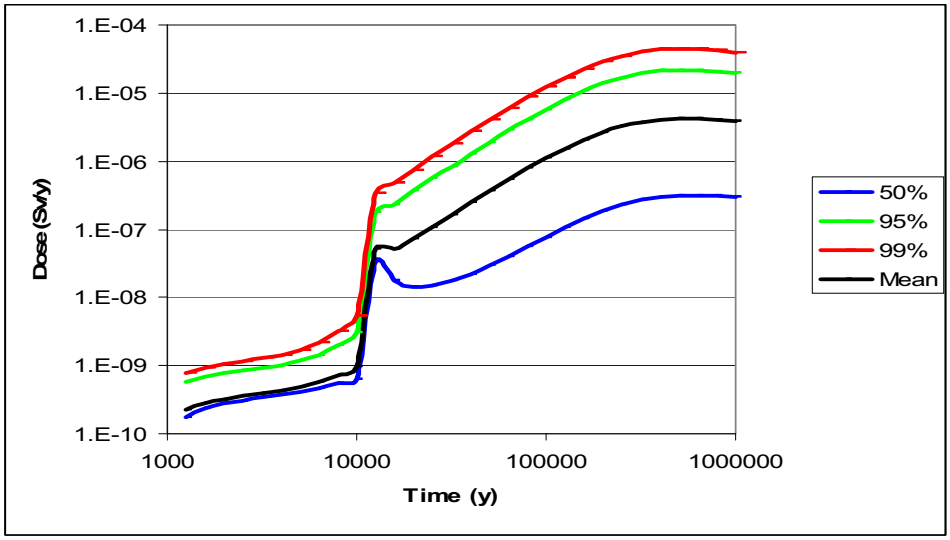

Figure 40: Calculated using Independent DFN Data (With Spalling) omitting Pb-210 and Po-210

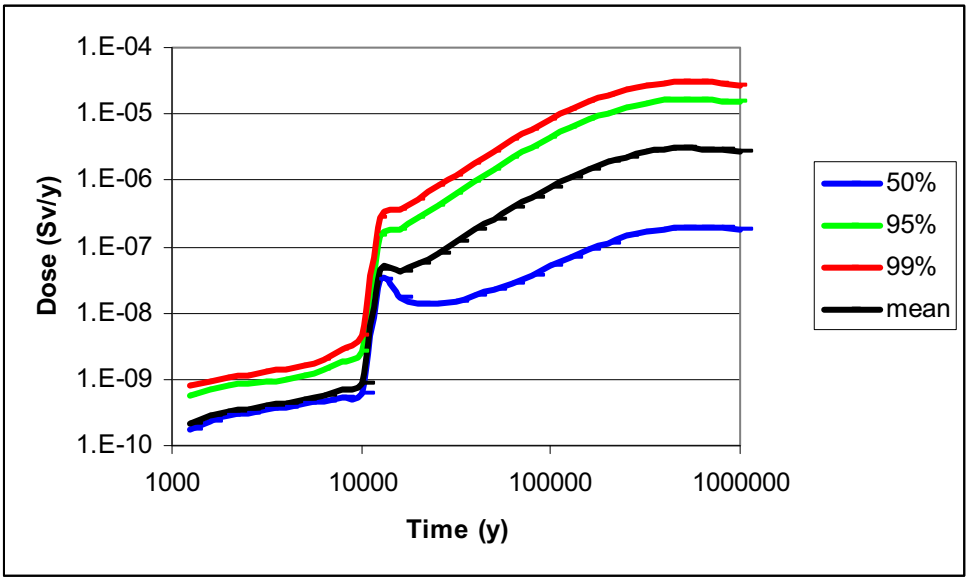

The primary reason for the higher doses calculated compared to the calculations in Section 6.3 with no spalling is the higher flux of radionuclides from the near field due to the higher values of the equivalent flow rate. This can be seen by comparing Figure 41 with Figure 38.

Figure 41: Scatter Plot of Near Field Dose at 1E6 y against Equivalent Flow Rate for Calculations using the Independent DFN Data (with spalling)

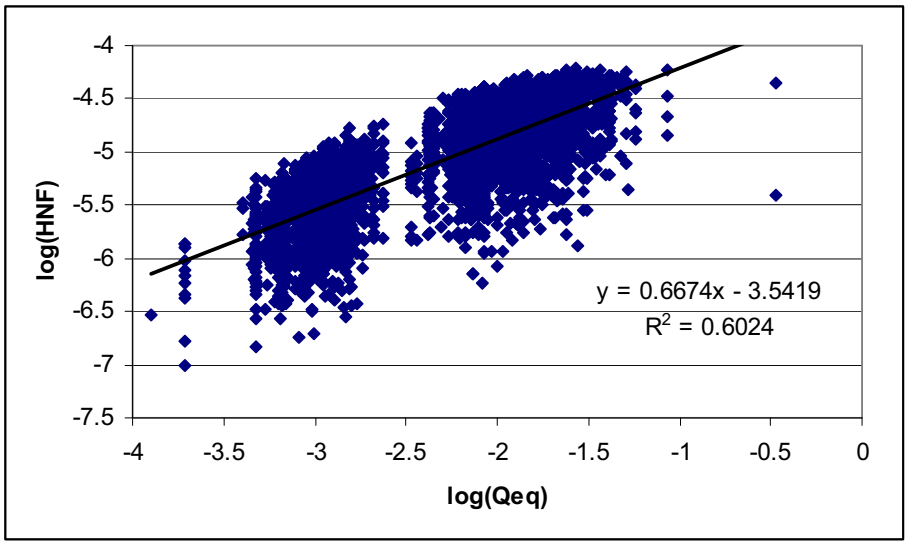

6.5 Conclusions

The main conclusions that can be drawn at this stage are:

- High dose runs have relatively high equivalent flow rates at the buffer/fracture interface, low geosphere travel times and low transport resistances compared with the overall population of runs.
- The AMBER calculations give significant contributions from Pb-210 and Po-210 for runs with very low geosphere travel times. This is not reflected in the SR-Can calculations.
- The independent DFN calculations have a higher fraction of runs with significant flows through the deposition hole; over half the SKB calculations do not, resulting in zero calculated doses.
- The independent DFN calculations have generally much smaller fracture apertures and geosphere travel times compared with the information supplied by SKB. This results in generally higher calculated doses.
- Detailed comparisons between the SR-Can and AMBER calculations is hindered by an imperfect understanding of the methods used by SKB to calculate the equivalent flow rates at the buffer/fracture interface.

7 Programme for Further Calculations

The discussion in the previous sections has identified several areas where further independent calculations would be valuable. In this section the most important of these are summarised.

7.1 Individual Processes

The discussion in Sections 3.3, 4.3 and 5.2 has highlighted the critical nature of the timescales for corrosion in the lost buffer failure mode. To date it has not been possible to reproduce the failure distribution function presented by SKB. Further consideration of both the calculations presented by SKB and independent evaluations are required in order to provide a more detailed assessment of this part of SKB's safety case.

As discussed in Section 3.2, SKB's approach to the representation of spalling appears reasonable, but this is clearly a preliminary assessment. Independent calculations for this process for comparison with SKB's evaluation would be useful.

7.2 Evolution of the EBS

SKB's representation of the evolution of the EBS in the period immediately following repository closure is superficial, with no fully-coupled assessment of the various processes involved. Additional independent QPAC-EBS calculations should be undertaken to investigate this period in more detail. Particular issues that need to be addressed include:

- Further consideration needs to be given to the thermal evolution of the repository, considering issues such as the heterogeneity of rock properties and the sensitivity of peak temperatures to the repository layout.

- QPAC-EBS calculations undertaken to date have not considered the resaturation of the bentonite. This involves complex processes that are currently being considered in benchmarking test cases in the EU THERESA project (Bond et al., 2007). At early times vapour transport may be an important process, possibly leading to the drying-out of bentonite close to the canister before incoming groundwater can resaturate it. In addition, the variation of thermal conductivity with the degree of saturation will need to be considered.

- Further QPAC-EBS calculations should be undertaken to investigate the interaction of hydrological processes with other processes in the immediate post-

closure period. This will require further work on the choice of appropriate relative permeability curves for use with the coarse system discretisation.

7.3 Canister Failure Modes

QPAC-EBS calculations have been initiated that will be able enable the buffer erosion scenario to be investigated in much more detail. These calculations will represent the evolving EBS (including groundwater chemistry), buffer erosion and canister corrosion.

In addition to the potential failure modes identified by SKB, consideration needs to be given to whether other scenarios for the evolution of the system could result in canister failures. Such scenarios could include mechanical failure modes.

7.4 Radionuclide Transport Calculations

SKB's radionuclide transport calculations still employ 1D methods that cannot consider time-dependent processes in the geosphere. SKB are aware of the limitations of this approach, but it would be useful to consider some specific issues, such as the effect of approximations introduced by integrating the F-factor over the transport pathway. In addition, further consideration needs to be given to the sensitivity of probabilistic calculations to the choice of parameter PDFs.

The current AMBER radionuclide transport model has been implemented in QPAC-EBS, and this will enable radionuclide transport calculations to be coupled to calculations for the evolution of the EBS in the future.

As shown in Dedross et al. (2006), it is possible to use information from DFN calculations to undertake 3D calculations using AMBER that are capable of considering time dependent processes. It would be useful to undertake some calculations using this approach in order to be able to assess any comparable calculations that are presented in SR-Site.

It is stated in SR-Can Section 4.2.12 that borehole seals must prevent short-circuiting of contaminated groundwater from the repository. The seals are 'under development'. It would be useful to undertake independent calculations to investigate the possible consequences if borehole seals fail.

8 Conclusions

The following conclusions have been drawn from the calculations presented in the preceding sections.

1. SKB has worked hard to respond to criticisms of previous performance assessments, and SR-Can is an impressive piece of work.

2. In several areas either insufficient or inconsistent information has been presented so that a full reproduction of SKB's calculations has not been possible. This is an important area where SKB will need to improve the presentation of its assessment for SR-Site.

3. There are several areas where SKB's description of post-closure repository evolution needs to be further reviewed. Overall SKB have given only limited consideration to the coupled processes that will operate before the system reaches a new equilibrium.

4. The calculations of thermal evolution suggest that some canisters may reach temperatures close to the maximum criterion of 100°C. It was not possible to reproduce fully the calculations presented by SKB because of uncertainties over the way that the repository layout was specified.

5. SKB's repository resaturation calculations are not definitive. The resaturation timescales obtained in the QPAC-EBS calculations are generally consistent with the relatively short timescales obtained by SKB, but timescales of much greater than 200 years have been obtained with some combinations of modelling assumptions. Further independent calculations will be undertaken, including consideration of bentonite resaturation.

6. Radionuclide transport calculations using the AMBER code have produced very similar results to those reported by SKB. However, this required a considerable amount of effort because of the need to check a large number of areas with SKB where the information provided in the SR-Can documentation was either incorrect or missing.

7. Insufficient deterministic calculations are given by SKB to enable the reader to understand the key issues presented and to facilitate the reproduction of SKB's calculations by a third party. It is suggested that for each set of probabilistic calculations undertaken in support of comparisons with regulatory criteria, a deterministic case should be documented to illustrate the key points. Further insight into the important features of probabilistic calculations can be obtained

by analysing the high consequence runs: this has been undertaken for the Quintessa calculations but was not considered by SKB in SR-Can.

8. The calculated risks may be more sensitive to the choice of parameter probability density functions (PDFs) than implied by SKB. For example, the choice between a triangular and log-triangular PDF for the fuel dissolution rate makes a difference of more than a factor of 2 in the calculated doses.

9. The lost buffer failure mode is critical to the overall risk quantification, and SKB's evaluation of this failure mode appears to be preliminary in nature. The distribution of failure times for canisters is critical, but it has not been possible to verify fully SKB's corrosion calculations. Further consideration of both the calculations presented by SKB and independent evaluations are required in order to provide a more detailed assessment of the validity of the approach taken in SR-Can.

10. The use of the independent Discrete Fracture Network calculations undertaken by Clearwater Hardrock Consulting has enabled alternative hydrogeological parameters to be used in the AMBER radionuclide transport calculations, contributing to an assessment of the robustness of the conclusions drawn by SKB.

Areas where additional independent calculations would be valuable have been identified and these can be considered for inclusion in the programme for 2008.

9 References

Allison J D, Brown D V and Novo-Gradac K J (1991). MINTEQA2/PRODEFA2. A Geochemical Assessment Model for Environmental Systems: Version 3.0 User's Manual. EPA/600/3-91/021.

Arcos D, Grandia F and Domenech C (2006) Geochemical Evolution of the Near Field of a KBS-3 repository. SKB Report TR-06-16.

Arthur R C and Wang J (2000). Claystone Constraints on Models of the Long-term Chemical Evolution of Buffer Porewaters. Scientific Basis for Nuclear Waste Management (R. W. Smith and D. W. Shoesmith, eds.), Materials Research Society Symposium 608**:** 551-556.

Bond A E, Maul P R, Robinson P C and Watson C E (2007). The Use of QPAC-EBS for Project THERESA Benchmarking Studies. Quintessa Report QRS-3009A-1 (in preparation).

Bradbury M H and Baeyens B (2002). Porewater Chemistry in Compacted Re-saturated MX-bentonite. Physicochemical Characterisation and Geochemical Modelling. PSI Report 02-10, Paul Scherrer Institute, Villigen, Switzerland.

Börgesson L and Sandén T (2006). Piping and Erosion in Buffer and Backfill Materials: Current Knowledge. SKB Report R-06-80.

Börgesson L, Fälth B and Hernelind J (2006). Water Saturation Phase of the Buffer and Backfill in the KBS-3V Concept: Special Emphasis given to the Influence of the Backfill on the Wetting of the Buffer. SKB Report TR-06-14.

Brantberger A Z, Torben A-N, Olsson T, Olssen I&T, Outters N and Pauli S (2006). Final Repository for Spent Nuclear Fuel: Underground Design Forsmark, Layout D1. SKB Report R-06-34.

Cliffe K A and Kelly M (2006). COMP23 version 1.2.2 User´s Manual. SKB Report R-04-64.

Dedross P, Benbow S J and Maul P R (2006). Particle Path Plotting Software for Analysing Discrete Fracture Network Flow Calculations. Quintessa Report QRS-1097H-1 version 2.0.

Duro L, Grivé M, Cera E, Gaona X, Domènech C and Bruno J (2006). Determination and Assessment of the Concentration Limits to be used in SR-Can. SKB TR-06-32.

Elert M, Gylling B and Lindgren M (2004). Assessment Model Validity Document-FARF31. SKB Report R-04-51.

Enviros Ltd and Quintessa Ltd (2007). AMBER version 5.1.

Geier J (2007). Discrete-Feature Modelling of Groundwater Flow and Solute Transport for the SR-Can Review. Draft Clearwater Hardrock Consulting report to SKI dated August 5 2007.

Grandia F, Domenèch C, Arcos D and Duro L (2006). Assessment of the Oxygen Consumption in the Backfill: Geochemical Modelling in a Saturated Backfill. SKB Report R-06-106.

Hartley L, Hoch A, Jackson P, Joyce S, McCarthy R, Rodwell W, Swift B and Marsic N (2006a). Groundwater Flow and Transport Modelling during the Temperate Period for the SR-Can Assessment: Forsmark Area – version 1.2. SKB Report R-06-98.

Hartley L, Hoch A, Jackson P, Joyce S, McCarthy R, Swift B, Gylling G and Marsic N (2006b). Groundwater Flow and Transport Modelling during the Temperate Period for the SR-Can Assessment: Laxemar Subarea – version 1.2. SKB Report R-06-99.

Hedin (2004). Integrated Near-Field Evolution Model for a KBS-3 Repository. SKB Report R-04-36.

Hedin A (2007a). E-mail to Bjorn Dverstorp and Bo Stromberg dated 15/3/07 in response to queries on SR-Can calculations from SKI and SSI.

Hedin A (2007b). E-mail to Bjorn Dverstorp and Bo Stromberg dated 19/3/07 on the subject of input files for SR-Can calculations.

Hedin A (2007c). E-mail to P R Maul dated 10/4/07 in response to further queries on the input files for SR-Can calculations.

Hökmark H and Fälth B (2003). Thermal Dimensioning of the Deep Repository: Influence of Canister Spacing, Canister Power, Rock Thermal Properties and Nearfield Design on the Maximum Canister Surface Temperature. SKB Report TR-03-09.

Jacquet O and Siegel P (2004). Local-Scale Modelling of Density-Driven Flow for the Phases of Repository Operation and Post-Closure at Beberg. SKB Report R-04-46.

Jacquet O and Siegel P (2006). Regional Groundwater Flow Model for a Glaciation Scenario. SKB Report R-06-100.

Karnland O, Olsson S, and Nilsson U (2006). Mineralogy and Sealing Properties of various Bentonites and Smectite-rich Clay Materials. SKB Report TR-06-30.

Kelly M and Cliffe K A (2006). Validity Document for COMP23. SKB Report R-06-76.

Lide D R and Kehiaian H V (1994). CRC Handbook of Thermophysical and Thermochemical Data. CRC Press LLC.

Liu J and Neretnieks I (2006). Physical and Chemical Stability of the Bentonite Buffer. SKB Report R-06-103.

Maul P R and Robinson P C (2005a). An Assessment of SKB's Performance Assessment Calculations in the Interim Main Report for the Safety Assessment SR-Can. SKI Report 2005:07. Quintessa Report QRS-1097F-3 version 1.1.

Maul P R and Robinson P C (2005b). Modelling Radionuclide Transport at Interfaces in the SKB Deep Repository Design. Quintessa Report QRS-1097G-2 version 1.0.

Maul P R, Benbow S J, Bond A E, Robinson P C and Watson C E (2007). QPAC-EBS version 1.0: A System Evolution Model for the Near Field of a Deep Repository for Spent Fuel. Quintessa Report QRS-3008B-1 version 1.0.

Moreno L and Gylling G (1998). Equivalent Flow Rate Concept used in Near Field Transport Model COMP23- Proposed Values for SR97. SKB Report R-98-53.

Neretnieks I (1979). Transport Mechanism and Rates of Transport of Radionuclide in the Geosphere as Related to the Swedish KBS-Concept. Proc. Symp. Underground Disposal of Radioactive Wastes, Otaniemi Finland, July 2-56 1979 vol. II p 108. International Atomic Energy Agency.

Neretnieks I (1986). Stationary Transport of Dissolved Species in the Backfill Surrounding a Waste Canister in Fissured Rock: Some Simple Analytical Solutions. Nuclear Technology 72, 196.

Neretnieks I (2006a). Flow and Solute Transport in a Damaged Zone due to Spalling. SKB Report R-06-91.

Neretnieks I (2006b). Flow and Transport through a Damaged Zone – Exploration of the Impact of a Cemented and an Eroded Buffer. SKB Report TR-06-33.

Rutqvist J and Tsang C-F (2007). Review of SKB's Work on Coupled THM Processes within SR-Can. Lawrence Berkeley National Laboratory draft report to SKI.

SKB (2004a). Interim Main Report of the Safety Assessment SR-Can. SKB Report TR-04-11.

SKB (2005). Preliminary Safety Evaluation for the Forsmark Area Based on Data and Site Descriptions after the Initial Site Investigation Stage. SKB report TR-05-16.

SKB (2006a). Long-term safety for KBS-3 Repositories at Forsmark and Laxemar - a First Evaluation. SKB Report TR-06-09.

SKB (2006b). Data Report for the Safety Assessment SE-Can. SKB Report TR-06-25.

SKB (2006c). Preliminary Safety Evaluation for the Laxemar Subarea Based on Data and Site Descriptions after the Initial Site Investigation Stage. SKB report TR-06-06.

SKB (2006d). Model Summary for the Safety Assessment SR-Can. SKB Report TR-06-26.

SKB (2006e). Initial State Report for the Safety Assessment SR-Can. SKB Report TR-06-21.

SKB (2006f). Fuel and Canister Process Report for the Safety Assessment SR-Can. SKB Report TR-06-22.

SKB (2006g). Buffer and Backfill Process Report for the Safety Assessment SR-Can. SKB Report TR-06-18.

SKI (2005). An Assessment of SKB's Performance Assessment Calculations in the Interim Main Report for the Safety Assessment SR-Can. SKI Report 2005:07.

SKI (2007). Review of SR-Can: Engineered Barriers. Report in Preparation.

Svensson U (2006a). The Forsmark Repository: Modelling Changes in Flow, Pressure and Salinity Fields due to a Repository for Spent Nuclear Fuel. SKB report R-05-57.

Svensson U (2006b). The Laxemar and Forsmark Repositories: An Analysis of the Water Inflow Distribution. SKB report R-06-102.

Vahlund F and Hermansson H (2006a). FVARF – a Direct Numerical Approach to Solving the Transport Equations for Radionuclide Transport in Fractured Rock. SKB Report R-04-50.

Vahlund F and Hermansson H (2006b). Compulink: Implementing the COMP23 Model in Simulink. SKB Report R-06-86.

Werme L, Johnson L H, Oversby V M, King F, Spahiu K, Gambow B and Shoesmith L W (2004). Spent Fuel Performance under Repository Conditions: a Model for Use in SR-Can. SKB Report TR-04-19.

Xu S (2007). E-mail to Philip Maul dated 30/3/07 giving details of discussion with Fredrik Vahlund.

Appendix A: The Buffer/Fracture Interface

In this Appendix a summary is given of the key results from Maul and Robinson (2005b).

A.1. Flow Resistances

It can be shown that the flux across the interface for a single fracture is given by

$$\Phi = Q_{eq}^{frac} C_1 = 4\,\varepsilon_i\, b\, v\, C_1 \sqrt{\frac{4 D_w L}{\pi v}}\,, \tag{A1}$$

So that:

$$Q_{eq}^{frac} = 4\,\varepsilon_i\, b\, v \sqrt{\frac{4 D_w L}{\pi v}}\,, \tag{A2}$$

$$= 8\,\varepsilon_i\, b \sqrt{\frac{D_w L\, v}{\pi}}\,.$$

SKB write this in terms of the Darcy velocity and introduce the 'width' of the surface area of contact into their formulae. This can be hard to interpret and depends (or seems to depend) on the precise choice of discretisation in the buffer. Here, we link this to the physical properties of the fractures.

The result is for a single fracture, of aperture $2b$. If we have a fracture separation of $2a$ (a>> b) and the distance of interest perpendicular to the fracture plane is W, then the number of fractures, N, is given by $W/2a$ (where we are implicitly assuming that N is an integer). The porosities and sizes are related by $\varepsilon_i b = a\varepsilon_f$, and the Darcy velocity and pore velocity are related by $q = v\varepsilon_f$. Thus, the total equivalent flow is given by

$$Q_{eq} = N Q_{eq}^{frac} = 8\, N\, \varepsilon_i\, b \sqrt{\frac{D_w L v}{\pi}}\,,$$

$$= 8\, N\, a\, \varepsilon_f \sqrt{\frac{D_w L\, q}{\pi \varepsilon_f}}$$

$$= 4\, W \sqrt{\frac{D_w L\, q\, \varepsilon_f}{\pi}}\,. \tag{A3}$$

This corresponds precisely to the result given by Moreno and Gylling (1998). Notice that the fracture aperture and separation do not appear in this formula, only the overall flowing porosity and Darcy velocity. This implies that the effect of two thin fractures is exactly the same as the effect of one twice as thick (given a fixed flowing porosity and Darcy velocity) – this enables the effect of fracture zones to be assessed without regard to the details of the fracturing within the zone.

For sparsely fractured systems, some care must be taken to avoid having a fraction of a fracture implied by the parameter choices. If a compartment is defined with a single fracture and a dimension perpendicular to the flow that is less than the fracture separation, *2a*, then *W* in (A3) should be replaced by *2a*. It is possible that, if this situation is not explicitly catered for, some choices of parameter values in probabilistic calculations could result in the effective value of the equivalent flow rate being underestimated.

A.2. Diffusive Resistances

It can be shown that the diffusive flux through the fissure is given by:

$$\Phi = \frac{A\,D(C_0 - C_1)}{F} = \frac{2\pi r_2\, b\, D_b (C_0 - C_1)}{F} \qquad \text{A4}$$

where

$$F = a\,\{\beta\,\delta + \frac{2}{\pi^2}\sum_{m=1}^{\infty}\frac{\tanh(m\pi\delta)\sin(m\pi\beta)}{m^2}\}$$

$$\frac{F}{b} = \delta + \frac{2}{\beta\pi^2}\sum_{m=1}^{\infty}\frac{\tanh(m\pi\delta)\sin(m\pi\beta)}{m^2}$$

$$\beta = \frac{b}{a}$$

$$\delta = \frac{R}{a}$$

where C_1 is the concentration at the fissure opening and A is the interface area. Note again that the total flux through the fissure is a factor of two higher than that given in equation (A4) due to the consideration of just half the aperture.

In Neretnieks (1986) it is incorrectly stated that F is dimensionless: in fact it has dimensions of length and it is the combination F/b that is dimensionless.

Note that F is related to the parameter B of equation (5.7) by

$$B = \frac{F}{A} = \frac{F}{2\pi r_2 b} \qquad \text{A5}$$

Neretnieks (1986) gives the following approximation for *F*, which it is assumed is obtained from a simple curve fitting to the calculated full solution over the range of values of β and δ that are considered to be relevant:

$$\frac{F}{b} \cong 1 - 1.35\log_{10}\beta + 1.6\log_{10}\delta \qquad \text{A5}$$

$$10^{-6} \leq \beta \leq 10^{-1}$$
$$0.03 \leq \delta \leq 1$$

An alternative approximation to the evaluation of the dimensionless quantity *F/b* can be obtained by assuming that δ~1 and β <<1. One then obtains:

$$\frac{F}{b} \cong \delta + \frac{2}{\pi}[\gamma - \frac{1}{12} - \ln(\pi\beta)] \qquad \text{A6}$$

The full evaluation of the summation in equation (A4) is not as straightforward as implied by Neretnieks, because it converges extremely slowly, but the following approximation can be obtained:

$$\frac{F}{b} \cong \alpha_1 + \alpha_2\log_{10}\beta + \alpha_3\log_{10}\delta\,. \qquad \text{A7}$$

where α_1 is around 0.9, α_2 -1.466 and α_3 1.58.

These values differ only slightly from those used by Neretnieks.

Although the approximation δ~1 may not be a particularly good one, the resulting estimate for *F/b* generally remains reasonable provided β <<1, which will usually be the case.

As Neretnieks points out, the quantity *F* can be interpreted as the effective distance over which the concentration gradient applies, and this is a factor of 1-10 times the fracture half-width.

Appendix B: Correlated Sampling from Triangular Distributions

As indicated in SR-Can Section 5.1.2, SKB use correlated groups of elements in specifying sorption coefficients. A value x is obtained from a uniform distribution [0, 1] and an input value y is then calculated as $y = F^{-1}(x)$, where $F(y)$ is the cumulative distribution function for the input variable in question. In a particular realisation, the same x is used for all elements belonging to the same correlation group.

SKB make frequent use of triangular (and log-triangular) probability density functions. If the PDF has a lower value L, a peak value P and an upper value U, then the cumulative density function can be written as follows:

$$\begin{aligned} F(y) &= 0 \quad y \le L \\ &= \frac{(y-L)^2}{(P-L)(U-L)} \quad L \le y \le P \\ &= 1 - \frac{(U-y)^2}{(U-P)(U-L)} \quad P \le y \le U \\ &= 1 \quad x \ge U \end{aligned} \tag{B.1}$$

So that for a given value of x, y can be determined as follows:

$$\begin{aligned} y &= L + (U-L)\sqrt{x\xi} \qquad 0 \le x \le \xi \\ &= U - (U-L)\sqrt{(1-x)(1-\xi)} \quad \xi \le x \le 1 \\ \xi &= \frac{(P-L)}{(U-L)} \end{aligned} \tag{B.2}$$

Appendix C: Canister Corrosion Calculations

In this Appendix details are given of the progress made to date on the QPAC-EBS calculations described in Section 4.3. At this stage the calculations are purely illustrative, but they will provide the basis for independent calculations of canister corrosion in 2008.

C.1 The Transport of Corrodants with an Intact Buffer

A QPAC-EBS model has been set up to simulate the transport of sulphide ions to the canister surface through a fracture that intersects the EBS. The geometry of the system is shown in Figure 42 and the system dimensions are given in Table 24. The canister region is a 'hole' in the model (i.e. it is not simulated). All interactions with the canister are modelled as surface processes on the canister boundary. Two fracture apertures are considered, 0.1 mm and 1mm.

The fracture is assumed to be filled with regional groundwater with a sulphide ion concentration of 1E-2 mol m^{-3}. No chemical evolution is simulated in the model except for the corrosive interaction of the sulphide ions with the canister surface.

A regional head gradient of 1E-2 (m/m) is imposed across the system (left to right as shown in Figure 42). This serves to provide a sufficiently large groundwater flow rate such that the sulphide concentration around the edge of the buffer remains close to the fixed regional concentration (although this will depend on the hydraulic conductivity, and hence aperture, of the fracture). The hydraulic properties assumed in the model are listed in Table 25.

Hydraulic boundary conditions are set around the edge of the fracture to be consistent with the regional head gradient assumption. All other boundaries in the system are assumed to be no flow.

Transport through the system is assumed to be via advection and diffusion. Given the large regional head gradient that is assumed, flow in the fracture regions is likely to be advection dominated (although this will vary with fracture aperture), whereas in the buffer, where the hydraulic conductivity is small, transport will be predominantly by diffusion. Transport property values are listed in Table 26.

Figure 42: System Geometry

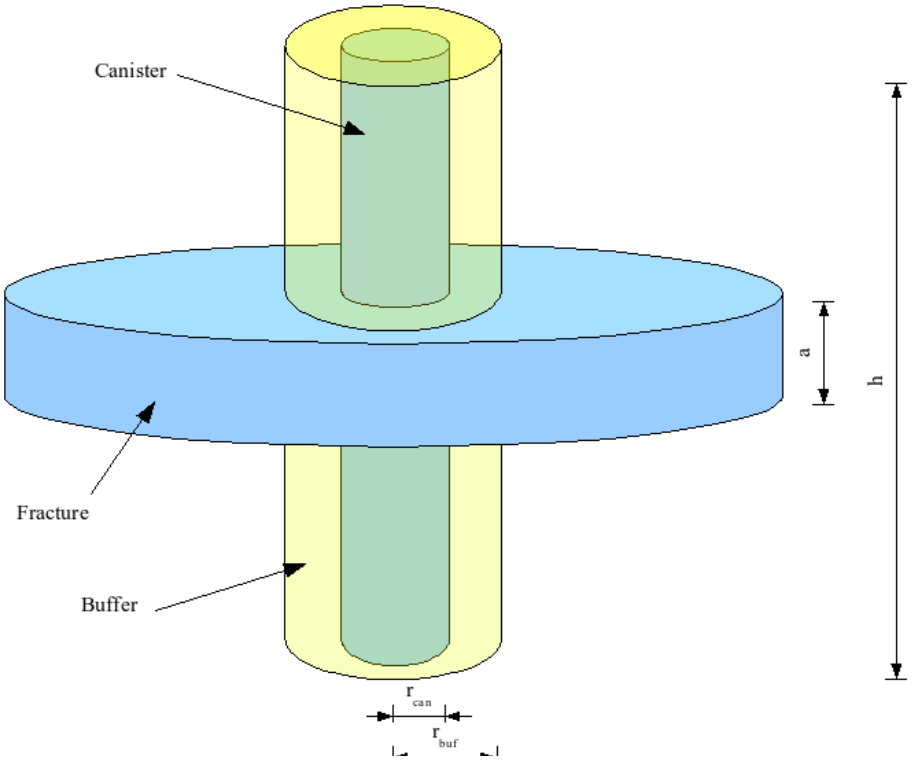

Table 24: System Dimensions

Property	Parameters	Value
Fracture aperture	a (m)	1E-4, 1E-3
Canister height	h (m)	5
Canister radius	r_{can} (m)	0.525
Buffer radius	r_{buf} (m)	0.85
Radial extent into fracture	r_{far} (m)	10

Table 25: Hydraulic Properties

Location	Porosity	Hydraulic conductivity ($m\ s^{-1}$)
Fracture (a = 1E-4 m)	0.2	1e-14
Fracture (a= 1E-3m)	0.2	1E-12
Buffer	0.43	5E-7

Note: porosity and hydraulic conductivity values for the buffer and the smaller fracture are taken from Table 5-2 of Arcos et al. (2006). The hydraulic conductivity for the larger fracture is derived from the Poiseuille assumption that this varies as the square of the aperture.

Table 26: Transport Properties

Location	Effective diffusion coefficient ($m^2\ s^{-1}$)
Fracture (all apertures)	1E-9
Buffer	1.2E-10

Note: The value of the diffusion coefficient in the buffer is taken from Table 5-2 of Arcos et al. (2006). The diffusion coefficient in the fracture is assumed to be that of free water.

The radial extent that is modelled in to the fracture is assumed to be sufficient that the concentration of sulphide ions at the boundary is held at the regional concentrations, i.e. it is assumed that this is a sufficiently large system that the perturbation caused to the sulphide concentrations by interactions within the EBS is small. In reality it may be the case that the fracture intersects more than one deposition hole, in which case this assumption may be invalid. It is however considered conservative. All other outer boundaries are assumed to have a zero flux condition.

To simulate corrosion at the canister surface it is assumed that all sulphide ions that arrive are instantaneously consumed in the corrosion process. Thus a zero sulphide concentration condition is imposed on the canister boundary.

The equation used in Appendix B of the SR-Can report for the bulk corrosion rate for an intact buffer (equation 3.1 in the main text) is:

$$e = [HS^-]Q_{eq}\frac{F f M_{Cu}}{2\pi r_{can} h_{can} \rho_{Cu}} \qquad \text{C.1}$$

Here the sulphide ion concentration [HS^-] (mol m^{-3}) is multiplied by an equivalent flow rate Q_{eq} (m^3 y^{-1}) to obtain the transport rate of sulphide ions to the canister. The second term is an averaging term over the whole canister surface. *F* is a 'buffer concentration factor' which is specified to account for variations in sulphide concentration up the length of the canister. The remaining terms *f*, M_{Cu} and ρ_{Cu} are a stoichiometric factor (equal to 2), and the molar mass (kg mol^{-1}) and density (kg m^{-3}) of copper.

Using the QPAC-EBS model it is possible to compute a corrosion rate on each 'surface element', ω on the discretisation of the canister surface, given by

$$e_\omega = Q_{[HS^-],\omega}\frac{1}{A_\omega}\frac{f M_{Cu}}{\rho_{Cu}}. \qquad \text{C.2}$$

Here $Q_{[HS^-],\omega}$ is the flux of sulphide ions at the canister surface (mol y^{-1}) and A_ω (m^2) is the area of the surface element. The three terms in the equation correspond to analogous quantities in SKB's formula. Using this formula it is possible to plot the corrosion rate at various locations on the canister surface. This allows the 'shape' of the corrosion profile along the canister length to be determined, and, in particular, how quickly the corrosion rate falls off away from the fracture plane.

The quantities in the QPAC-EBS model can also be used to derive an equivalent flow rate. This can be expressed as

$$Q_{eq(QPAC)} = \frac{1}{\left[HS^-\right]_{regional}} \sum_{\omega} Q_{\left[HS^-\right]}, \omega \qquad \text{C.3}$$

and can be compared with equivalent flow rates quoted by SKB.

Due to the assumption of instantaneous corrosion and constant boundary conditions, the system tends towards a steady state at the point where the consumption rate of sulphide ions at the canister surface matches the maximum rate at which they can be transported. After this time the sulphide concentrations in the system remain constant. The constant profiles across the system in the plane of the fracture are shown in Figure 43 and Figure 44 where the axes are distances in m. The 1E-3 m aperture fracture is sufficient to maintain regional sulphide concentrations around the circumference of the buffer whereas the slower transport rates associated with the 1E-4 m fracture lead to greater variation in sulphide concentration around the circumference, although the concentrations are still generally 'high'.

The corrosion rate profile along the length of the canister for the 1E-4 m fracture is shown in Figure 45 for upstream and downstream locations on the canister surface. The maximum corrosion rate is around 2.75E-12 m y^{-1} and occurs at the upstream location in and near to the fracture plane (as would be expected) and falls off rapidly moving away from the fracture plane. The corrosion rate is essentially zero at distances beyond 1.75 m along the canister length. At the downstream location, the maximum corrosion rate is around 1E-12 m y^{-1} and falls off with a similar rate. A derived equivalent flow rate of 2.5E-5 m^3 y^{-1} is obtained from this model (Figure 46).

The corrosion rate profile along the length of the canister for the 1E-3 m fracture is shown in Figure 47 for upstream and downstream locations on the canister surface. The maximum corrosion rate is around 9E-11 m y^{-1} and occurs at the upstream location in and near to the fracture plane. Again, the rate falls off quickly moving away from the fracture plane. The corrosion rate is essentially zero at distances beyond 1.75 m along the canister length. Due to the larger fracture aperture the downstream corrosion rate is similar to the upstream rate. A derived equivalent flow rate of 1.15E-3 m^3 y^{-1} is obtained from this model (Figure 48).

The peak corrosion rates calculated here are consistent with the values presented in Figure 9-62 of the SR-can report.

Figure 43: Steady State Sulphide Concentration in the Fracture Plane (1E-4 m Aperture)

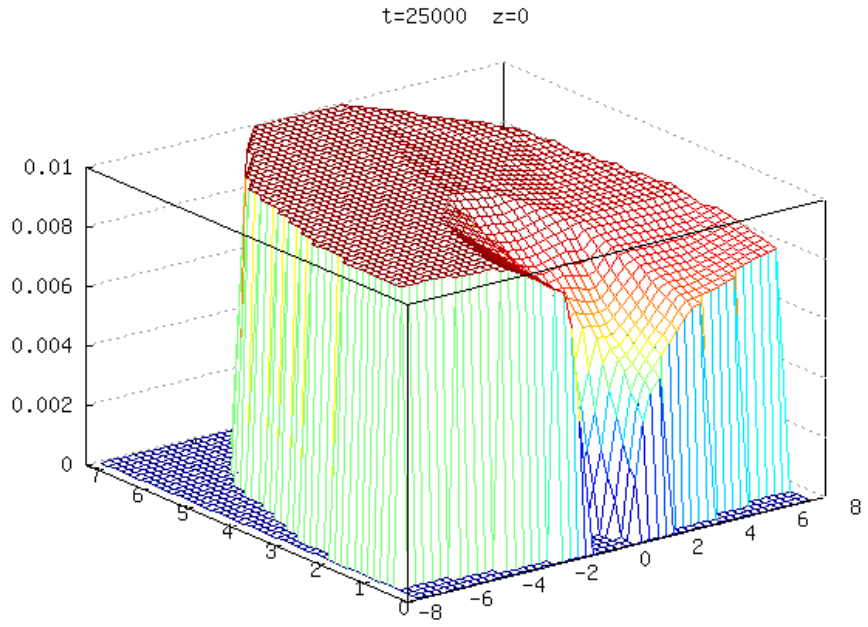

Figure 44: Steady State Sulphide Concentration in the Fracture Plane (1E-3 m Aperture)

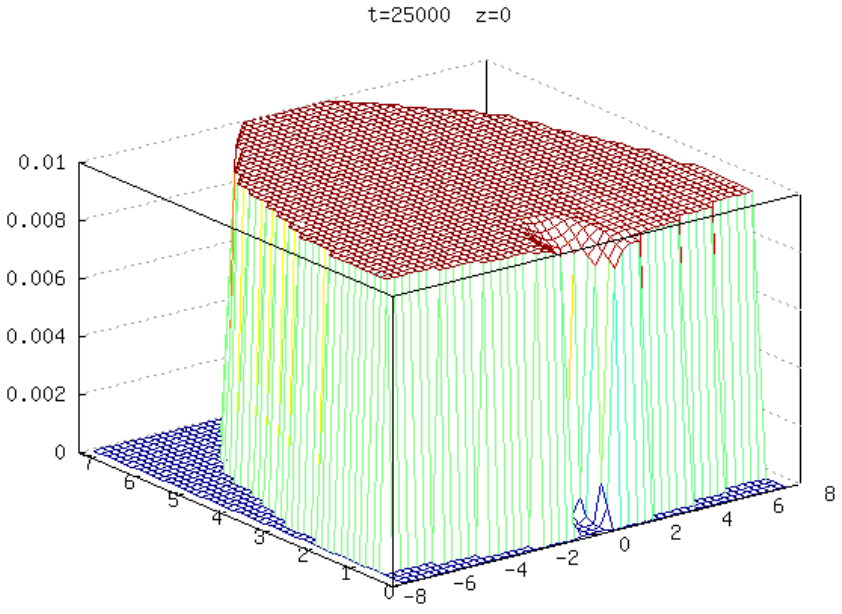

Figure 45: Corrosion Rates (1E-4 m Aperture Fracture)

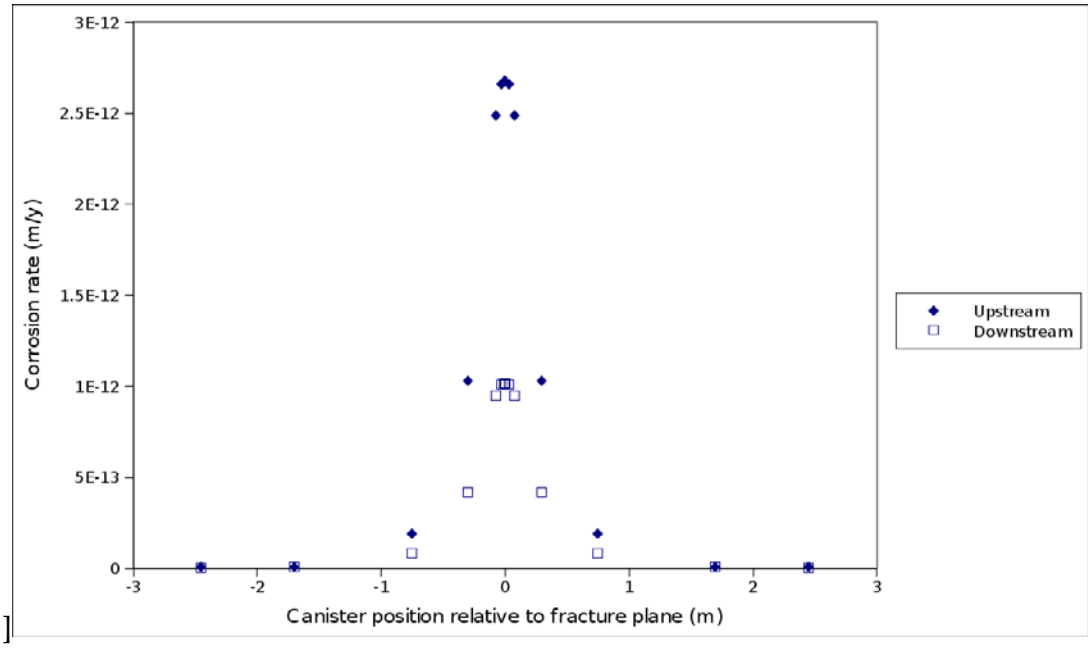

Figure 46: Derived Equivalent Flow Rate (1E-4 m Aperture Fracture)

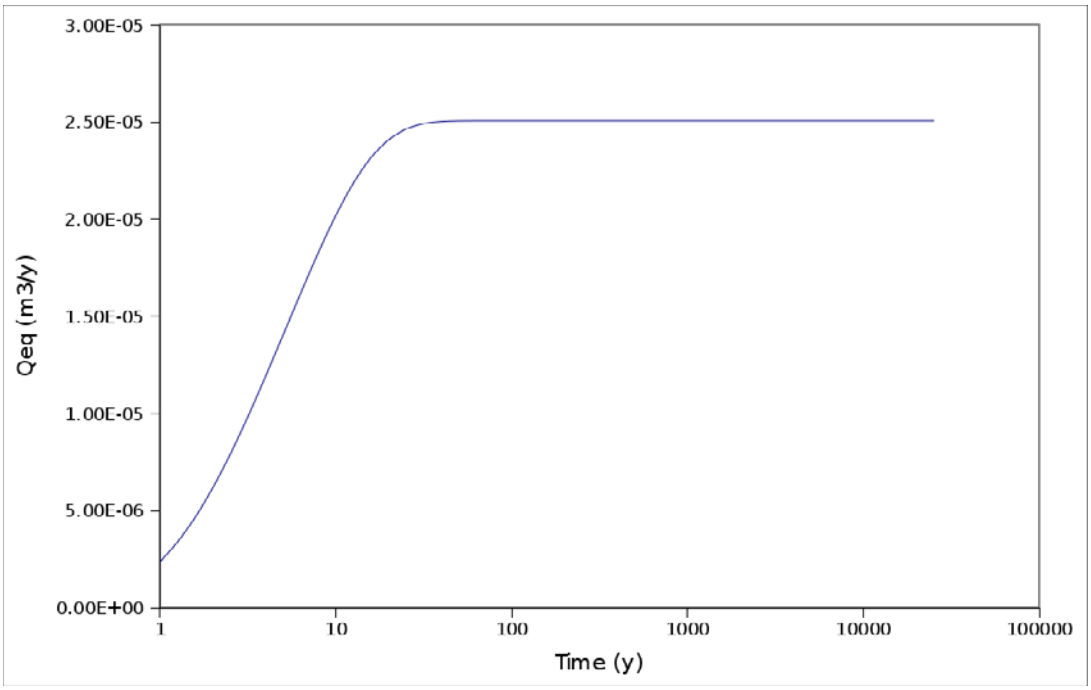

Figure 47: Corrosion Rates (1E-3 m Aperture Fracture)

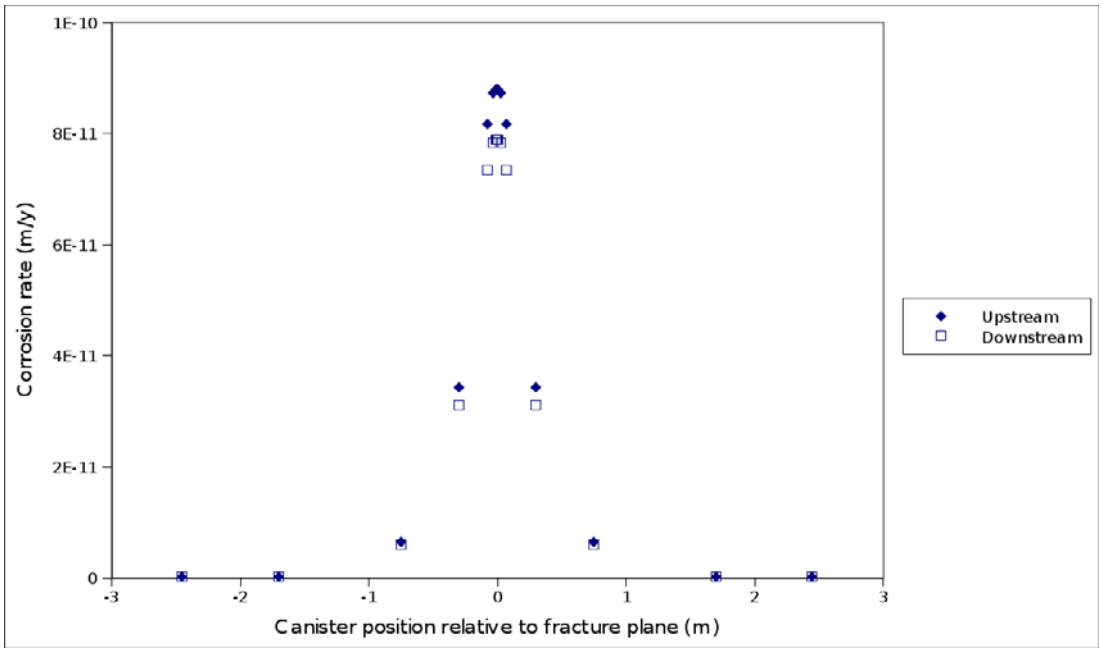

Figure 48: Derived Equivalent Flow Rate (1E-3 m Aperture Fracture)

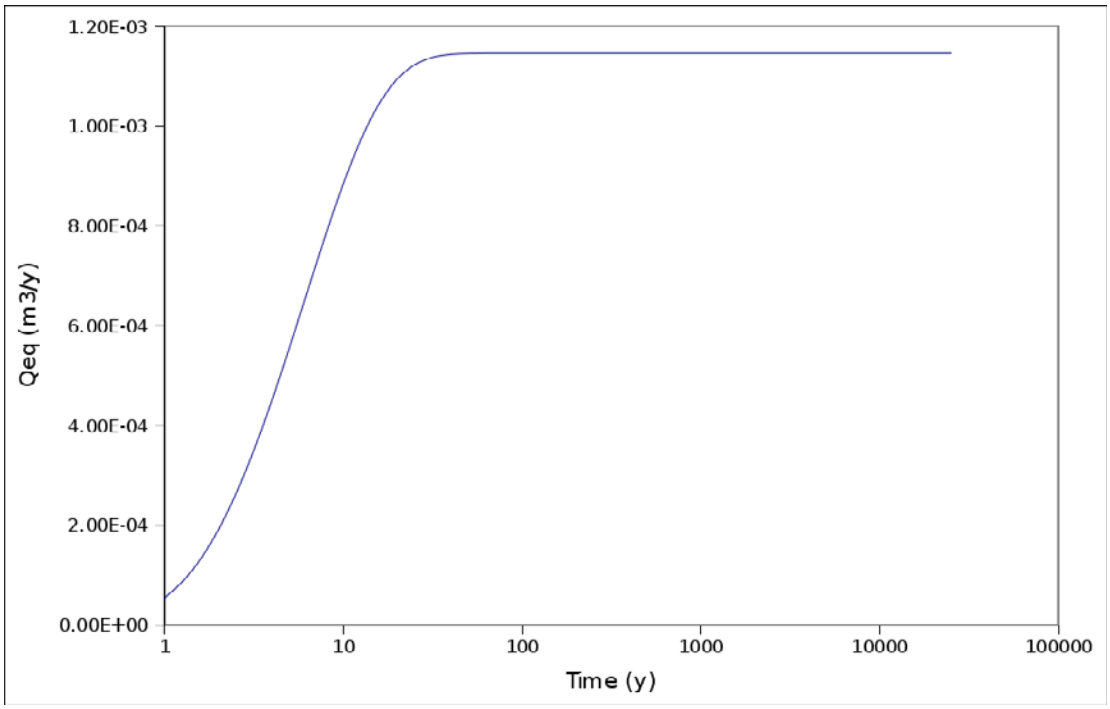

C.2 The Transport of Corrodants with an Eroding Buffer

The QPAC-EBS calculations given in the previous section for an intact buffer are currently being developed to consider the more complex situation when the buffer is eroding. Results from these calculations will be presented in 2008.

C.3 Chemical Processes

The chemical model to be employed has not yet been implemented, but a discussion is given here of the processes that need to be represented and the data that are available.

For the near-field evolution model employed in SR-Can, the concentration of divalent cations is important in that their presence decreases the stability of colloids. In dilute groundwaters, montmorillonite colloids may be transported away if $[M^{2+}] < 0.001$ mol l^{-1}. Available experimental data suggests that montmorillonite colloids are not stable at concentrations above this limit. Consequently, SKB 'switch on' the bentonite erosion model when interactions of bentonite pore fluids with glacial meltwater decrease the concentration of Ca^{2+} less than 0.001 mol l^{-1}.

Arcos et al. (2006) consider that the key processes impacting upon the buffer chemistry relating to the erosion of the buffer are:

- cation exchange reactions in the montmorillonite;
- protonation-deprotonation surface reactions of the montmorillonite;
- dissolution-precipitation of solid carbonate minerals; and
- dissolution-precipitation of solid sulphate minerals.

Dissolution-precipitation processes involving montmorillonite itself have been excluded, since they consider it to be too slow to be of significance. However, it should be noted that other authors have a different view of the importance of this process (e.g. Arthur and Wang, 2000).

Other reactions which are of relevance to canister corrosion are those that potentially control Eh, such as pyrite oxidation and siderite dissolution. These reactions are not considered here.

Table 27 gives the key reactions and data considered by SKB. Data for pyrite and goethite hydrolysis quoted in Table 5-3 of Arcos et al. (2006) have been omitted. It

should be noted that siderite and dolomite are not present in MX-80 bentonite. Site capacities for ZOH and YOH are each 4.0 10^{-2} mol kg^{-1}. Data for dolomite, siderite, pyrite and goethite hydrolysis have been omitted in the interests of simplicity.

Mineralogical data for MX-80 and Deponit CA-N are presented in Table 28. With regard to chemical buffering reactions it is noteworthy that solid carbonate minerals are absent in MX-80, whereas, they amount to 13 wt % in Deponit CA-N.

Arcos et al. (2006) quote a value of 0.43 for diffusion-accessible porosity and effective diffusion coefficient (D_e) of 1.2 10^{-10} m^2 s^{-1} in bentonite with a dry density of 1570 kg m^{-3}.

The chemical compositions of bentonite pore waters and groundwater compositions considered by Arcos et al. (2006) are reproduced in Table 29 and Table 30. The bentonite pore water compositions were achieved by reacting Forsmark groundwater with bentonite with a porosity of 0.43 using the data for exchange and surface complexation reactions and the dissolution-precipitation of trace carbonates and sulphate minerals.

Table 27: Geochemical Modelling Data

Mineral hydrolysis			
Mineral	**Reaction**	**Log K**	**Source**
calcite	$CaCO_3 = Ca^{2+} + CO_3^{2-}$	-8.48	Allison et al. (1991)
gypsum	$CaSO_4{:}2H_2O = Ca^{2+} + SO_4^{2-} + 2H_2O$	-4.85	Allison et al. (1991)
dolomite	$CaMg(CO_3)_2 = Ca^{2+} + Mg^{2+} + 2CO_3^{2-}$	-17.90	Allison et al. (1991)
siderite	$FeCO_3 = Fe^{2+} + CO_3^{2-}$	-10.80	Allison et al. (1991)
Cation exchange reactions			
NaX	$X^- + Na^+ = NaX$	0.00	Bradbury & Baeyens (2002)
KX	$X^- + K^+ = KX$	0.60	Bradbury & Baeyens (2002)
CaX_2	$2X^- + Ca^{2+} = CaX_2$	0.41	Bradbury & Baeyens (2002)
MgX_2	$2X^- + Mg^{2+} = MgX_2$	0.34	Bradbury & Baeyens (2002)
Protonation-deprotonation reactions			
	$ZOH + H^+ = ZOH_2^+$	4.50	Bradbury & Baeyens (2002)
	$ZOH + H^+ = ZO^- + H^+$	-7.90	Bradbury & Baeyens (2002)
	$YOH + H^+ = YOH_2^+$	6.00	Bradbury & Baeyens (2002)
	$YOH + H^+ = YO^- + H^+$	-10.50	Bradbury & Baeyens (2002)

Table 28: Mineralogical Composition and Cation Exchange Capacity of the Clay Fraction of bentonites MX-80 and Deponit CA-N. From Arcos et al. (2006).

Mineral wt %	**MX-80**	**Deponit CA-N**
Montmorillonite	87	81
Quartz	5	2
Feldspar + mica	7	2
Dolomite	0	3
Calcite + siderite	0	10
Pyrite	0.07	0.5
Gypsum	0.7	1.8
CEC (meq/10 g)	75	70
NaX (%)	72	24
KX (%)	2	46
CaX_2 (%)	18	29
MgX_2 (%)	8	2

Table 29: Calculated Compositions of Bentonite Porewaters Saturated with Forsmark Groundwater. Concentrations are in mol l^{-1}. From Arcos et al. (2006).

	MX-80	Deponit CA-N
pH	7.08	7.09
pe	-2.19	-2.30
HCO_3^-	2.14e-3	2.33e-3
Ca	9.97e-3	2.37e-2
Cl	1.53e-1	1.53e-1
Fe total	3.31e-5	1.72e-4
K	1.14e-3	1.34e-3
Mg	2.39e-2	2.39e-2
Na	7.11e-3	7.11e-2
SO_4^{2-}	2.94e-2	1.32e-2
Si	6.60e-5	6.64e-5

Table 30: Compositions of Groundwaters Considered in the Chemical Modelling. Concentrations are in mol l^{-1}. From Arcos et al. (2006).

	Forsmark	Laxemar Saline	Grimsel ice-melting
pH	7.2	7.9	9.6
pe	-2.42	-5.08	-3.38
HCO_3^-	2.20e-3	1.00e-4	4.50e-4
Ca	2.33e-2	4.64e-1	1.40e-4
Cl	1.53e-1	1.28	1.60e-4
Fe total	3.31e-5	8.00e-6	3.00e-9
K	8.75e-4	7.00e-4	5.00e-6
Mg	9.30e-3	1.00e-4	6.20e-7
Na	8.88e-2	3.49e-1	6.90e-4
SO_4^{2-}	6.80e-3	9.00e-3	6.10e-5
Si	1.85e-4	8.00e-5	2.05e-4

www.ski.se

STATENS KÄRNKRAFTINSPEKTION
Swedish Nuclear Power Inspectorate

POST/POSTAL ADDRESS SE-106 58 Stockholm
BESÖK/OFFICE Klarabergsviadukten 90
TELEFON/TELEPHONE +46 (0)8 698 84 00
TELEFAX +46 (0)8 661 90 86
E-POST/E-MAIL ski@ski.se
WEBBPLATS/WEB SITE www.ski.se